Deterministic ratchets for larger-scale separation of suspensions

Yvette Sylvia Lubbersen

Thesis committee

Promotor

Prof. Dr R.M. Boom

Professor of Food Process Engineering

Wageningen University

Co-promotor

Dr M.A.I. Schutyser

Assistant professor, Laboratory of Food Process Engineering

Wageningen University

Other members

Prof. Dr E. van der Linden, Wageningen University

Prof. Dr M. Wessling, RWTH Aachen, Germany

Dr M. Biesheuvel, Wetsus, Leeuwarden and Wageningen University

Prof. Dr M. Kreutzer, Delft University of Technology

Deterministic ratchets for larger-scale separation of suspensions

Yvette Sylvia Lubbersen

Thesis

submitted in fulfillment of the requirements for the degree of doctor

at Wageningen University

by the authority of the Rector Magnificus

Prof. Dr M.J. Kropff,

in the presence of the

Thesis Committee appointed by the Academic Board

to be defended in public

on Wednesday 23 April 2014

at 11 a.m. in the Aula.

Table of Contents
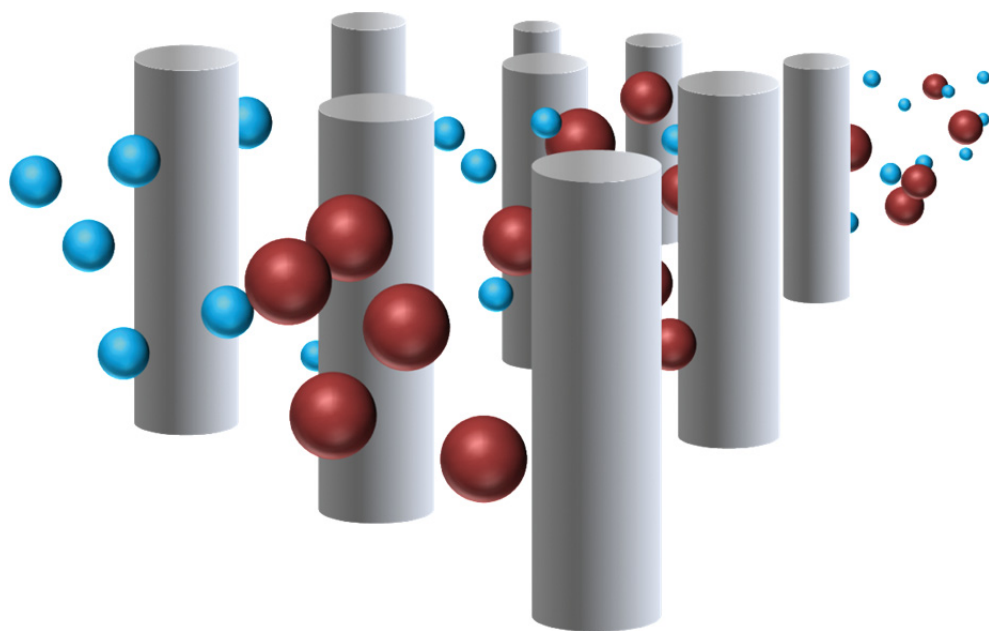
General Introduction

Illustration of particles flowing through an obstacle array.

1. General Introduction

This chapter provides an introduction to this PhD thesis, which aims at understanding the mechanisms, and developing design guidelines for deterministic ratcheting systems for large scale separation of suspensions. The chapter starts with an introduction on suspension separation and is followed by a factual overview of the development history of deterministic ratchets for separation purposes. It furthermore states the aims and scope of the research and finalizes with a short description of the chapters in this thesis.

1.1. Suspension separation

Separation processes are essential operations in the process industry to concentrate or fractionate raw materials to obtain a product or stream of desired specifications. On an industrial scale these processes represent over fifty percent of the capital and operating costs in industry [1]. Although many different separation technologies are readily available, all these technologies have their restrictions, and thus there is a continuous need for new technologies. The main reasons for innovation are the increasing demand for high product purity, the stricter environmental regulations on waste treatment and the need for technologies that use less energy, water, and chemicals.

This thesis focuses on the separation of suspensions, which can be defined as heterogeneous mixtures of a dispersed phase, usually small solid particles in a fluid, which can be either a liquid or a gas. In this work, suspensions of solid particles in water are separated, with particle sizes of at least one micrometer. The reason for separation can be either the purification of the liquid by the removal of the particles or the recovery of valuable particles (fractions) from the suspension. Examples of liquid purification are the regeneration of laundry rinsing water, sewage treatment and clarification of fruit juices and alcoholic beverages like beer and wine. Examples of

particle recovery are the harvesting of algae and the fractionation of blood components.

The main three basic principles for solid-liquid separation are filtration, sedimentation and centrifugation [2-4]. A further classification of those separation processes is given in fig. 1.1. In filtration a solid-liquid mixture is directed towards a filter, for example a screen, woven cloth, paper or membrane. The liquid flows through the filter (permeate or filtrate), while a concentrate with most of the particles remains behind (retentate or filter cake). This separation is based on the difference in solid particle size and characteristic pore size of the filter material. In the case of classical filtration, much of the separation is not due to the particle size of the filter cloth, but due to the capture of the particles in an accumulation layer of particles that are added as filter aid.

A serious drawback of filtration is the inherent accumulation of particles on the filter surface. The accumulation reduces the permeation rate and increases the energy demand. Sedimentation technologies principally rely on a difference in medium density to separate solid particles from the liquid. If the density difference is small, the sedimentation velocity can be enhanced by increasing particle size via flocculation or coagulation. During centrifugal separation, solid-liquid separation by density differences is enhanced by application of centrifugal forces. Other suspension separation processes rely on force fields such as magnetic fields [5], acoustic fields [6] or optical trapping [7], which are not shown in fig. 1.1.

Processing industries traditionally process large volumes and preferably treat concentrated streams to avoid unnecessary dilution and related energy use. This requires separation technologies that allow high throughputs, while retaining good separation efficiencies, have low energy use and do no suffer from fouling problems. In the pharmaceutical and biomedical analysis areas, process volumes are very small and usually very dilute. Previous research showed that microfluidic separation devices can process these dilute streams with high resolution and sensitivity, at low cost, short analysis times and with small foot print [8]. Examples of microfluidic separation technologies are flow focusing [9, 10] and flow line sieving [11], which are based on particle exclusion from certain pathways through a sieving structure. Among

the microfluidic separation technologies, deterministic ratchets are identified as highly promising for separation of food or waste water suspensions [12]. They do not need the use of an external force field, additional chemicals or water, are relatively simple in system design and operation and have potential for large scale application.
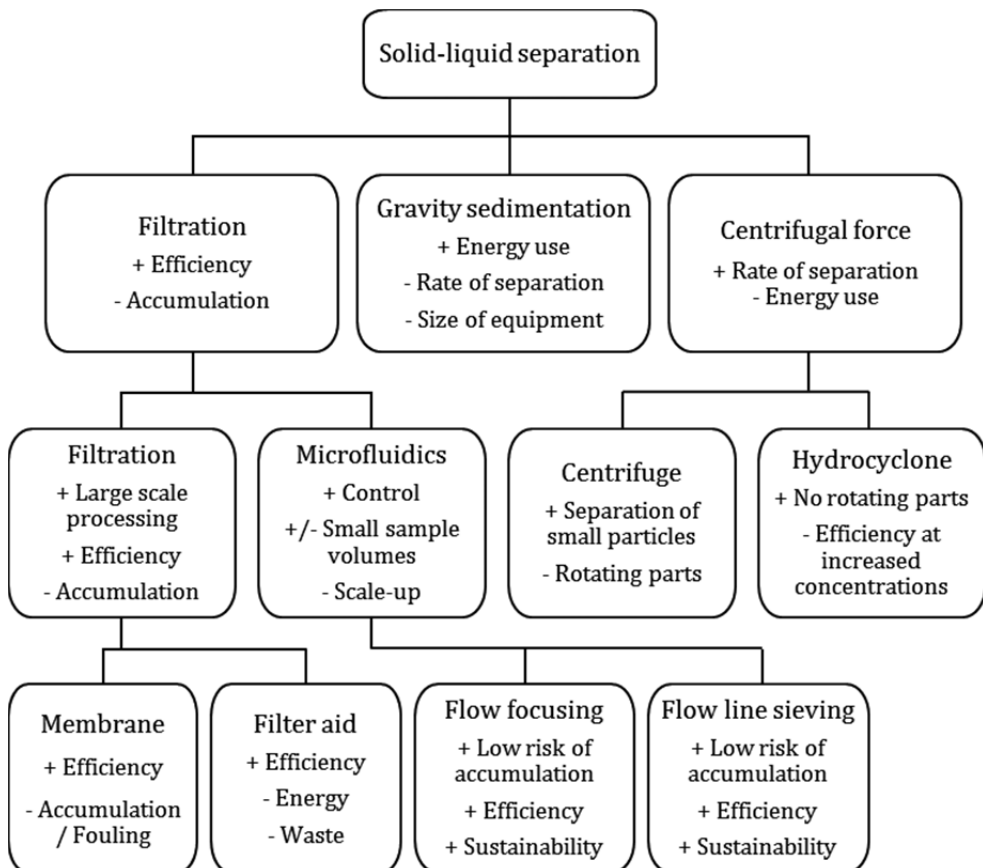
Fig. 1.1. Classification of several important solid-liquid separation processes (not exhaustive).

1.2. Deterministic ratchet technology

This thesis studies deterministic ratchet technology. Deterministic ratchets, also known as deterministic lateral displacement arrays, have been introduced by Huang *et al.* [13]. It is a continuous separation principle based on the physical displacement of particles by obstacles in a flow. Particles have a preferential direction of movement

which depends on their interaction with the obstacles. Particles below a critical size follow the streamlines through the array and move along with the fluid, in a so-called zigzag trajectory. Particles above a critical size are forced from their streamlines when they interact with an obstacle and have a migration path (displacement direction) other than the main flow direction. The critical size depends on the design of the obstacle array. Important design parameters are the gap size between adjacent obstacles, and the shift, i.e., the relative displacement of each row of obstacles.

The *gap size* is always larger than the particle to be separated to enable a particle to move through the array. The major advantage of this design criterion is indeed the lower risk of particle accumulation compared to filters with pores smaller than the particles.

The *shift* is the distance each obstacle row is shifted compared to the previous one in a direction perpendicular to the flow. It determines the displacement of a particle at each obstacle line. A schematic drawing of the separation principle is given in fig. 1.2. Since Brownian diffusion of the particles hinder the separation, deterministic ratchet technology is limited to particles with a minimum size in the order of one micrometer. An alternative for smaller particles is Brownian ratchet technology [14-16]. The design of a Brownian ratchet is comparable with a deterministic ratchet, but asymmetric obstacles are essential. If the Brownian motion of a particle is large enough, the particle diffuses in perpendicular direction to the fluid. Brownian ratchets are however outside the scope of this thesis.

Previous research was primarily aimed at understanding the flow profile and determining the critical particle size for a set of design parameters [13, 17-20].

Initially, Huang *et al.* assumed a uniform liquid flow profile in between the obstacles [13]. The width of each flow lane, and thus the critical flow lane width, $D_{f,c}$, is then equal to:

$$D_{f,c} = \frac{D_y}{N} \tag{1.1}$$

Here, D_y is the gap size between the obstacles and N equals the periodic number of the array:
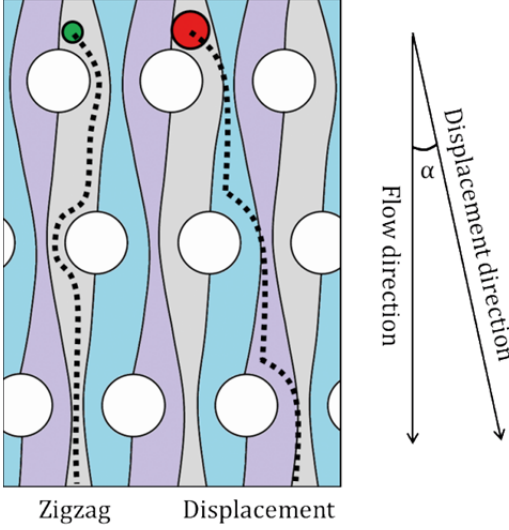
Fig. 1.2. Schematic drawing of the separation principle of deterministic ratchets. The flow is divided in flow lanes. Particles smaller than a critical size stay in one flow lane and move along with the fluid in a zigzag trajectory. Particles larger than a critical size are displaced to the adjacent flow lane at each obstacle and follow a displacement trajectory which has an angle (α) with the flow direction.

$$N = \frac{\lambda}{\Delta\lambda}$$

(1.2)

λ is the center to center distance between two adjacent obstacles on the same row and $\Delta\lambda$ is the shift. The number of flow lanes in the gap between two obstacles is equal to N. The design parameters are depicted in fig. 1.3. Based on this hypothesis, particles with a radius, $R_p < D_y / N$ will follow a zigzag path through the array and particles with $R_p > D_y / N$ will follow a displacement path.

Inglis *et al.* stated a new hypothesis, in which they assumed a conventional, symmetric parabolic flow profile through the gap [17].

$$\left[\frac{D_{f,c}}{D_y}\right]^3 - \frac{3}{2}\left[\frac{D_{f,c}}{D_y}\right]^2 + \frac{1}{2N} = 0$$

(1.3)

Each flow lane has an equal volumetric flow rate and because the flow rate is zero along the obstacle, the first and last flow lanes have the largest width and thus equal to $D_{f,c}$. Particles are displaced when $R_p > D_{f,c}$.
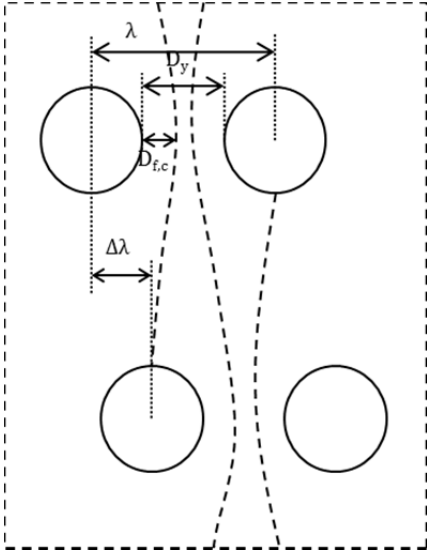
Fig. 1.3. Main design parameters of a deterministic ratchet. Flow is from top to bottom.

This flow profile was further detailed by Loutherback *et al.* who showed that the flow profile is asymmetric in an array with asymmetric, triangular, obstacles [20, 21]. The flow velocity is higher next to the triangular vertex than next to the flat side of the triangle, which results in an asymmetric flow profile. $D_{f,c}$ is smaller at the vertex side than at the flat side. $D_{f,c}$ thus depends on the flow direction. Particles with a radius in between those two values follow a zigzag path when they flow along the flat sides of the obstacles, but a displacement path when they flow along the vertex sides of the obstacles.

Kulrattanarak *et al.* found that anisotropy of the permeability of an array with symmetric obstacles also introduces asymmetry in the flow profile [18, 19]. The main flow direction and the pressure gradient are thus not aligned. A particle can follow a displacement path for more than *N* obstacle rows before it makes a zigzag motion. The last flow lane is in fact a collection of many mini flow lanes and has a width, $D_{f,N}$, larger than the first flow lane width, $D_{f,1}$, which makes the flow profile asymmetric. Similar to Loutherback, this asymmetry results in two critical particle sizes. If $R_p < D_{f,1}$ the particle has a zigzag motion, if $R_p > D_{f,N}$ it has a displacement motion and if $D_{f,1} < R_p < D_{f,N}$ it has a so-called mixed motion.

Besides on the understanding the flow profile, different papers have been published on the use of deterministic ratchets for microfluidic separations. These studies, all in the field of biomedical analysis, proved that deterministic ratchets can separate small volumes with high resolution. Examples are the fractionation of blood components and the isolation of cancer cells [22, 23]. Before deterministic ratchets can be applied on larger scale with high particle concentrations and increased flow rates, there are however several issues to investigate, such as an optimal ratchet design, finding the best hydrodynamic conditions and understanding and steering the effect of high particle concentrations. Only one research paper discussed on the treatment of larger process streams, in which the feasibility of deterministic ratchets for dewatering of microalgae for biofuel production was conceptually evaluated [24]. It was concluded that the technology would be both technically and commercially feasible when stacking numerous microfluidic deterministic ratchets.

1.3. Research objective

The main research objective of the work reported in this thesis is to understand the mechanisms relevant for deterministic ratchets to be applied at larger scales, and to develop guidelines for the design of these deterministic ratchets for suspension separation at a large-scale. High throughput separation requires increased understanding of deterministic ratchet designs and operation conditions suitable for separation at high particle concentrations and increased flow rates. Deterministic ratchet modules were thus constructed that allowed simple and quick experimentation for multiple deterministic ratchet designs. Experiments were carried out with model suspensions comprising particles with diameter of 100 μm or larger.

1.4. Outline

Chapter 2 describes the design of an up-scaled module to simplify the investigation of deterministic ratchets for large-scale application. The up-scaled module, in which all features of a microfluidic device were enlarged in size, was used to study the effect of

obstacle design, high flow rate and high particle concentrations on the separation efficiency. The results indicate a strong dependency of the separation efficiency on the local hydrodynamics in the deterministic ratchet, which has not been reported before.

Chapter 3 elaborates on the results of chapter 2 and presents the results of high speed camera visualization of fluid flow in the up-scaled module and corresponding computational fluid dynamic simulations. The high speed camera images give insight in the influence of flow rate on local hydrodynamics and these results are confirmed by the simulations. Moreover, the change in hydrodynamics could be coupled to increased separation efficiency at high flow rates.

Chapter 4 introduces a new deterministic ratchet design making use of mirrored obstacle arrays that allows more efficient concentration. Additionally, a second and smaller up-scaled module was developed to investigate the effect of the length scale of the design, while maintaining high flow rates and high particle concentrations. Different mirrored designs in both modules were extensively evaluated for their separation efficiency of mono- and bidisperse mixtures of particles.

Chapter 5 describes the development of sparse deterministic ratchets as simplified designs suitable for large-scale application. A theoretical analysis provides insight on how particle retention is influenced by the particle volume fraction along obstacle lines and how a maximum particle volume fraction that can be separated is coupled to the number of obstacle lines. Experimental results, including high speed camera images confirm these analysis data. Computational fluid dynamic simulations were carried out to map the flow distribution in the device.

Chapter 6 provides a general discussion and gives an outlook on the future perspective of deterministic ratchets. Furthermore, some preliminary results are presented of the development of a new separation system employing metallic microsieves to mimic deterministic ratchet obstacle arrays. This new system would allow further up-scaling of deterministic ratchet technology also allowing separation of particle suspensions with particles smaller than 100 μm.
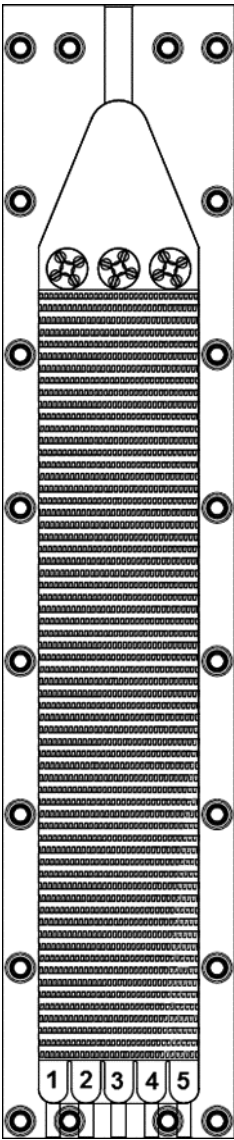
Schematic drawing of the deterministic ratchet device.

2. Suspension separation with deterministic ratchets at moderate Reynolds numbers

2.1. Abstract

Deterministic ratchets were evaluated in this study as continuous separation devices for suspensions. Compared to conventional microfluidic ratchets (gap width ≈ 10 µm), ratchet designs in this study were 70 times larger. Apart from the hydrodynamic regime (2 < Re < 34 versus Re < 1) no other changes were introduced. Three deterministic ratchet designs were constructed and evaluated for their separation efficiency with polystyrene particles having sizes between 309 and 532 µm. The separation efficiency was defined as the ratio between the highest and the lowest outlet concentration.

The separation efficiency increased with increasing flow rate from a ratio of 1 (Re = 2) at the lowest flow rates up to a ratio of 47 at the highest flow rates (Re = 18). An explanation for this strong dependence on flow rate may be the presence of inertial lift forces and a pair of vortices behind the obstacles (typically for Re > 1), which lead to additional displacement. Furthermore, there was a maximum concentration of particles in the device above which the separation decreased, e.g. 12 v/v% for a design with cylindrical-shaped obstacles. The high suspension concentrations did not lead to blockage of the device and were much higher compared to concentrations normally achieved for membrane separations.

The up-scaled deterministic ratchets show potential for fractionation. Particles above a critical particle size were better separated than particles below that critical particle size.

2.2. Introduction

A deterministic ratchet is a particle separation device that uses the fluid flow distribution through periodic arrays of obstacles to separate and fractionate

suspended particles based on their size. Deterministic ratchets have been explored as microfluidic devices for analytic separation of biomedical suspensions mainly [22, 25-31]. Recently, also the potential for fractionation of food suspensions was suggested [12].

Although microfluidic deterministic ratchets have demonstrated their potential, the application of this separation technique to larger liquid volumes is not straightforward. Therefore, 70x up-scaled deterministic ratchets were designed and constructed in this study. An up-scaled device has several advantages; easier operation in continuous mode, larger volumes of samples collected, easier visual system observation and less influence of small disturbances. This speeds up the research process. Despite the mentioned advantages of an up-scaled system, all studies with deterministic ratchets have been carried out with microfluidic ratchets, excluding the study of Balvin [32]. In this study the motion of single stainless steel balls through an array of obstacles (LEGO® pegs) was investigated. Instead of focusing on single particle motion we here look to the separation efficiency of the whole system with a substantial volume fraction of particles.

In this paper we report about separation and fractionation experiments of concentrated model suspensions with three different 70x up-scaled ratchet systems. The different ratchet designs were evaluated for their separation and fractionation efficiencies as a function of various operating conditions.

2.2.1.   Theory

In deterministic ratchets the fluid flow is split up between the obstacles and forced through the gaps, which can be visualized with fluid streams or lanes, separated by streamlines [13]. Under laminar flow conditions particles are thought to follow the streamlines. However, a slightly tilted obstacle arrangement gives particles above a critical size a slight off-set from each streamline at each row of obstacles, which after several rows gives a microscopic displacement of particles. The off-set, $\Delta\lambda$, is called shift and is a fraction of the distance between the centers of the obstacles, λ. The ratio $N = \lambda/\Delta\lambda$ indicates the number of obstacle rows in one periodic cell. Depending on the ratio between flow lane width and particle size, the particle will follow a certain

migration path. Two different types of migration paths are identified, viz. zigzag and displacement.

Huang and Inglis assumed that the fluid through the gaps would follow a parabolic flow profile [13, 17]. By using triangular obstacles instead of circular obstacles Loutherback found out that the flow profile is asymmetric [21]. Later on he described the effect of vertex rounding and obstacle shape in more detail [20]. More recently, it became clear that anisotropy of the permeability of the obstacle array also introduces asymmetry in the flow profile [18, 19]. An asymmetric fluid flow profile, results in a third type of particle migration, mixed motion that could not be explained by the parabolic flow theory, but may be essential in calculating the appropriate critical diameter. The third type of trajectory was also noticed by Quek [33].

The hydrodynamic conditions of suspension flow through a ratchet device can be characterized by two Reynolds numbers: the channel Reynolds number (Re_c) and the particle Reynolds number (Re_p). Re_c describes the hydrodynamic conditions of the fluid and is defined as the ratio of inertial force to viscous force (Eq. 2.1) and Re_p describes the effect of Re_c on a particle and is defined as Re_c multiplied by a factor that takes into account the particle diameter (Eq. 2.2) [10, 34].

$$Re_c = \frac{U_m D_y}{\nu} \tag{2.1}$$

$$Re_p = Re_c \frac{d^2}{D_y{}^2} = \frac{U_m d^2}{\nu D_y} \tag{2.2}$$

Here, U_m [m/s] is the maximum fluid velocity (for the ratchets in this study the average fluid velocity in the gap between two obstacles is taken), D_y [m] is the gap width between two obstacles, ν [m²/s] is the kinematic viscosity of the fluid, d [m] is the average particle diameter. The critical flow lane width is the determining factor for separation with deterministic ratchets. For the definition of the flow lanes only the fluid flow is considered. Therefore we use Re_c to describe the hydrodynamic conditions in our up-scaled device. Typically, for microfluidic ratchets viscous forces dominate the particle flow; Re_c << 1, resulting in Stokes flow. From this point onwards $Re_c = Re$, unless mentioned otherwise. For Re << 1, as long as the flows are truly laminar (*i.e.* Stokes flow), the streams in each flow lane do not cross or mix [13].

2.3.Materials and methods

2.3.1. Chemicals

The separation experiments are done with model suspensions. We used spherical, polystyrene particles with a density of 1.05 g/ml (Maxiblast, USA). Two types of particles were used; small and large particles. The small particles had a diameter between 209 (d_{10}) and 277 μm (d_{90}), with a d_{50} of 234 μm; the large particles had a diameter between 309 (d_{10}) and 532 μm (d_{90}), with a d_{50} of 441 μm. Separation experiments were carried out with the large particles only. For the fractionation experiments a mixture of both types of particles was prepared. In the first and third set of experiments a 20 v/v% glycerol, 1.5 w/v% sodium dodecyl sulfate (SDS) solution is used as liquid. Glycerol (Boom chemicals, The Netherlands) was added to demi-water to match the density of the particles (1.05 g/ml). SDS (J.T. Baker, Boom chemicals, The Netherlands) was added as surfactant to avoid any undesired particle agglomeration. In the second set of experiments polyethylene glycol 400 (PEG-400, Merck, The Netherlands) was added in different amounts to demi-water to obtain viscosities of 164 and 220 mPa·s, respectively [35].

Particle size analyses were carried out by optical measurements (Eyetech, Ankersmid Lab, Netherlands). In this method a LED produces a white area on a video lens. If a particle comes in this area, it blocks the light from reaching the video lens, producing a black spot on the detector. The area of this black spot is measured, from which many other parameters are calculated. The diameter is used to describe the particle sizes in this report.

2.3.2. Design and construction of the ratchet devices

Three different ratchets were designed (fig. 2.1). Design parameters are given in table 2.1 and indicated in fig. 2.1. Ratchet designs 1 and 2 had 64 obstacles rows (N_{rows} = 64) with on average 32 quadrilateral-shaped obstacles on each row; ratchet design 3 had 120 obstacles rows (N_{rows} = 120) with on average 36 cylindrically shaped obstacles on each row. The obstacle pattern of design 2 was mirrored around the central axis. The

obstacles around this central axis had a slightly different shape and size as can be seen in fig. 2.1. The obstacles of all the three designs had a height of 2.5 mm and were created by a milling machine. The material used for the ratchets is polyether ether ketone (PEEK). The designs allow us to differentiate between obstacle shapes, non-symmetric (designs 1 and 2) and symmetric (design 3).
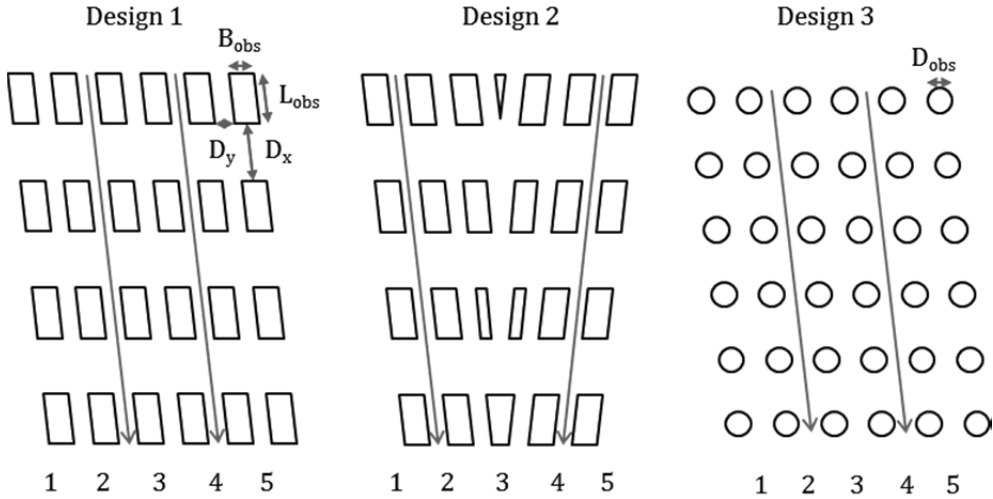
Fig. 2.1. A small part of the ratchet designs. Geometrical parameters are indicated with their symbols. In design 2 obstacles around the central axis are given to show the different obstacle shapes and sizes. The numbers 1-5 indicate the outlet numbering. The arrows indicate the particle trajectories.

Tabel 2.1. Geometry data of the devices is given in this table. N is the number of obstacle rows in one periodic cell, D_x is the gap width between the obstacles in the flow direction, D_y is the gap width between the obstacles perpendicular to the flow, B_{obs} and L_{obs} are the width and length of the quadrilateral-shaped obstacles, D_{obs} is the diameter of the cylindrical-shaped obstacles, λ is the distance between the centers of the obstacles, Δλ is the shift and is calculated as the ratio Δλ = λ/N.

	N	D_x	D_y	B_{obs}	L_{obs}	D_{obs}	λ	Δλ
	[-]	[mm]	[mm]	[mm]	[mm]	[mm]	[mm]	[mm]
Design 1	4	1.80	0.60	0.80	1.60	n/a	1.40	0.35
Design 2	4	1.80	0.60	0.80	1.60	n/a	1.40	0.35
Design 3	6	1.13	0.56	n/a	n/a	0.68	1.24	0.21

The ratchet was placed in a module with a stainless steel body and covered with a transparent polymethyl methacrylate (PMMA) lid for visual inspection. The module consists of one inlet channel and five outlet channels. In fig. 2.2 a picture of the module is shown. Three magnetic stirrers just before the ratchet assisted in achieving an even distribution of particles across the ratchet. In the experiments the module was operated in a vertical position; suspension flow was from top to bottom. The outlets were connected via a small tube to different sample vessels.

In the current study the calculation of the critical particle diameter is based on the work of Kulrattanarak [19] as the ratchet designs in this study were similar in geometry. The only major difference was the scale of the designs which was approximately 70 times larger. The increased dimensions lead to different hydrodynamic conditions ($Re > 1$), when compared to the regular Stokes flow regime for microfluidic devices. The different conditions are expected to go along with the formation of secondary flow structures, i.e. steady vortices, behind the obstacles, which may affect migration trajectories of the particles.
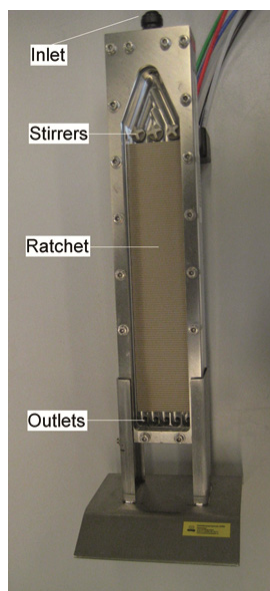

Fig.2.2. Ratchet module.

2.3.3. Experiments

In deterministic ratchets the fluid is expected to move freely through the obstacles. Because of the open structure the fluid is expected not to be influenced by the ratchet design. For our set-up with five outlets it is expected that 20% of the fluid ends up in each outlet. To confirm this hypothesis the five outlet flows of ratchet designs 1 and 3 were measured. A solution of demi-water with 20 v/v% glycerol and 1.5 w/v% sodium dodecyl sulfate (SDS) was pumped through the ratchets at a flow rate of 80 ml/min. As a control the same experiment was done without a ratchet in the module. The outlet fractions were collected and the volumes determined. The experiments were repeated twice.

In the first set of experiments the up-scaled deterministic ratchet designs were evaluated for their separation efficiency as a function of design, flow rate and inlet concentration. The separation efficiency, ε, was defined as the ratio between the highest outlet concentration and the lowest outlet concentration. The deterministic ratchets were fed with suspensions (20 v/v% glycerol, 1.5 w/v% SDS) at flow rates between 20 (Re = 2) and 150 ml/min (Re = 18) and particles of 309-532 μm at concentrations of 2.78 v/v% and 3.67 v/v%. Five outlet fractions were collected and particle concentrations were determined.

In the second set of experiments ratchet design 3 was fed with suspensions at flow rates 150 ml/min and 200 ml/min and particles of 309-532 μm at a concentration of 2.78 v/v%. PEG-400 was added to the suspension at mass fractions 0.58 for the experiment at 150 ml/min and 0.63 for the experiment at 200 ml/min. Under these conditions the Reynolds number of the flow was kept constant at Re = 2. Again the five outlet fractions were collected and particle concentrations and separation efficiencies were determined.

In the third set of experiments the upper limits for flow rate and particle concentration were determined. The parameter combination that gave the highest separation efficiency was investigated. Suspensions (20 v/v% glycerol, 1.5 w/v% SDS) with particles of 309-532 μm at concentrations up to 8.70 v/v% were fed to ratchet device 3 at flow rates between 50 (Re = 6) and 275 ml/min (Re = 34).

In the fourth and last set of experiments the fractionation behavior was investigated. A suspension (20 v/v% glycerol, 1.5 w/v% SDS) with equal number of particles of 209-277 μm and 309-532 μm at a total concentration of 2.78 v/v% was fed to ratchet device 2 at flow rates 20, 80 and 150 ml/min. The particle concentrations, fractionation efficiencies and the particle size distributions were determined.

2.4. Results and discussion

2.4.1. Fluid flow distribution

The results of the fluid flow distribution measurements are given in fig. 2.3. The lowest measured volume was 16.5% and the highest measured volume was 25.5%, with a maximum standard deviation of 2%. These variations in fluid flow could be completely attributed to flow resistances in the outlet tubing, which was checked by exchanging the tubes connected to the five outlets. Therefore, it can be concluded that the fluid flow was not significantly influenced by the design.
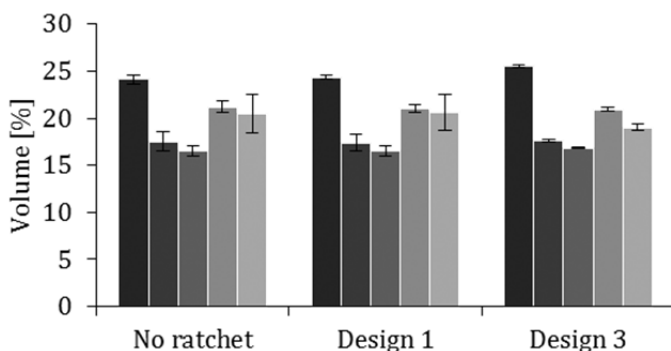

Fig. 2.3. Fluid flow distribution over outlet 1 (dark grey) to outlet 5 (light grey).The average volume is 20%.

2.4.2. Separation of particles from fluid

In calculating the maximum (theoretical) separation efficiency, ε_{max}, the critical particle size for displacement, $D_{p,c}$, the particle size distribution of the suspension as

well as the ratchet geometry is important. $D_{p,c}$ is twice the largest flow lane width, $D_{f,c}$. Values for $D_{f,c}$ are estimated from the paper of Kulrattanarak (figures 5 and 6) [19], assuming that these values also apply for $Re > 1$ and different obstacle shapes. For design 1 and 2 $D_{p,c} = 400$ µm, for design 3 $D_{p,c} = 330$ µm. Approximately 0% and 29% of the particles in the suspension were less than 330 and 400 µm, respectively. For designs 1 and 2 the maximum distance that a particle may be displaced is 22.4 mm (= $\Delta\lambda \cdot N_{rows}$), for design 3 this distance is 24.8 mm. Based on $D_{p,c}$ and the maximum displacement values the estimated particle concentrations in the different outlets and ε_{max} are calculated (table 2.2).

Tabel 2.2. Estimated particle concentrations in the different outlets. Values are given as percentage of the total number (100%) of particles present. The estimated maximum separation efficiency, ε_{max}, is the ratio of the highest value and lowest value of the design.

	Outlet 1	Outlet 2	Outlet 3	Outlet 4	Outlet 5	ε_{max} [-]
Design 1	5.7	5.7	12.9	20.0	55.7	9.8
Design 2	5.7	5.7	77.1	5.7	5.7	13.5
Design 3	0.0	0.0	4.8	20.0	75.2	∞

The results of the separation experiments are shown in fig. 2.4. The flow rate is found to have a large influence on the results. At low flow rates below 20 ml/min ($Re = 2$) the particle concentrations in the outlets are quite similar and the separation efficiency is small. The separation efficiencies under the latter conditions are less than expected from theory (table 2.2). This may be explained from interaction between particles, which cause particles to move more randomly rather than following a displacement trajectory. The ratchet displacement theory is based on displacement without any hindrance from neighboring particles. Commonly, in microfluidic experiments very dilute suspensions are applied, so more ideal displacement behavior is expected. With increasing flow rates it is found that the separation efficiency increases. It is expected that other forces than particle-particle interactions become dominating at increased flow rates.
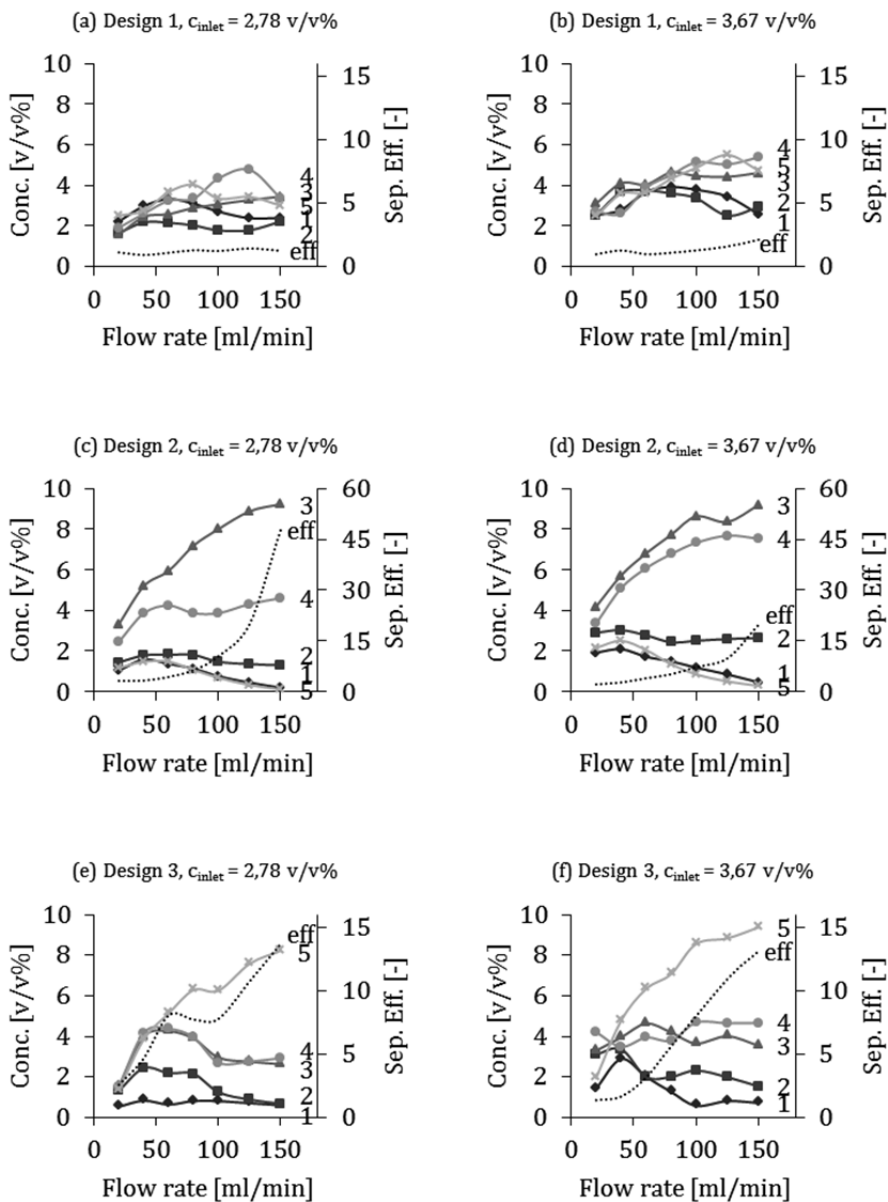
Fig. 2.4. Concentration of outlet fractions of design 1 (fig a and b), design 2 (fig c and d) and design 3 (fig e and f) as function of the flow rate. Symbols: diamonds = outlet 1, squares = outlet 2, triangles = outlet 3, circles = outlet 4, crosses = outlet 5. The separation efficiency of outlet 5 is plotted as a dotted line. All lines are drawn to guide the eye. The inlet concentrations are 2.78 v/v% (left) and 3.67 v/v% (right).

The geometric parameters of design 1 are the same for design 2, except for the mirrored structure. However in design 2 much higher separation efficiencies are obtained: $\varepsilon > \varepsilon_{max}$. The particle concentrations in the outer outlets 1 and 5 decreased to almost 0 at a flow rate of 150 ml/min (Re = 18). The obtained separation efficiencies in design 3 are higher than for design 1, although not all particles are directed to outlet 5, ε = 14. Also for design 3 the separation efficiency strongly depends on the flow rate. Such strong dependence of separation efficiency on flow rate has not been reported before for deterministic micro-engineered ratchets. Evidently, the theory that only particles with size larger than $D_{p,c}$ are displaced does not apply in this situation. Also particles smaller than $D_{p,c}$ are following a displacement path.

The explanation for the improved separation at high flow rates is most probably related to the fluid dynamics. Microfluidic devices are operated at conditions $Re << 1$, while in our experiments $2 < Re < 18$. At $Re > 1$ inertial forces become more dominant than the viscous forces. Studies to flow behavior around cylindrical structures at increased Reynolds numbers ($Re > 1$) have reported the occurrence of symmetric vortices behind cylinders [36, 37]. These vortices change the streamline profile and exert a shear-gradient induced lift force, pushing the particles away from the vortex to the adjacent flow lane. This leads to an additional displacement, dependent on the magnitude of the shear gradient. With increasing flow rate the vortex increases in size and the shear-gradient intensifies. A larger vortex narrows the gap between two subsequent obstacle rows and thus could hinder particles from following a zigzag trajectory. A similar phenomenon is observed during continuous focusing of particles when using secondary rotational flows to induce lateral migration forces in multi-orifice channels [34].

The effect of fluid flow on a particle is characterized by Re_p. Because in our experiments $Re_p > 1$, the influence of both viscous and inertial forces on a particle should be considered. Viscous drag forces cause particles following streamlines, while inertial lift forces cause particles crossing streamlines. Di Carlo described the inertial effects in a quantitative way [38]. There are two lift forces; shear gradient lift and wall lift. The shear gradient lift, F_{LS}, is directed down the shear gradient and pushes

particles from the center of the channel to the wall and can be described by Eq. 2.3. The wall lift, F_{LW}, is directed away from the wall and can be described by Eq. 2.4.

$$F_{LS} = \frac{f_L \rho U_m{}^2 d^3}{D_y} \tag{2.3}$$

$$F_{LW} = \frac{f_L \rho U_m{}^2 d^6}{D_y{}^4} \tag{2.4}$$

Here, f_L [-] is a dimensionless lift coefficient, ρ [kg/m³] is the fluid density, U_m [m/s] is the maximum fluid velocity, d [m] is the average particle diameter, D_y [m] is the channel width. Particles experiencing these forces will cross streamlines and find an equilibrium position in the channel. To reach this equilibrium position a minimum channel length and flow rate is required. The channel length is equal to the length of a single obstacle. The flow rate, Q, required for focusing to equilibrium positions for an obstacle with length L and height H is also described by Di Carlo (Eq. 2.5) and is 700 ml/min for our devices [38].

$$Q \approx \frac{2\pi \mu D_y H^3}{3\rho L d^2 f_L} \tag{2.5}$$

In our experiments the maximum flow rate is 150 ml/min and thus particles do not find the equilibrium position. However, during their migration to the equilibrium position particles may cross streamlines, leading to additional displacement.

In the second set of experiments it was investigated whether the observed separation efficiencies are indeed caused by the different hydrodynamics leading to different displacement behavior. In these experiments the viscosity was increased by adding PEG-400 to the water, while the flow rate was varied such that the Reynolds number was constant. The separation efficiency was low at Re = 2 for all flow rates of 20 (ε = 1), 150 (ε = 1.8), and 200 ml/min (ε = 1.5), while the separation efficiencies for the 150 and 200 ml/min experiments were low compared to the earlier experiments. Indeed, the hydrodynamic regime as indicated by the Reynolds number is therefore crucial in the increased separation efficiency.

Another factor that may affect separation efficiency is the concentration of the suspended particles. Outlet concentrations of up to 9 v/v% were observed, which did not lead to problems such as particle blockage. One might expect that at a maximum concentration exists at which the number of particles is simply too high and thus

blockage occurs. However, from the results it appears that particles will distribute themselves across more outlets, leading to a decrease in separation efficiency. Fig. 2.5 shows the results of an experiment in which the maximum concentration is determined without particle accumulation and the separation efficiency is still reasonably high. For an inlet concentration of 5.41 v/v%, outlet concentrations of 12 %v/v were obtained with ε = 20. Other attempts were done with inlet concentrations up to 10 v/v%. However, in these cases the maximum separation efficiency decreased significantly.
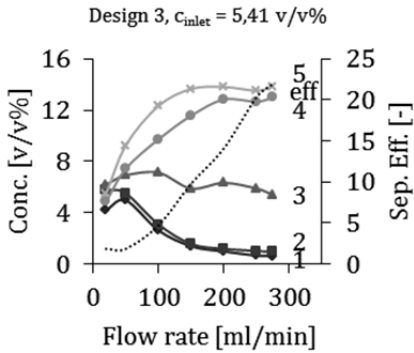

Fig. 2.5. Concentration of outlet fractions of design 3 as function of the flow rate. Symbols: diamonds = outlet 1, squares = outlet 2, triangles = outlet 3, circles = outlet 4, crosses = outlet 5. The separation efficiency of outlet 5 is plotted as a dotted line. All lines are drawn to guide the eye. The inlet concentration is 5.41 v/v%.

2.4.3. Fractionation of particles on size

In paragraph 2.4.2 we noticed that also particles smaller than $D_{p,c}$ are following a displacement path. The hydrodynamic regime is assumed to be a main reason. A second explanation might be that small particles are carried along with large particles. However, if small particles are carried along with large particles the fractionation efficiency (mutual separation between the particles) will actually decrease. Fractionation on particle size was evaluated by introducing bidisperse suspensions (2.78 v/v%, prepared from an equal mixture of small and large particles) into ratchet design 2. The particle size distribution of the feed suspension (inlet) is shown in fig. 2.6.
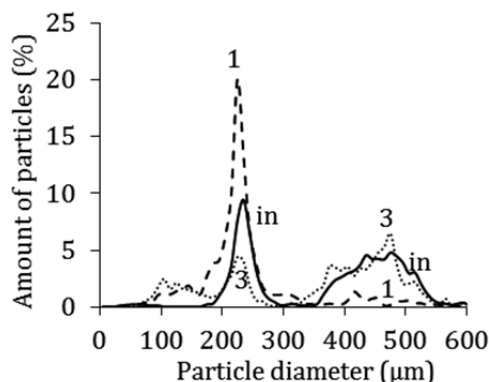
Fig. 2.6. Particle size distributions (number based) of inlet stream (solid line) and outlet fractions 1 (dashed line) and 3 (dotted line) of design 2 (quadrilateral-shaped obstacles mirrored around central axis) operated at 150 ml/min. The inlet concentration is 2.78 v/v%.

The feed consists as expected of approximately the same amount of small particles as large particles. During the experiments the flow rate was varied and the resulting particle size distribution of the collected suspensions at the different outlets was determined. In fig. 2.6 the results are shown for fractionation at a flow rate of 150 ml/min (Re = 18). Outlet 1 consists of mainly small particles; d_{50} = 242 μm, while outlet 3 consists of large particles and a smaller amount of small particles; d_{50} = 456 μm.

Table 2.3 shows the percentages of smaller (< 310 μm) and larger particles (> 310 μm) that end up in the five outlets for three different flow rates. With increasing flow rates, the percentage of large particles that is present in the central outlet 3 increases. Assuming that the small particles would indeed not be affected by the ratchet, each outlet would contain approximately 20% of small particles. This is apparently not the case. Outlets with a high percentage of large particles also have a relative higher percentage of smaller particles. From these data it can be concluded that even particles that are much smaller than the critical particle size are displaced in the ratchet, which might be induced by the presence of the larger ones. In spite of this, small and large particles can be well fractionated at increasing flow rates.

Table 2.3. Percentage of small (N_s) and large particles (N_l) that leave the device at a specific outlet for three different flow rates. Results are shown only for ratchet design 2.

	Outlet 1		Outlet 2		Outlet 3		Outlet 4		Outlet 5	
Q	N_s	N_l	N_s	N_l	N_s	N_l	N_s	N_l	N_s	N_l
[ml/min]	[%]	[%]	[%]	[%]	[%]	[%]	[%]	[%]	[%]	[%]
20	6.2	10.3	6.7	14.5	53.9	34.3	20.8	29.4	12.5	11.5
80	14.0	9.8	7.4	13.6	23.7	40.4	18.2	26.0	36.7	10.2
150	22.2	2.3	7.5	7.5	36.3	55.0	9.2	33.6	24.8	1.5

2.5. Conclusions

We investigated the separation and fractionation of concentrated suspensions with 70x up-scaled deterministic ratchet systems. Three different ratchet designs were evaluated for their separation efficiencies as a function of design and operating conditions. The separation efficiency is strongly dependent on the flow rate; it increased with increasing flow rate from a ratio of 1 (Re = 2) at the lowest flow rates, to a ratio of 47 at the highest flow rates (Re = 18). The highest efficiency value was obtained with a design with quadrilateral-shaped obstacles which were mirrored around the central axis. Such strong dependence of separation efficiency on flow rate has not been reported before for deterministic ratchets.

A possible explanation for this observation is found in the presence of symmetric vortices behind the obstacles (typically for Re_c > 1) and shear-induced lift forces (typically for Re_p > 1), affecting particle displacement and thus separation. The influence of hydrodynamic conditions on separation efficiency was confirmed by using liquids with increasing viscosity and applying higher flow rates. Comparable separation behavior was observed when operating at similar Reynolds numbers, but different flow rates.

The devices showed very high separation efficiencies with inlet particle concentrations of up to 5.41 v/v% particles, leading to 12 v/v% particles in the concentrated outlets, with a separation efficiency ratio of 20. The high suspension concentrations did not lead to blockage of the device and were much higher compared

to concentrations normally achieved for membrane separations. Higher inlet concentrations led to lower separation efficiencies.

The ratchet with quadrilateral-shaped obstacles mirrored around the central axis was also evaluated for its fractionation. It was found that fractionation of small and large particles improved with increasing flow rates. At the highest flow rate, it was found that 55% of the large particles left the device at outlet 3.

The large separation and fractionation efficiencies and tolerance for high suspension concentrations found in this study may open up ways for efficient separation processes, not only for analytical purposes, but also for larger-scale, preparative applications. If one would apply the same hydrodynamic conditions of the described up-scaled ratchets to microfluidic devices the pressure drop will become an important issue as well as the effect of high fluid velocities on the particle properties.

2.6.Acknowledgements

Visualization of inertial flow in deterministic ratchets
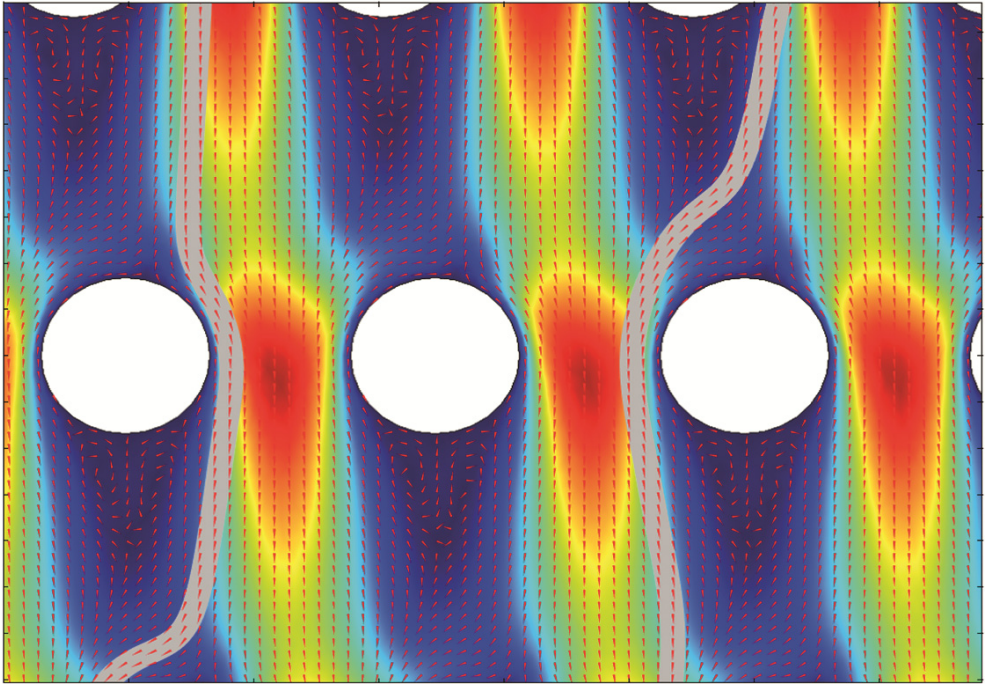
2D flow field simulation of water flowing around obstacles in a deterministic ratchet.

3. Visualization of inertial flow in deterministic ratchets

3.1. Abstract

Recently it was found that at moderate Reynolds numbers, $Re > 1$, the displacement behavior of suspended particles in deterministic ratchets changes with increasing flow rates, resulting in superior separation at higher flow rates. This change was attributed to the inertial flow regime where the flow pattern strongly depends on Re. The objective of this study was to visualize the fluid streamlines of inertial flow in deterministic ratchets, using 2D flow field simulations and high speed camera images. Analysis of the flow field revealed two effects contributing to improved separation efficiency in the inertial flow regime. The first effect is the formation of vortices, which was observed from both simulations and experiments for two ratchet designs at increased flow rates. For cylindrical-shaped obstacles a pair of vortices developed at $Re = 9$ and grew to 70% of the gap size between two consecutive obstacle rows at $Re = 30$. For quadrilateral-shaped obstacles these values are $Re = 2$ and 75% at $Re = 26$. The supposed effect of vortex formation on particle movement is preventing the 'zigzag' motion of particles by narrowing the gap between two consecutive obstacle rows. The second effect is an increase of the number of flow lanes at higher Re. This is explained by the asymmetry of the fluid velocity profile in the gaps, caused by the anisotropy of the obstacle arrays in combination with the development of vortices. The increase in number of flow lanes reduced the critical particle size for displacement by 14% and 24%. This gives opportunities for new designs with larger gap sizes, which reduces the chance for clogging and lowers the pressure drop.

The observations underline that anisotropy or asymmetry of the obstacles and the flow regime are both important parameters for the separation efficiency of deterministic ratchets.

Chapter
3

3.2. Introduction

Deterministic ratchets, also called lateral displacement or bump arrays, are microfluidic devices used to separate particles according to their size. Examples are the separation of chromosomes [13], blood components [22], parasites [26] and leukocytes [28]. The separation principle (fig. 3.1) makes use of Stokes flow through a periodic array of obstacles, where each obstacle row is shifted by a distance $\Delta\lambda$ compared to the previous row. The fluid in the gap between two obstacles may be split up into N number of imaginary flow lanes, equal to the number of obstacle rows in one periodic cell. Particles with a radius larger than the critical flow lane width, $D_{f,c}$, cross dividing streamlines and are displaced by $\Delta\lambda$ at each obstacle row. These particles follow a displacement path that makes an angle, α, to the main flow direction. Particles with a radius smaller than $D_{f,c}$ move in the main flow direction by following the streamlines of the fluid. These particles follow a so-called zigzag path.
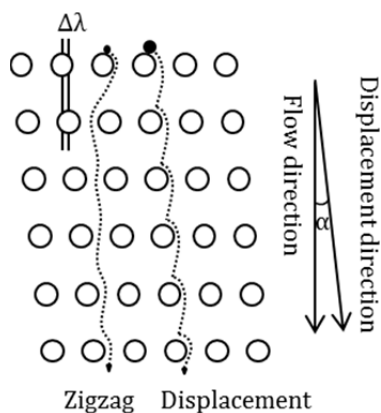
Fig. 3.1. Separation principle.

Deterministic ratchets have proven to be successful in the analytical research field, because of the high selectivity, short separation time and low sample volumes. Additionally, deterministic ratchets are considered promising with respect to separation and fractionation of concentrated suspensions at larger, preparative or even industrial scale, for example in the food industry [12], waste water treatment [39] or dewatering of algae [24]. Microfluidic deterministic ratchets are normally

operated in the Stokes flow regime, $Re \ll 1$, where Re is the fluid Reynolds number and is defined as $Re = Ud/\nu$, with U the average flow velocity, d the specific length scale, which equals the gap width between two neighboring obstacles D_y, and ν the kinematic fluid viscosity. Recently, up-scaled deterministic ratchets have been investigated [40]. These up-scaled ratchets have the advantage that their operation in continuous mode is easier. These ratchets were operated in the inertial flow regime, $Re > 1$. In our previous study it appeared that under the applied hydrodynamic conditions displacement behavior of suspended particles and thus separation efficiency was enhanced with increasing Reynolds numbers [40].

The objective of this work is to investigate and understand the underlying separation mechanism at inertial flow conditions by visualization and modeling of the fluid flow patterns in the up-scaled deterministic ratchets. This paper reports on 2D simulations visualizing the flow field under inertial conditions and experimental flow observations using high speed camera techniques.

Several studies have made extensive analysis of flow fields in deterministic ratchets. Deterministic ratchet technology was first developed by Huang *et al.* [13]. They showed that particle displacement could be predicted reasonably well with a parabolic flow profile in the gap between obstacles. Inglis *et al.* described this parabolic flow model in detail, predicting how the critical particle size depends on the ratchet geometry [17]. More recent work showed that asymmetry in obstacle shape [20, 21] and anisotropy in the permeability of the obstacle array [18, 19] creates asymmetry in the flow profile and changes the critical particle size calculated with the parabolic flow model. These studies provide the underlying mechanisms of particle separation, but all these theories are only valid for low Reynolds number (Stokes) flow.

The flow profile at Re > 1 is more difficult to describe, since inertial effects start to dominate the viscous forces. A vortex street or vortex shedding is a well-known phenomenon, creating a repeating pattern of swirling vortices behind an object. It is caused by unsteady fluid flow and typically observed for $Re > 40$ [37]. In deterministic ratchets the obstacles are quite densely packed and a longer vortex street cannot be created [36]. Instead a single pair of vortices is likely to be formed, which is present at

5 < Re < 40 [37]. These vortices could be a reason for the separation behavior at moderate Reynolds numbers as we described recently [40]. Therefore it is important to visualize the vortex development in deterministic ratchets to determine the underlying effect on the separation efficiency. The obstacle shape is just like the Reynolds number a factor in vortex development. Asymmetric obstacles and sharp obstacle edges are expected to create larger vortices than symmetric and streamlined obstacles at similar Re. Another inertial effect besides vortices is the migration of particles to other flow lanes under influence of inertial lift forces [38].

3.3.Materials and Methods

3.3.1.   2D simulation of inertial flow in deterministic ratchets

Two-dimensional geometries with cylindrical-shaped and quadrilateral-shaped obstacles were implemented in COMSOL multiphysics 4.2a to simulate flow through these designs. The designs and geometric parameters are given in fig. 3.2. Cylindrical-shaped obstacles had a diameter D = 675 μm, a gap between obstacles D_y = 563 μm, a gap between obstacle rows $D_x = 2D_y$ and a row shift $\Delta\lambda$ = 206 μm. Quadrilateral-shaped obstacles had a width W = 800 μm, a length L = 1600 μm, D_y = 600 μm, $D_x = 3D_y$ and $\Delta\lambda$ = 350 μm. These geometries are identical to the devices used in our previous work [40]. In the simulation design 1 counted 15 rows of 24 obstacles and design 2 counted 15 rows of 29 obstacles. These numbers are chosen to reduce the influence of the outer walls on the flow. For the models an extra fine mesh was selected with a maximum element size of 0.0975 mm and for all the boundaries no-slip conditions were applied. The fluid was assumed to be incompressible with the properties of water: density ρ = 1000 kgm^{-3} and viscosity η = 0.001 kgm^{-1}s^{-1}. The fluid velocity at the entire inlet was assumed to be constant; the fluid velocity at the outlet was based on the pressure drop. Laminar flow conditions were set to all the simulations. The simulations were carried out at inlet fluid velocities of 0.003-0.042 m/s, corresponding to 2 < Re < 34. The output of the simulations is a flow velocity field with streamlines visualizing the flow direction.
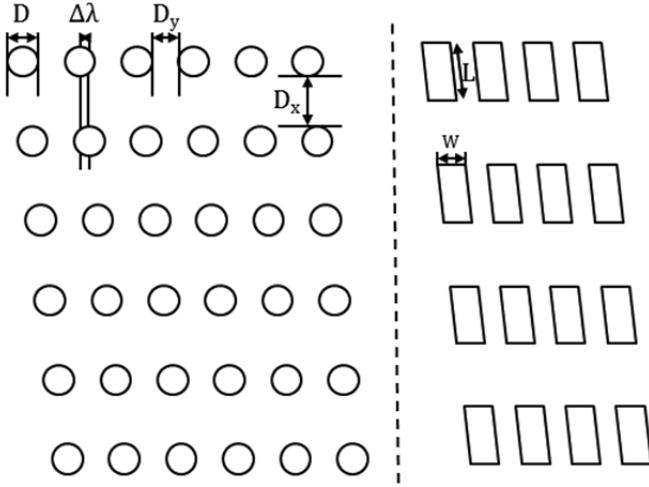
Fig. 3.2. Detailed view of the two deterministic ratchet geometries used; left: design 1 with cylindrical-shaped obstacles and right: design 2 with quadrilateral-shaped obstacles.

3.3.2. Experimental observations of inertial flow in deterministic ratchets

For the flow observations we used the up-scaled deterministic set-up and two ratchet designs as described in our previous work [40]. The particle movements were observed and recorded with a high speed camera (Photron SA 1.1), which was equipped with a long distance lens (Navitar). Images were recorded at frame rates between 250 and 1000 fps and shutter exposure times between 100 and 1500 μs. Suspensions were made of demineralized water and polyethylene particles of 90-104 μm which were wetted with a few drops of surfactant Tween-80. These particles are below the critical particle size for separation, and therefore it can be assumed that they follow the fluid streamlines. The applied flow rates were similar as in the simulations. Recorded images are analyzed with ImageJ software. First, the recorded image sequence is imported and the brightness and sharpness are adjusted. Second, the image sequence is stacked into one image using Z-projection to show the particle trajectories. The particle concentration was kept below 0.5 g/L in order to clearly identify individual particles and to obtain no overlapping particle trajectories.

3.4.Results and discussion

The change in outlet concentrations with increasing flow rate resulting in higher separation efficiency was shown in our recent study [40]. This change was attributed to the higher Reynolds numbers ($Re > 5$) in the deterministic ratchet, leading to vortex formation, which again influenced particle displacement. Separation efficiency increases with Reynolds number and this effect is strongest for ratchet design 1 (fig. 3.3). This difference can be partially explained by the two designs having different critical particle sizes and the particles separated. The dependency of separation efficiency on flow rate was not observed previously in ratchets under Stokes flow conditions. Therefore it was decided to investigate the inertial flow regime in the ratchets in more detail.
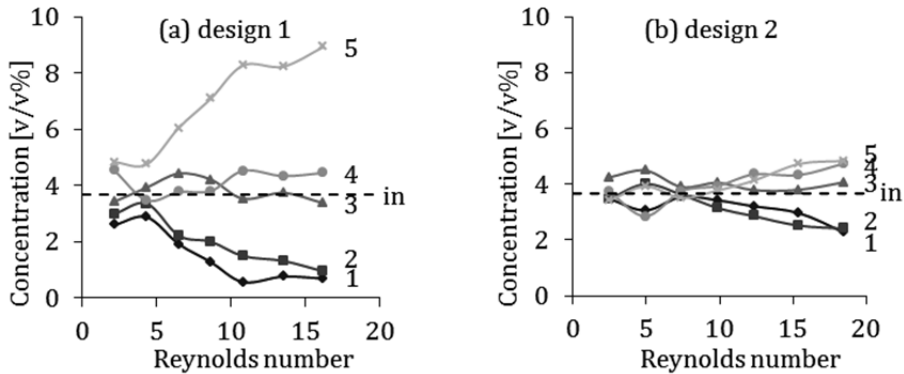

Fig. 3.3. Graphs showing the dependency of the outlet concentration on the Reynolds number for (a) design 1 and (b) design 2. Symbols: diamonds = outlet 1, squares = outlet 2, triangles = outlet 3, circles = outlet 4, crosses = outlet 5. The inlet concentration (3.7 v/v%) is given as a dashed line.

The results of the 2D simulations are shown in fig. 3.4. For cylindrical-shaped obstacles at $Re = 2$ the fluid profile is comparable to viscous flow. At $Re = 9$ a small pair of vortices is developing behind the obstacles. These vortices become larger at higher Re. At $Re = 30$ the vortices are about 70% of the gap size between two consecutive obstacles rows. Compared to cylindrical-shaped obstacles the development of vortices behind quadrilateral-shaped obstacles starts earlier, due to the sharp corners; namely

at $Re = 2$. Here the vortices increase in size to 75% of the gap between rows at $Re = 26$. Particles that are smaller than the critical size for separation normally zigzag between the two obstacle rows which are separated from each other by a distance D_x. Because of the vortices the streamline profile has been changed and particles are forced to zigzag just before the second row, after they passed the vortex. The stagnation point shifts from the top of an obstacle at low Re to the right side of an obstacle at high Re. Due to the presence of vortices there is only a fraction of D_x left for the zigzag motion of small particles. For the cylindrically-shaped obstacles and $Re = 30$ the gap is only 338 μm, 30% of D_x, and for the quadrilateral-shaped obstacles at $Re = 26$ the gap is 450 μm, 25% of D_x. The obstacles and associated vortices along the displacement direction act as a membrane with pore sizes smaller than the particle size. Particles are thus retained in a displacement trajectory.
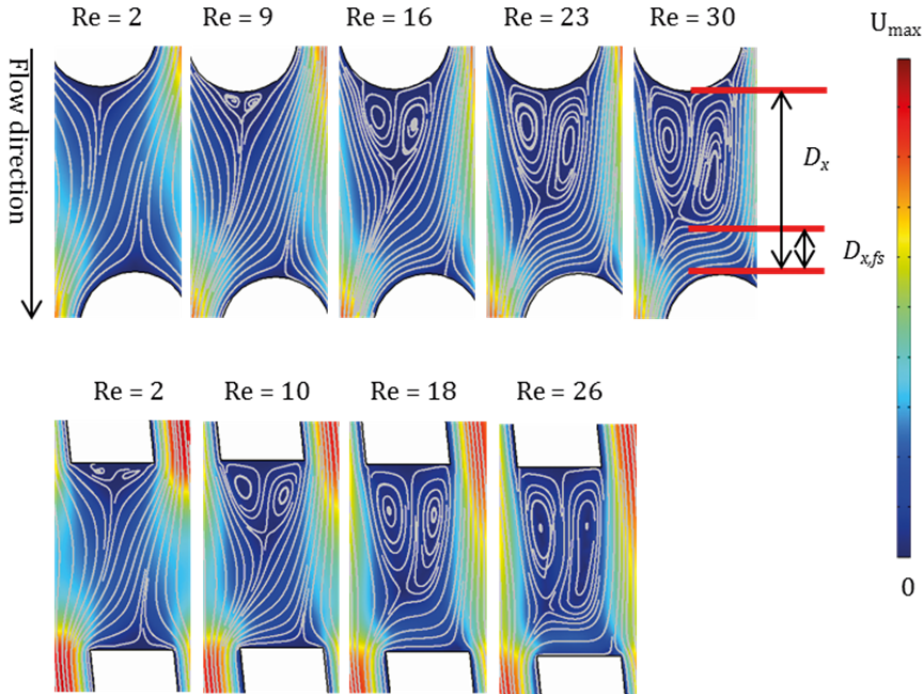
Fig. 3.4. Simulated streamlines at different Reynolds numbers (Re) on the inertial flow regime in deterministic ratchets. The fluid velocity is between 0 (dark blue) and U_{max} (dark red). (a) U_{max} = 0.100; 0.039; 0.072; 0.100; 0.134 m/s, (b) U_{max} = 0.012; 0.047; 0.093; 0.130 m/s.

The experimental results are shown in fig. 3.5. For cylindrical-shaped obstacles the created particle trajectories show that particles indeed swirl behind obstacles from Re = 16, indicating vortices. For quadrilateral-shaped obstacles the particles start to swirl from *Re* = 10. These swirls are similar to the simulated vortices. It can be concluded that the high speed camera results confirm the 2D simulations. One can also observe, especially for the quadrilateral-shaped obstacles, the change in the trajectories of the particles at increasing flow rates. At low flow rates the zigzag motion of particles can be described as close to diagonal, while at higher flow rates particles move straight until the next obstacle row and then make a sharp turn. This observation is comparable to the streamline profile in fig. 3.4, where we see a shift of the stagnation point. This behavior can be explained by the development and grow of vortices with increasing flow rate.
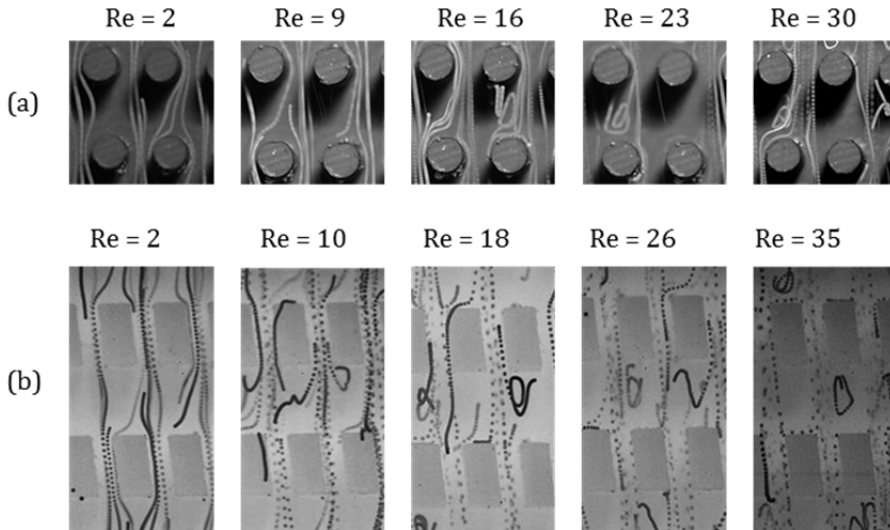
Fig. 3.5. Particle trajectories obtained by image analysis of high speed camera images. Flow was from top to bottom. The images were taken at different Reynolds numbers (Re) on the inertial flow regime in deterministic ratchets with (a) cylindrical-shaped obstacles and (b) quadrilateral-shaped obstacles.

Considering the differences between design 1 and design 2 it can be concluded that the obstacle shape is an important factor in the design of deterministic ratchets. For

Re < 1 the obstacle shape does not have a significant influence on the critical particle size as long as they are symmetric [20, 21, 41], but for *Re* > 1 the design of the obstacles has great influence. Asymmetric obstacles or obstacles having sharp edges, like design 2, induce larger vortices than symmetric and streamlined obstacles, like design 1. For future designs the obstacle shape could be an important factor in the design. By using specific shapes which induce a large vortex the separation efficiency may be further improved.

The velocity profiles, *U(x)* in the gap between two neighboring obstacles are shown in fig. 3.6. For design 1 the velocity profile is close to symmetric for *Re* = 2 and *Re* = 9 and can be described by a parabolic equation as described by Inglis *et al.* [17]. For higher Reynolds numbers the velocity profiles are increasingly asymmetric, with the largest velocity moving to larger *x*, with *x* the position in the gap between two neighboring obstacles. For design 2 the velocity profile is only close to symmetric for *Re* = 2. For higher Reynolds numbers the velocity profiles are slightly asymmetric, with the largest velocity moving to smaller *x*.
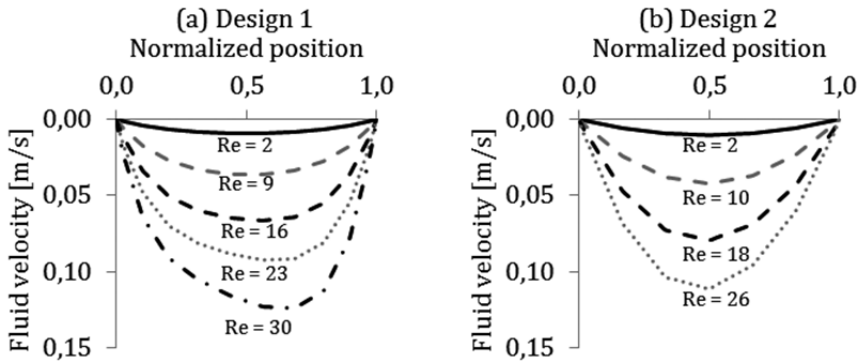
Fig. 3.6. Fluid velocity profiles in the gap between obstacles at different Reynolds numbers. (a) Design 1; Re = 2 (black solid line), Re = 9 (grey dashed line), Re = 16 (black dashed line), Re = 23 (grey dotted line), Re = 30 (black dashed/dotted line). The inlet fluid velocities are between 0.003 m/s (Re = 2) and 0.042 m/s (Re = 30). (b) Design 2; Re = 2 (black solid line), Re = 10 (grey dashed line), Re = 18 (black dashed line), Re = 26 (grey dotted line). The inlet velocities are between 0.003 m/s (Re = 2) and 0.031 m/s (Re = 26).

Analysis of the streamline profiles for different inlet velocities shows that the number of flow lanes, N, increased at higher inlet velocities (fig. 3.7). At the lowest measured velocities, N equaled the number of obstacle rows in one periodic cell; at the other measured velocities, N was higher. The experimental results were comparable with the simulations. The number of flow lanes at different Re for both designs is given in table 3.1.
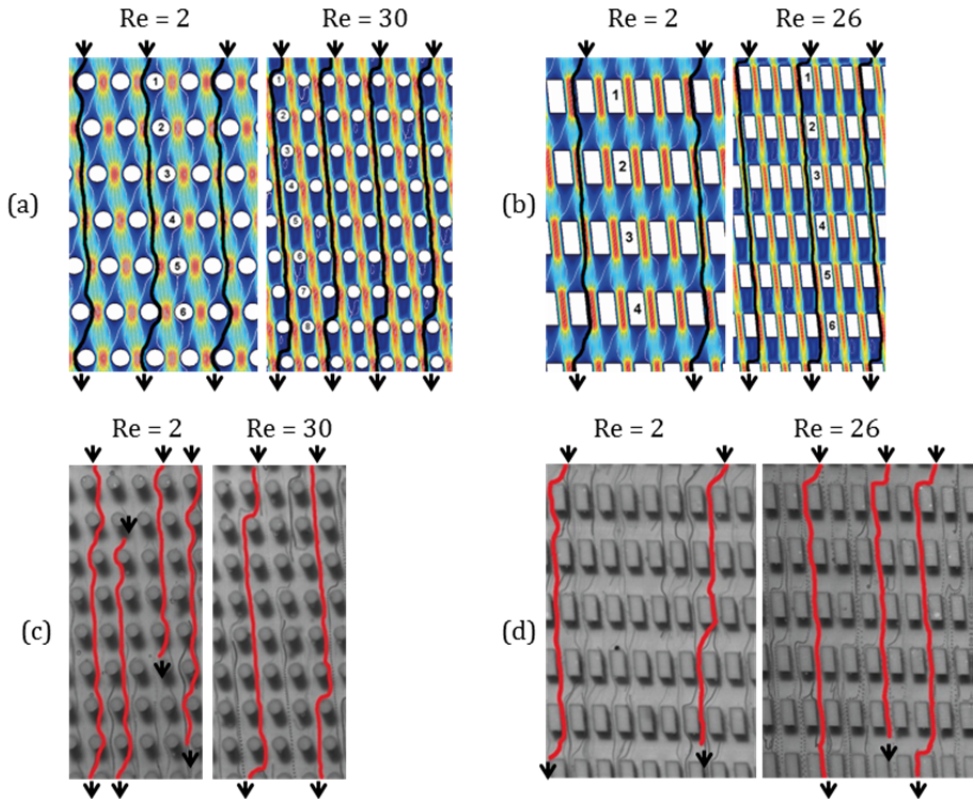
Fig. 3.7. Simulated streamlines (black) and experimentally observed particle trajectories (red lines) in (a), (c) design 1 and in (b), (d), design 2 for low and high Reynolds number. Flow was from top to bottom.

From the velocity profiles and the number of flow lanes we have determined the flow lane width distributions, fig. 3.8. Each flow lane is assumed to have equal fluid flux. Similar to fig. 3.6 the asymmetry can be observed in the distribution of the flow lanes.

Table 3.1. Number of flow lanes (N) at different Reynolds number (Re).

Design 1		Design 2	
Re	N	Re	N
2	6	2	4
9	6	10	5
16	7	18	6
23	7	26	6
30	8		

Chapter
3

As discussed previously, asymmetry in the flow profile may originate from asymmetry in obstacle shape [20, 21] and anisotropy in the permeability of the obstacle array [18, 19]. The obstacle shape of design 1 is symmetric; the obstacle shape of design 2 is slightly asymmetric. A deterministic ratchet contains anisotropy if the primitive cell is oblique and the flow direction is orthogonal to the lattice direction. This is true for the devices used in this study. The pressure field and the main flow direction are not aligned, creating an asymmetric flow profile. This mainly applies for design 1 with $D_x/D_y < 3$ and it results in $D_{f,1} < D_{f,N}$ [19]. This explanation does not fully explain the results in fig. 3.8, in which a clear influence of the Reynolds number is seen. The development of vortices as shown in fig. 3.4 probably influences the flow profile and contributes to the asymmetry. This asymmetry leads to a smaller first flow lane, so the critical particle size is reduced as well. An increase in number of flow lanes decreases the critical particle size even more. Applying Inglis' parabolic flow profile [17] yields $D_{p,c}$ = 292 μm for design 1 and $D_{p,c}$ = 392 μm for design 2. Fig. 3.8 shows that an asymmetric flow profile at Re = 2 gives $D_{p,c}$ = 264 μm for design 1 and $D_{p,c}$ = 380 μm for design 2. At the highest measured flow rates, where vortices are present and the number of flow lanes has been increased, $D_{p,c}$ = 226 μm for design 1 and $D_{p,c}$ = 290 μm for design 2. This is a reduction in critical particle size of 14% for design 1 and 24% for design 2. A smaller critical particle size allows us to design new devices with similar critical particle size, but wider gap size. Such devices have a reduced chance for clogging and a decreased pressure drop across the deterministic ratchet, enlarging the throughput of the device.
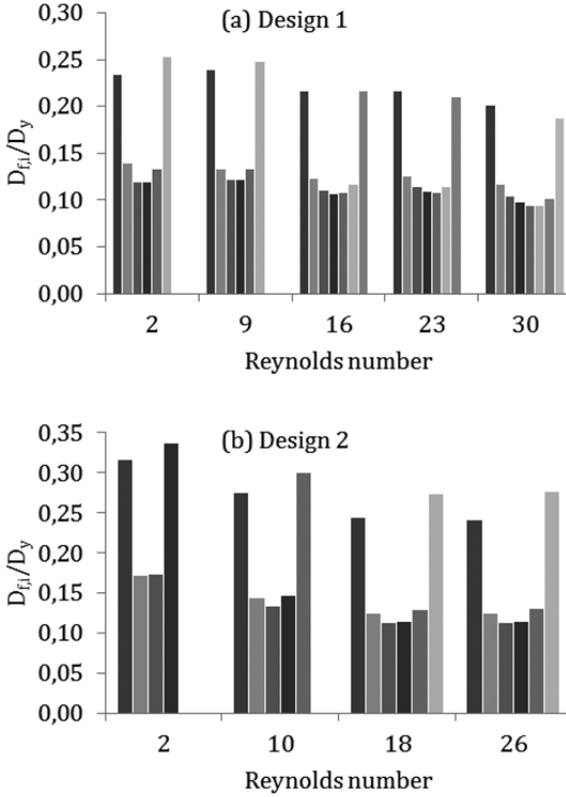
Fig. 3.8. Flow lane width distributions of (a) design 1 and (b) design 2, for different Re values. The number of bars equals the number of flow lanes at that specific Re. The first bar represents the first flow lane.

3.5.Conclusions

The separation efficiency of deterministic ratchets depends on design parameters and hydrodynamic conditions. In the viscous flow regime with low Reynolds numbers the flow pattern is well described and the particle separation can be predicted for different ratchet geometries and obstacle shapes. Previous work showed that at moderate Reynolds number the particle separation is different.

From 2D flow field simulations it could be concluded that for cylindrical-shaped obstacles a pair of vortices develops behind obstacles from $Re = 9$. These vortices become larger for higher Re. At $Re = 30$ the vortices are about 70% of the gap between

two obstacles rows. For quadrilateral-shaped obstacles the vortices develop at Re = 2 and become 75% of the gap between rows at Re = 26. Analysis of high speed camera images from particle motion in experimental ratchet devices confirmed the simulation results. The supposed effect of vortices on particle movement is prevention of the 'zigzag' motion of particles by narrowing the gap between two consecutive obstacle rows. This narrowing effect decreases the critical particle size for separation.

With both simulation and experiments an increase in number of flow lanes with Re was observed. This increase can be explained by asymmetry of the fluid velocity profile in the gaps. Asymmetry is caused by anisotropy of the obstacle array and the development of vortices. More flow lanes lead to a reduced critical particle size and are evident in better separation. For the design with cylindrical-shaped obstacles the critical particle size decreased by 14% from 264 to 226 μm, for the design with quadrilateral-shaped obstacles the critical particle size decreased by 24% from 380 to 290 μm. This reduction is important for the development of new devices with less chance for clogging and lower pressure drop.

These results provide better understanding of the inertial flow behavior in deterministic ratchets. It shows that we can make use of specific asymmetric ratchet designs and hydrodynamic conditions to develop new deterministic ratchets which facilitate high throughput.

3.6.Acknowledgements

High throughput particle separation with a mirrored deterministic ratchet design
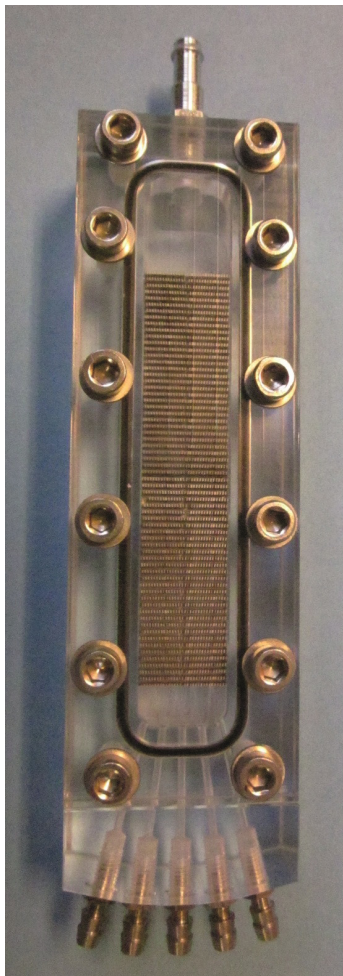
Picture of the smaller up-scaled device used in the experiments described in chapter 4.

4. High throughput particle separation with a mirrored deterministic ratchet design

4.1. Abstract

Deterministic ratchets, also called lateral displacement arrays, consist of periodic arrays of obstacles, spaced such that suspended particles having a minimum size are displaced. They have potential for suspension separation and fractionation. We report on the development of designs with obstacle arrays mirrored along the center plane providing more efficient displacement compared to non-mirrored designs. Depending on the application (e.g. concentration or cleaning) the design can be oriented to the center or to the sides. Highest recovery of incoming particles was found 88% in the center orientation, while the strongest depletions were achieved with the side orientation. Halving the length of the array did not always yield similar separation to the conventional design, especially at higher concentrations. This implies that particle displacement was not pure deterministic, but influenced by stochastic particle-particle interactions. Fractionation experiments demonstrated high recoveries of large particles, which were not much influenced by presence of small particles.

4.2. Introduction

Interactions between the flow field and the steric interactions of particles with confining walls or obstacles drive separation in flow line sieving devices. Three separation technologies which use this flow line sieving principle are deterministic ratchets, hydrodynamic filtration and asymmetric pinch flow fractionation [12]. Deterministic ratchets, also named lateral displacement arrays, were identified as the most promising route for continuous suspension separation. These devices consist of periodic obstacle arrays positioned in a flow channel, where each obstacle row is shifted laterally with respect to the previous row. Separation is based on physical displacement of particles from their streamlines by steric interaction with the

Chapter

4

periodic obstacle arrays. Particles below a critical diameter ($D_{p,c}$) follow the fluid streamlines, while those larger than $D_{p,c}$ interact with the obstacles, are displaced from the fluid streamlines and move at an angle (α) with the main flow direction.

Since the introduction of deterministic ratchets for suspension separation purposes by Huang *et al.* [13], several research groups demonstrated the efficacy to separate polymeric beads and a variety of biological cells [13, 17-23, 25, 26, 28-32, 40, 42, 43]. Most of these applications were demonstrated with microfluidic devices at low volumetric flow rates in the order of 0.1-10 mL/h. Deterministic ratchet technology has also shown potential for larger-scale applications that operate at high flow rates in the order of 0.5-10 L/h [23, 40, 44]. Scale-up of deterministic ratchets can be realized by increasing flow rate through a single device, or by out-scaling by stacking multiple devices [44]. Stacking involves practical challenges such as increased pressure drop across the device, complicated internal connections, and the design of the stack itself. By increasing the flow rate, the hydrodynamics in the deterministic device becomes different. The fluid Reynolds number (*Re*), defined as the ratio between inertial and viscous forces, characterizes different fluid flow regimes. In this work *Re* was calculated as *Ud/v*, with *U* the average flow velocity between two neighboring obstacles, *d* the specific length which equals the gap width between two neighboring obstacles and *v* the kinematic fluid viscosity. Smooth laminar flow occurs at low Reynolds numbers (*Re < 1*); viscous forces are dominant, while fluid instabilities due to presence of more inertial forces gradually arise at higher Reynolds numbers. In previous research it was observed that due to these changes in fluid flow, particle displacement behavior and thus separation behavior are significantly affected with increasing flow rates [40]. Via high-speed camera observations and numerical fluid flow calculation, vortex formation behind obstacles and an increasing number of fluid flow lanes were observed at increasing flow rates [45]. It was also hypothesized that inertial lift forces have beneficial effect on particle displacement. In two other studies using deterministic ratchets, successful separation of cancer cells and algae was demonstrated at increased flow rates of 0.6 L/h (*Re ≈ 40*) [23, 44]. In yet other studies controlled instabilities were used to improve the separation behavior during Dean vortex microfiltration [46, 47].

The Stokes number (St) characterizes behavior of particles in suspension flow and is defined as the ratio between the response time of the particle (τ) and the fluid response time (d_c/U). Here $\tau = \rho_p d_p^2/18\mu$, with ρ_p the particle density, d_p the particle diameter, μ the fluid viscosity, U the fluid velocity and d_c the characteristic dimension of the obstacle [48, 49]. At St << 1 particles follow fluid streamlines closely. However, at St >> 1 particles will deviate from the fluid flow especially at sudden changes in fluid velocity; inertial effects dominate. In this work St varies between approximately 0.02 and 0.45. Therefore, it can be concluded that most particles will follow the fluid streamlines in our experiments. Only at St > 0.1 the contribution of inertial effects cannot be neglected anymore [48, 49]; especially at locations with sudden changes in fluid velocity particles may be deflected from the fluid streamlines. Additionally, under these conditions the chance increases that particle-particle collisions occur as particles approach each other closer.

For the current study two deterministic ratchet devices were constructed at two size scales of 200 and 800 µm. The size scale is defined as the obstacle width. The 800 µm device was constructed using a precision milling technique; the 200 µm device was constructed using electric discharge machining (EDM) or spark machining. EDM is a process in which rapidly repetitive sparks remove material from the system. The sparks are discharges between two electrodes, which are separated from each other by a dielectric liquid and subjected to an electric voltage. A major advantage of the EDM technique is the large height to diameter ratio that can be achieved. For the 200 µm device this ratio was 7.5 compared to a ratio of 3.1 for the 800 µm device.

The main objective of this paper is to investigate the potential of deterministic ratchets with a mirrored design for a more efficient separation and fractionation process. The obstacle arrays of such a design are mirrored along its vertical center line (fig. 4.1). The advantage of mirrored designs is that particles need to be displaced only half the width of the device. If all particles show full displacement behavior the separation will be completed in half the length of a conventional non-mirrored design with the same width. This implies that the length of the device may be reduced by a factor two. It should be noticed that the particle displacement per obstacle, i.e. the shift, is not changed. The total displacement per unit length of the device is the same

in mirrored and non-mirrored designs. The difference is that with mirrored designs all particles can be concentrated with half the number of obstacle rows compared with non-mirrored designs. By mirroring, two different operating modes are possible; 1) particles are concentrated in one stream in the center of the deterministic ratchet and 2) particles are concentrated in two streams at both sides of the deterministic ratchet (fig. 4.1). The advantage of the first option is that all particles can be concentrated into a center outlet of the device with maximal concentration. The advantage of the second option is that higher inlet concentrations are possible without clogging the obstacle array, because the particles are divided into two concentrated streams at the sides of the device.
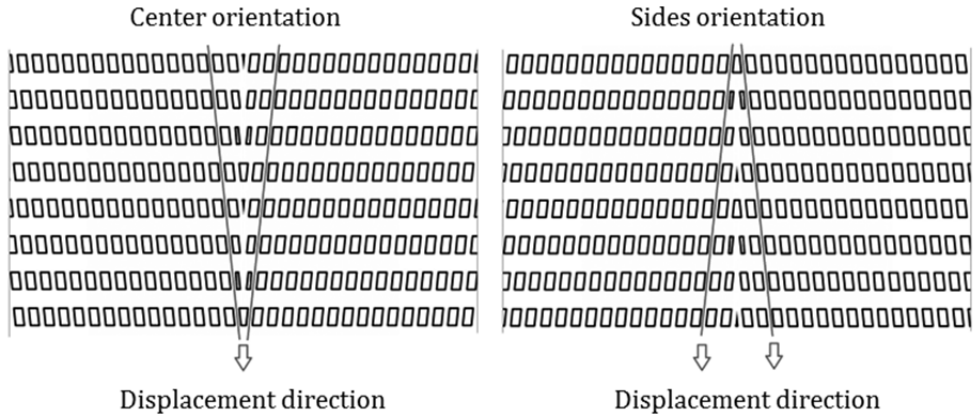
Fig. 4.1. Mirrored deterministic ratchet design with two operational modes: 1) center orientation and 2) sides orientation (note that only 8 of the 64 obstacle rows are shown). Suspended particles with $d_p > D_{p,c}$ follow a displacement direction which is directed to the center or the sides of the obstacle array. Flow is from top to bottom.

This paper presents the separation results for the mirrored deterministic ratchet design with two operational modes at two size scales. Subsequently the influences of flow rate, particle concentration and device length on separation recovery are discussed. Finally, the designs are evaluated for fractionation of mixtures of particles.

4.3.Materials and methods

4.3.1.   Device design and manufacture

We operated the mirrored deterministic ratchet in two modes (fig. 4.1). The left and right halves of both operational modes are mirrored around the vertical axis. Particles in operational mode 1 migrate to the center of the obstacle array and particles in operational mode 2 migrate to the sides of the obstacle array. The obstacles are quadrilateral and the obstacle width is used as the typical size scale of the design. The mirrored design is manufactured at two size scales, 800 µm and 200 µm. The 800 µm ratchet is made by controlled milling of polyether ether ketone (PEEK), a thermoplastic material. The 200 µm ratchet is made by spark machining of hardened metal as described in paragraph 4.2 of this chapter. The 800 µm ratchet is placed in an up-scaled device as described in previous work [40]. A schematic drawing is provided in fig. 4.2.
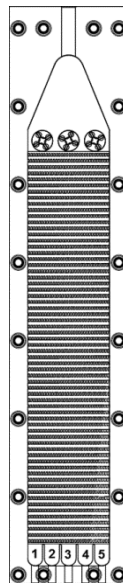
Fig.4.2. Schematic drawing of the device used for holding the 800 µm ratchet. The suspensions are fed at the top, while five outlet fractions are collected at the bottom.

For the 200 μm ratchet a smaller version of this up-scaled device was made.

The full length of the deterministic ratchet is composed of 16 periodic obstacle arrays of 4 obstacle rows. A single obstacle in the 800 μm ratchet has width W = 800 μm, length L = 1600 μm and height H = 2500 μm (fig. 4.3). The gap between adjacent obstacles D_y = 600 μm and the gap between two consecutive obstacle rows D_x = 1800 μm. A single obstacle in the 200 μm ratchet has W = 200 μm, L = 400 μm, H = 1500 μm, D_y = 150 μm and D_x = 450 μm. The displacement angle α = 6°. The obstacles along the center line have different shapes and sizes, see fig. 4.3. For the 800 μm device, which is made of one piece, W_1 = 300 μm, W_2 = 700 μm and W_3 = 400 μm. An important criterion for designing these center obstacles is that the smallest distance between the obstacles should be equal to D_y. The 200 μm device is made of four equal quarters; with spark machining it is not feasible to create the mirrored designs in one piece. The quarters can be combined in various ways to get the preferred operational modes. The mode in which the particles are displaced to the center line is slightly different than for the 800 μm device, see fig. 4.3. For the 200 μm device, W_2 = 25 μm and W_4 = 375 μm.

Assuming a parabolic flow profile in the deterministic ratchets [17] the critical particle size for displacement ($D_{p,c}$) is 392 μm for the 800 μm designs and 98 μm for the 200 μm designs. This assumption is justified for low Reynolds number flow regimes (Re < 10). For Re > 10, $D_{p,c}$ may well be decreased due to inertial effects [45].

4.3.2. Suspension preparation

The suspensions for the 800 μm device were prepared with water/glycerol solution (80/20 wt.%), polystyrene particles (ρ = 1.05 g/ml) and surfactant (SDS, 2.5 wt.%) to obtain neutral buoyancy. The particles had an average diameter d_{50} = 415 μm with d_{10} = 342 μm and d_{90} = 541 μm. These values are volume based and determined with an EyeTech particle size analyzer (Ankersmid). The particles were suspended to a concentration of 0.5-4.6 v/v%. The suspensions for the 200 μm device were prepared with water and polyethylene particles (0.98-1.0 g/ml) which were wetted with surfactant Tween-80 applying a concentration of 2 w/v% in the final suspension. For
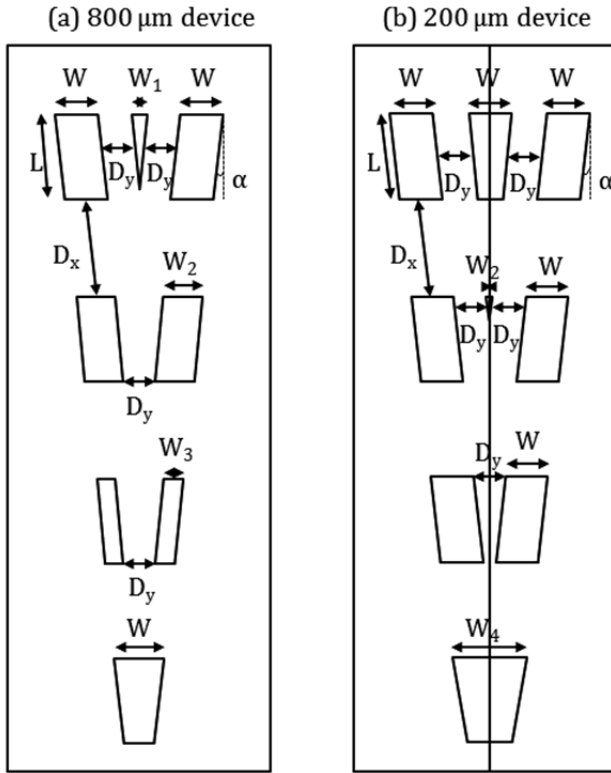
Fig.4.3. Schematic drawing of the obstacles along the center line; (a) 800 µm device and (b) 200 µm device, indicating the obstacle widths W, W_1, W_2, W_3 and W_4 the obstacle length L, the displacement angle α, the gap width between two obstacles on the same row D_y and the distance between two rows D_x. The left and right halves of the 200 µm device are separate parts as indicated by the vertical line in the figure. The parts are combined into one ratchet.

the separation experiments, the particles had an average diameter d_{50} = 104 µm, d_{10} = 92 µm and d_{90} = 112 µm. These values are volume based and obtained with a Mastersizer 2000 particle size analyzer (Malvern). The particles were suspended to a concentration of 0.1-1.5 v/v%. For the fractionation experiments, mixed suspensions were prepared with different volume fractions of red colored particles (d_{10} = 32 µm, d_{50} = 36 µm, d_{90} = 41 µm) and blue colored particles (d_{10} = 92 µm, d_{50} = 104 µm, d_{90} = 112 µm). The volume fractions used (red/blue) are 0/100, 20/80, 50/50, 80/20 and 100/0. The total concentration of these mixed suspensions was 0.5 v/v%.

4.3.3.   Experiments

Both devices with the mirrored design were analyzed for their recovery, which we define as the total volume of particles in a specific outlet divided by the total volume of particles in all the outlets, multiplied by 100%. The sum of the recoveries of all the five outlets is 100%. The suspensions were pumped into the device at the top of the module and collected in five equal sized outlets. The composition of the outlet fractions was analyzed by determining the volume fraction of the particles and the particle size distribution.

The separation using both operational modes at both size scales was investigated by determining the recovery per outlet as function of the flow rate, feed concentration and deterministic ratchet length. For the 800 μm device the flow rates were between 20 and 280 ml/min (*Re* is between 2 and 35), the feed concentrations were between 0.5 and 4.6 v/v%, the particle size was in the range of 342-541 μm and only the full deterministic ratchet length was used. For the 200 μm device the flow rates were between 10 and 150 ml/min (*Re* is between 4 and 56), the feed concentrations were between 0.1 and 1.5 v/v%, the particle size was in the range of 92-112 μm and both the full deterministic ratchet length and the half-length were investigated. The half-length was obtained by replacing the upper two quarters by a unit without obstacles.

The fractionation of mirrored designs was only investigated with the 200 μm device. The flow rate was set at 150 ml/min (*Re* = 56), the total feed concentration was 0.5 v/v% and both the full length and the half-length were investigated. The investigated suspensions had different volume fractions of red colored 32-41 μm and blue colored 92-112 μm particles; 0/100, 20/80, 50/50, 80/20 and 100/0. From each of the five outlet streams we determined the recovery of the small and large particles by measuring the total particle volume and the particle size distribution with a Malvern Mastersizer 2000.

4.4. Results and Discussion

4.4.1. Separation experiments

The recovery per outlet as a function of the Reynolds number (*Re*) is shown in fig. 4.4. For the 800 µm design operated in center mode (fig. 4.4 (a)) the recovery of outlet 3 increases from 37% at *Re* = 2 to 88% at *Re* = 35. These recovery values correspond to concentrations of 0.9 v/v% at *Re* = 2 and 2.1 v/v% at *Re* = 35. This 2.1 v/v% means a fourfold concentration increase compared to the inlet concentration of 0.5 v/v%. The recovery in outlet 1 and 5 is 0% at *Re* = 18, *Re* = 26 and *Re* = 35. The particles are thus completely removed from the wall area. For the 800 µm design operated in sides mode (fig. 4.4 (b)) the particles are completely removed from the center at *Re* = 18, *Re* = 26 and *Re* = 35. The recovery at both sides is approximately 50%, corresponding to a concentration of 1.2 v/v%, a twofold increase in concentration compared to the inlet concentration. Depending on the application one could opt for the center or sides mode. The center mode is preferred for concentration purposes where the recovery should be maximized in only one outlet. The sides mode is preferred for cleaning purposes where the largest part of the outlet stream is clear from particles. For the 200 µm device operated in center mode (fig. 4.4 (c+d)), similar effects as a function of *Re* are observed. This increase in separation efficiency as a function of *Re* was described in detail in our previous papers [40, 45]. We concluded that the reason for this dependence arises from vortices behind the obstacles and shear-induced lift forces that affect particle displacement. Both effects start to appear at *Re* > 1 and become stronger with increasing *Re*.

The recovery per outlet as a function of the inlet concentration is given in fig. 4.5. Only for the 800 µm design operated in the center mode (fig. 4.5 (a)), the recovery is to a limited extent dependent on the inlet concentration. The recovery of outlet 3 decreases from 79% at 0.5 v/v% to 46% at 3.7 v/v%. A maximum inlet concentration was found where the recovery dramatically decreased due to clogging of the device. When displacing the particles to the sides the maximum concentration was
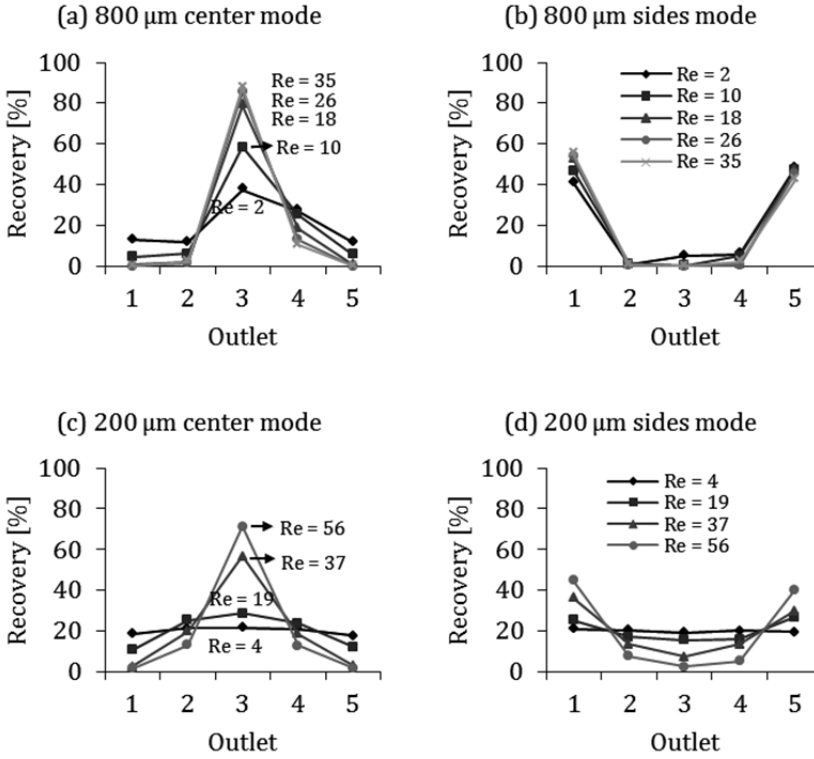
Fig.4.4. Recovery per outlet for different fluid Reynolds numbers (Re) at an inlet concentration of 0.5 v/v%. (a) 800 μm center mode, (b) 800 μm sides mode, (c) 200 μm center mode and (d) 200 μm sides mode. Symbols: (a)+(b) diamonds: Re = 2, squares: Re = 10, triangles: Re = 18, circles: Re = 26, crosses: Re = 35; (c)+(d) diamonds: Re = 4, squares: Re = 19, triangles: Re = 37, circles: Re = 56. Lines are drawn to guide the eye.

approximately 25% higher than for the center mode, at least for the 800 μm device. This is expected because when displacing the particles to the sides, particles are distributed across two concentrated streams, while in the center mode particles are collected in only one concentrated stream.

The maximum concentration that can be achieved is approximately a factor 3 lower for the 200 μm devices compared to the 800 μm devices. This may be explained by the increasing number of particles for the smaller particle size mixtures, which leads to a higher chance for particle-particle interactions and thus risk for clogging of the device. At similar volume concentration the number of 92-112 μm particles is approximately $d_{50(342-541)}^3/d_{50(92-112)}^3$ = 64 times higher than for 342-541 μm particles. The surface

area of one single 92-112 μm particle is $d_{50(342-541)}^2/d_{50(92-112)}^2 = 16$ times smaller than for a single 342-541 μm particle. Combining both factors shows that at similar volume concentration the total particle surface area of the 92-112 μm particles is approximately $d_{50(342-541)}/d_{50(92-112)} = 4$ times larger. The concentration at which for both particle sizes the total particle surface area is similar coincides approximately with the maximum concentrations we found in our device.
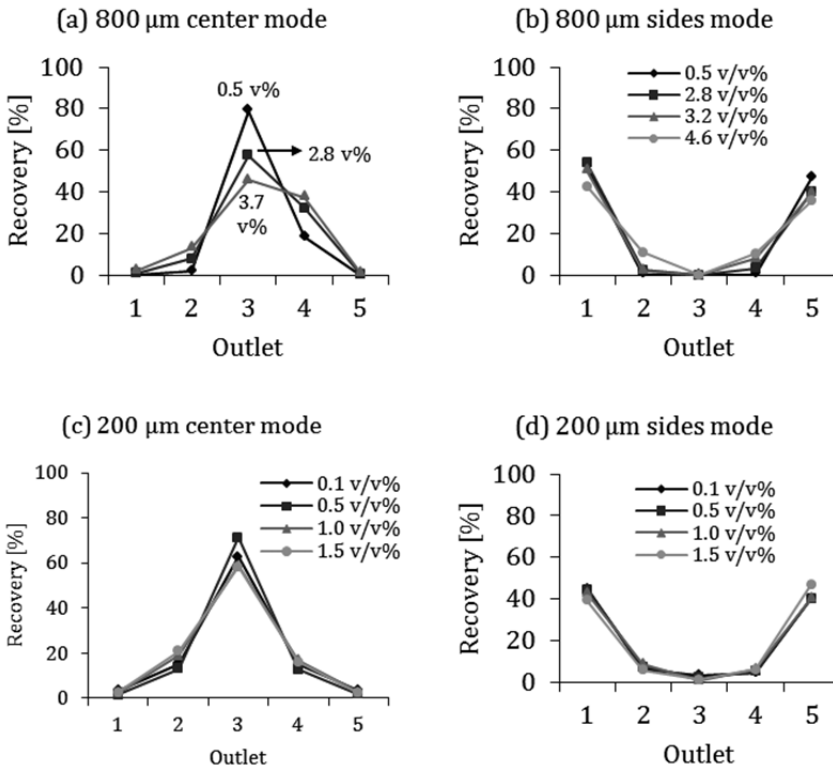
Fig.4.5. Recovery per outlet for different inlet concentrations. Lines are drawn to guide the eye.

(a) 800 μm center mode, Re =18, diamonds: 0.5 v/v%, squares: 2.8 v/v%, triangles: 3.7 v/v%;

(b) 800 μm sides mode Re = 18, diamonds: 0.5 v/v%, squares: 2.8 v/v%, triangles: 3.2 v/v%, circles: 4.6 v/v%;

(c) 200 μm center mode Re = 56, diamonds: 0.1 v/v%, squares: 0.5 v/v%, triangles: 1.0 v/v%, circles: 1.5 v/v%;

(d) 200 μm sides mode, Re = 56, diamonds: 0.1 v/v%, squares: 0.5 v/v%, triangles: 1.0 v/v%, circles: 1.5 v/v%.

The measured recovery per outlet as function of the deterministic ratchet length is given in fig. 4.6. The recovery of outlet 3 in the center mode is 71% for the full length

and 41% for the half-length design. The recovery of outlet 1 in the sides mode is 45% for the full length and 31% for the half-length design. If the deterministic particle displacement behavior for both lengths would be completely deterministic the outlet 3 recovery of the full length device (center mode) equals 100%, while the outlet 3 recovery of the half-length equals 70 % (outlet 2 and 4 both 15%).
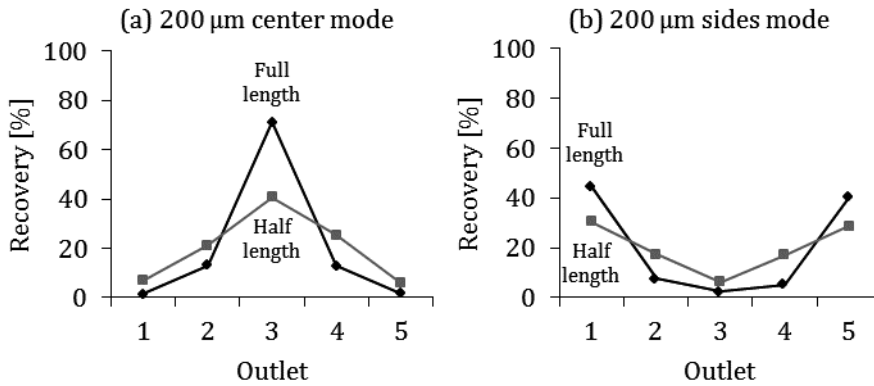
Fig. 4.6.Recovery per outlet for the full length design (diamond symbol) and the half-length design (square symbol) at Re = 56 and an inlet concentration of 0.5 v/v%. (a) 200 μm center mode and (b) 200 μm sides mode. Lines are drawn to guide the eye.

The maximum horizontal displacement equals the number of obstacle rows multiplied by the shift (87.5 μm). For the full length device this distance is 64 rows x 87.5 μm = 5600 μm. This means that all particles, including the particles that enter the array at the walls, will end up in outlet 3, which collects all particles between 4480 and 6720 μm from the left wall. For the half-length device this distance is 32 rows x 87.5 μm = 2800 μm. This means that particles entering the array at 4480-2800 = 1680 μm (or less) from the wall end up in outlet 2. Assuming an equal distribution of particles this is 1680 / 2240 (width of one outlet) x 20% = 15% recovery. The outlet 3 recovery for the full length device is thus a factor 1.4 lower and the recovery for the half-length device a factor 1.7 lower than expected based on completely deterministic behavior. The separation process must therefore be slightly stochastic. This can be due to hydrodynamic particle-particle interactions or by a different flow profile. For the sides mode the outlet 1 recovery is only a factor 1.1 lower for both the full length device and

the half-length device. Since the particle concentrations in sides mode are lower than in center mode it is likely that there are less particle-particle interactions in the sides mode. In each case, it is recommended to make the length of deterministic ratchets several periodic arrays longer than theoretically needed, especially when attempting to displace particles to one concentrated outlet.

4.4.2. Fractionation experiments

Fractionation of bi-disperse suspensions into suspensions of small and large particles was evaluated with the 200 μm device. Suspensions with different ratios of small particles ($d_p < D_{p,c}$) and large particles ($d_p > D_{p,c}$) were fractionated into five outlet fractions. The small particles were red and the large particles were blue. Visual inspection of the outlet fractions gives a qualitative impression of the fractionation achieved (fig. 4.7). For the center mode no or only red particles can be seen in outlets 1 and 5 and the blue color in outlet 3 changes into a red color as the ratio of small particles increases. For the sides mode no or only red particles can be seen in outlet 3 and the blue color in outlets 1 and 5 changes into a red color as the ratio of small particles increases. These results are expected based on the particle size of the red and blue particles, and the results correspond to those of the separation experiments with the blue particles only. The recovery is not to be dependent on the ratio between small and large particles.
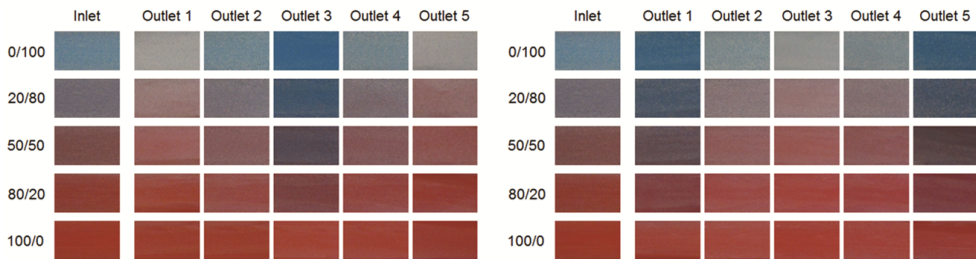

Fig. 4.7. Results of the fractionation experiments with the center mode (left) and the sides mode (right). The results are pictures of the five outlet fractions for inlet suspensions with different volume based ratios of small particles (red) and large particles (blue). At dilute concentrations a grey color is visually observed.

Fig.4.8. Recovery per outlet for feed suspensions with different volume ratios of 32-41 μm particles ($d_p < D_{p,c}$) and 92-112 μm particles ($d_p > D_{p,c}$). The 200 μm device is <u>full length</u>, the applied flow rate is 150 ml/min (Re = 56) and the total inlet concentration is 0.5 v/v%. The recovery of the 32-41 μm and the 92-112 μm particles for both operational modes are given in separate figures: Lines are drawn to guide the eye.

(a) center mode, 32-41 μm particles, diamonds:100/0, squares: 80/20, triangles: 50/50, circles: 20/80;

(b) center mode, 92-112 μm particles, squares: 80/20, triangles: 50/50, circles: 20/80, crosses: 0/100;

(c) sides mode, 32-41 μm particles, diamonds:100/0, squares: 80/20, triangles: 50/50, circles: 20/80;

(d) sides mode, 92-112 μm particles, squares: 80/20, triangles: 50/50, circles: 20/80, crosses: 0/100.

The quantitative analysis of the fractionation results is given in fig. 4.8. With the operational mode that displaces the particles to the center, the recovery of small particles in the center (outlet 3) is less than 20% for the 100/0 suspension, but slightly increases with more large particles present (fig. 4.8(a)). When operating in the sides mode there are no clear differences between the ratios (fig. 4.8(c)). The recovery of the large particles is not influenced by the ratio of small and large particles (fig. 4.8(b+d)), but is similar as obtained in the separation experiments (fig. 4.6). The

displacement of large particles is not influenced by the presence of both small and large particles, but some small particles are dragged along with the large particles. A similar effect was observed with the 800 μm device as described in a previous paper [40]. The same fractionation experiments are done with the half-length deterministic ratchets (fig. 4.9); no clear dependency on the suspension composition is seen here; the obtained recoveries are similar as obtained in the separation experiments (fig. 4.6).

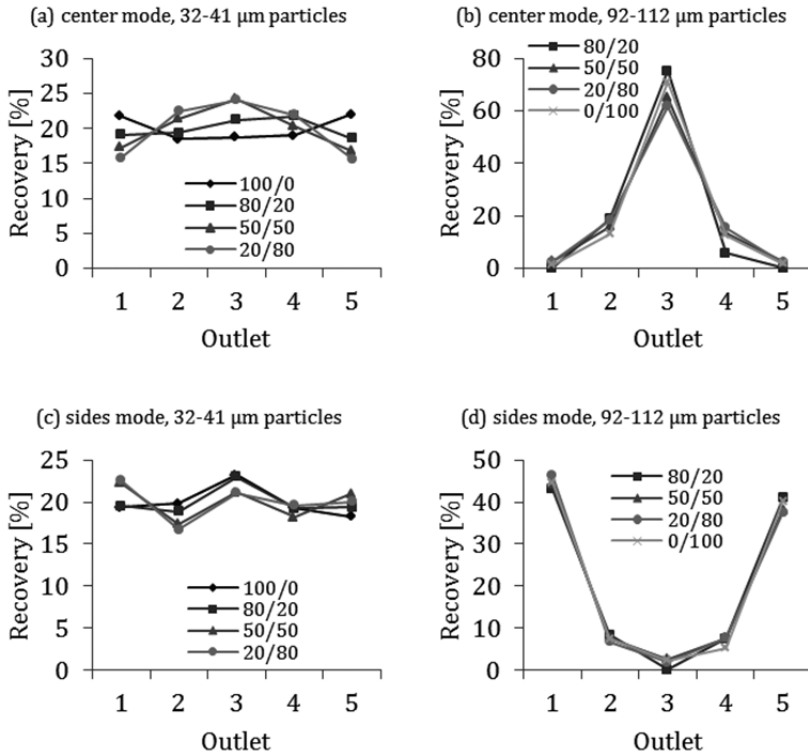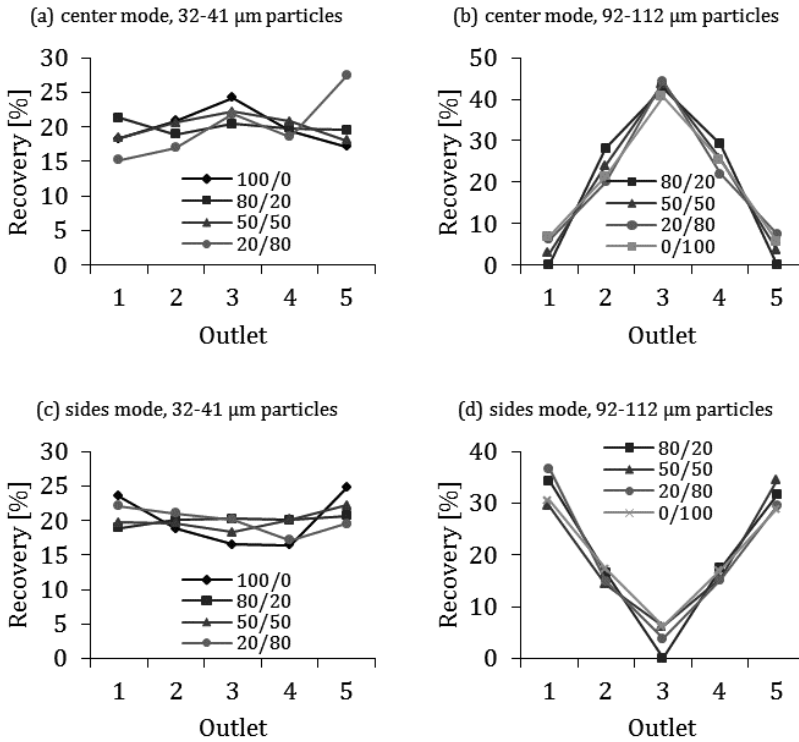*Fig. 4.9. Recovery per outlet for feed suspensions with different volume ratios of 32-41 μm particles ($d_p < D_{p,c}$) and 92-112 μm particles ($d_p > D_{p,c}$). The 200 μm device is __half- length__, the applied flow rate is 150 ml/min (Re = 56) and the total inlet concentration is 0.5 v/v%. The recovery of the 32-41 μm and the 92-112 μm particles for both operational modes are given in separate figures: Lines are drawn to guide the eye.*

(a) center mode, 32-41 μm particles, diamonds:100/0, squares: 80/20, triangles: 50/50, circles: 20/80;

(b) center mode, 92-112 μm particles, squares: 80/20, triangles: 50/50, circles: 20/80, crosses: 0/100;

(c) sides mode, 32-41 μm particles, diamonds:100/0, squares: 80/20, triangles: 50/50, circles: 20/80;

(d) sides mode, 92-112 μm particles, squares: 80/20, triangles: 50/50, circles: 20/80, crosses: 0/100.

4.5.Conclusions

A maximum recovery of 88% was obtained with the operational mode that collects particles in the center. With the operational mode that collects the particles at both sides it is possible to displace 100% of the particles into two side streams. The lower recoveries for the center mode could be explained by increased particle-particle interactions in the center regions influencing displacement. Less high volumetric inlet concentrations could be reached for the smaller deterministic ratchet (200 μm), which appeared to scale inversely with the total particle surface area. Fractionation experiments showed that movement of small particles did not hamper displacement of large particles, while a small effect was noticeable for the influence of large particles on small particles. These results show that mirroring of ratchet designs is much more effective and allows displacement of particles to center or sides. Further development is required to translate these results to practical application, which may be either cleaning or concentrating of suspensions.

4.6.Acknowledgements

Suspension separation with sparse deterministic ratchets

Picture of a sparse deterministic ratchet with quadrilateral-shaped obstacles.

5. Suspension separation with sparse deterministic ratchets

5.1. Abstract

We report on the development of a sparse deterministic ratchet for particle size-based suspension separation. The new design consists of just four obstacle lines in a flow channel and is based on the observation that in principle one line should be sufficient to fully displace particles.

A theoretical analysis indicates a decreasing retention along the obstacle line due to particle-particle interactions at increasing concentrations. This provides the insight that while the angle of the lines determines the primary separation, the number of lines is coupled to the maximum particle volume fraction that can be separated. Insertion of multiple lines prevents accumulation of particles and maintains separation. Experiments with four obstacle lines indeed showed full displacement at low particle concentrations, but at increasing concentrations the separation efficiency decreased. This behavior could be confirmed with visual high speed camera observation. Computational fluid dynamics simulations showed that the flow resistance in sparse deterministic ratchets is so low, that the flow distribution across five outlets is easily controlled by the flow resistance in the outlet tubing. The extension with some more lines to accommodate for large particle volume fractions poses no problem.

We thus believe that sparse deterministic ratchets have great potential for efficient and simple separation of suspensions.

Chapter
5

5.2. Introduction

Separation of solid-liquid suspensions is carried out in many industries. While analytical applications require only small throughput, e.g. cell separation for biological and medical analysis [50], separation in the food, chemical and waste water treatment

industry occurs at a much larger scale, e.g. removal of bacteria or fat globules from milk by microfiltration [51]. The separation can be achieved by using different separation principles, such as sedimentation, separation using steric effects and separation using force fields. Sedimentation [2, 4] requires a difference in solid-liquid density to separate particles from liquid. Alternatively, steric effects are introduced to separate particles, e.g. during membrane filtration [52], or by using flow focusing [9, 10] or flow line sieving [11], which are based on particle exclusion from certain pathways through a sieving structure. Other technologies rely on the application of external force fields such as magnetic fields [5], acoustic fields [6] or optical trapping [7]. The advantage of techniques using steric effects compared to those using external forces is the lower energy costs. Membranes are common, but suffer inherently from particle accumulation on the membrane surface. Deterministic ratchets, also called lateral displacement systems, can be regarded as a promising alternative without severe particle accumulation [12]. Moreover, ratchet separation does not require an additional external force field, dilution or the addition of chemicals.

Deterministic ratchets consist of periodic arrays of obstacles positioned in a flow channel (fig 5.1a). Each obstacle row is shifted by a fixed distance, which is a fraction of the distance between two adjacent obstacles on the same row and the periodic number. The periodic number is an integer, indicating the number of obstacle rows in one periodic array. Particles smaller than a critical size follow the fluid streamlines through the array, while particles larger than a critical size are laterally displaced at each obstacle they encounter. Deterministic ratchets have been found to be efficient, continuous, size based separation and fractionation devices for small dilute sample volumes. Since the first description of Huang *et al.* in 2004 [13] several improvements to the original design have been reported. These improvements concern the shape of the obstacles [20, 21, 53], the design of the walls of the system [54] and the asymmetry in the array (using different displacement angles) [18, 19, 31, 43, 55]. The flow rate significantly influences the recovery [40, 45] while the fluid viscosity influences the critical particle size [56].

Deterministic ratchets can be made suitable for large scale application by out-scaling (i.e. parallelizing large number of devices) or by up-scaling (increasing the dimensions

of the system itself). We here chose for up-scaling rather than out-scaling. In up-scaling, minimizing the flow resistance and minimizing the complexity of the system are key factors. The most important simplification possible is the reduction of the number of obstacles rows. In theory not all the obstacles of an array are needed for the displacement of the particles. In fact, only one or a few diagonal lines of obstacles are sufficient. We name such a design a sparse deterministic ratchet (fig 5.1b).
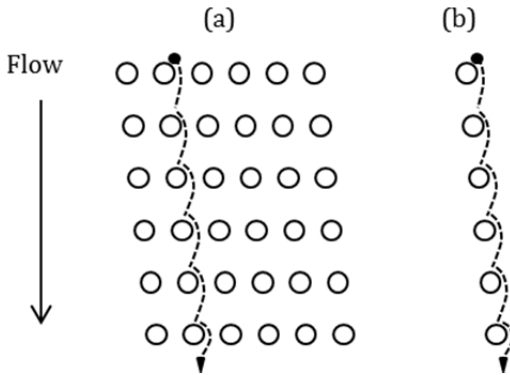
Fig. 5.1. (a) One periodic array of a deterministic ratchet; (b) One obstacle line of a sparse deterministic ratchet.

In a normal deterministic ratchet the risk of internal fouling is low since the gap sizes are bigger than the particle size, but in a sparse ratchet the risk of fouling lowers correspondingly with the number of obstacle lines. A sparse deterministic ratchet has also advantages for fractionation of multi-component mixtures; with original ratchets one needs to stack multiple arrays with different critical particle sizes, for example to separate blood as done by Davis *et al.* [22]. This stacking is not required in a device with one or a few obstacle lines for each particle size to be separated.

Bowman *et al.* demonstrated with a drop settling experiment that the critical angle of a single line ratchet agrees with the critical angle of a normal deterministic ratchet, and concluded that individual obstacle-drop collisions determine the drop migration trajectory [42]. This conclusion is probably valid only for highly diluted systems, in which suspended particles do not interact with other particles. In more concentrated suspensions, particle-particle interactions are expected to be a determining factor in

the particle displacement behavior [55]. One single obstacle line may not be sufficient for high particle retention; instead a sparse deterministic ratchet with more obstacle lines may well be more suitable for suspensions with higher volume fraction.

We start this paper with an investigation of the effect of particle concentration by a theoretical analysis of the particle flux near the obstacle lines. Next we discuss the experimental separation of polystyrene particles in sparse deterministic ratchets, and their interpretation based on the theory. Finally, we analyze the flow and pressure field inside a sparse deterministic ratchet with computation fluid dynamics.

5.3. Materials and Methods

5.3.1.   Sparse deterministic ratchet design

We investigated two different sparse deterministic ratchet designs; one with quadrilateral obstacles and one with cylindrical obstacles (fig. 5.2). The basic geometry of these designs originates from previous work with common obstacle arrays [40]. The quadrilateral obstacles are 0.8 mm wide and 1.6 mm long, the cylindrical obstacles have a diameter of 0.7 mm. All obstacles have a height of 2.5 mm, and are constructed by computer-controlled milling of a solid slab of polyether-ether ketone (PEEK). The designs are placed in a module with one inlet and five outlets. Each single line ends between two outlets. The device is operated vertically with liquid flowing from top to bottom. The flow is regulated by a peristaltic tubing pump (Masterflex).

5.3.2.   Experiments

Suspensions were prepared with 80/20 wt. % water/glycerol solution (glycerol obtained from Merck), polystyrene particles with density 1.05 g/ml (Maxiblast, USA) and 1.5 wt. % surfactant (SDS, obtained from VWR BDH Prolabo), such that the particles were neutrally buoyant. For the experiments we used particles of different
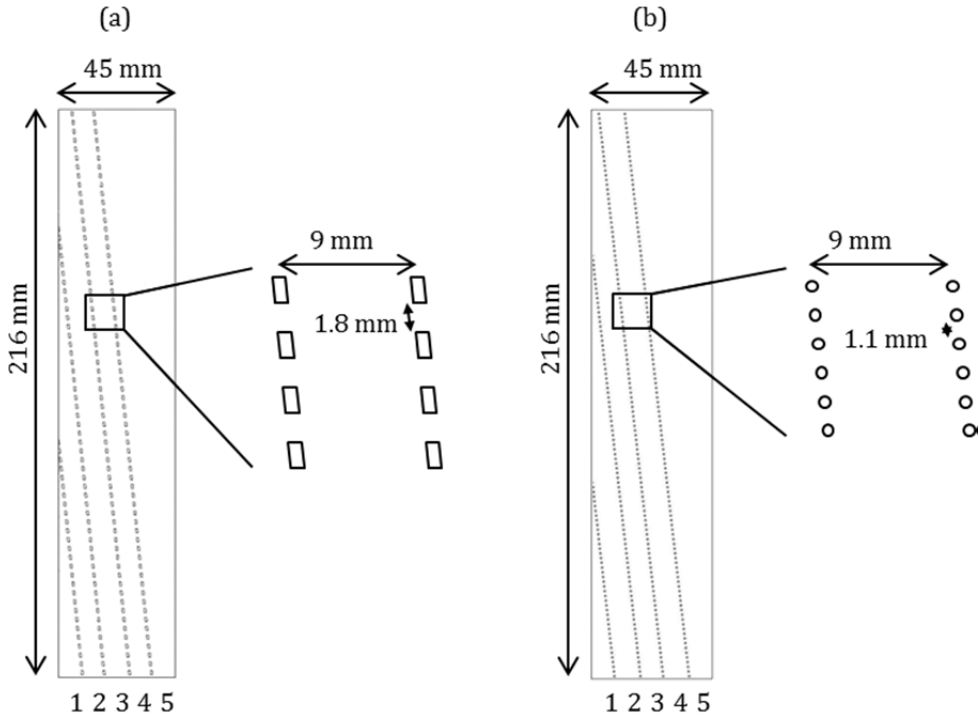
Fig. 5.2. Sparse deterministic ratchet designs. Flow is from top to bottom. At the bottom there are five outlets, numbered 1 to 5, separated by the lines. (a) Quadrilateral obstacles with length 1.6 mm and width 0.8 mm; (b) Cylindrical obstacles with diameter 0.7 mm.

size ranges: 0.36-0.61 mm, 0.61-0.99 mm and 0.99-1.68 mm (supplier sizing specification: minimum 99% ± 0.13 mm of target size range). The quadrilateral obstacle design was analyzed for its recovery of particles of 0.61-0.99 mm and 0.99-1.68 mm, which is a factor 1.8 to 3.0 and 1.1 to 1.8 smaller than the gap between two obstacles (1.8 mm). The recovery was defined as the volume percentage of particles per outlet, such that the sum of the five outlets is always equal to 100%. The inlet concentration was varied between 0.1-7 v/v%; the flow rate was varied between 50-800 ml/min. The cylindrical obstacle design was analyzed for its recovery of particles of 0.36-0.61 mm and 0.61-0.99 mm, which is a factor 1.8 to 3.1 and 1.1 to 1.8 smaller than the gap between two obstacles (1.1 mm). Notice that this gap is smaller than the gap of the quadrilateral obstacle design. The inlet concentration was 2.8 v/v%, the

flow rate was varied between 50-800 ml/min. The experiments with 2.8 v/v% particles were done in triplicate and a 95% confidence interval was calculated.

To observe the particle behavior close to the single lines we recorded the suspension flow with a high speed camera (Photron SA 1.1), which was equipped with a long focal distance lens (Navitar). The images were recorded at a frame rate of 500 fps. Suspensions with 2.8 v/v% particles of 0.61-0.99 mm were continuously recirculated through the sparse ratchet with cylindrical shaped obstacles at 100, 400 and 800 ml/min.

5.3.3.   CFD modeling of the fluid flow distribution

The sparse deterministic ratchet design as shown in fig. 5.2b was implemented in STAR-CCM+ as a three-dimensional geometry to simulate steady-state fluid flow distribution in this design. A mesh of polyhedral cells was generated, which refined in the neighborhood of obstacles and outlets. The base size was set at 4 mm. Rectangular cells were generated along the walls of the outlets by the prism layer mesher with a relative thickness size of 10%. The surface remesher was selected to improve the mesh quality. The relative minimum surface size was set at 5%. For all boundaries no-slip conditions were applied. The fluid was considered incompressible with the properties of water at 293 °C; ρ = 998 kgm^{-3} and μ = 8.9·10^{-4} kgm^{-1}s^{-1}. The fluid flow was set either at 100 ml/min or at 800 ml/min. The Navier-Stokes equations were solved to obtain the fluid flow, distribution of fluid velocities, and pressure field in the ratchet. Laminar flow conditions were assumed in all simulations and outlet boundary conditions were varied as described in the results and discussion section.

5.4. Results and Discussion

First the effect of larger particle concentrations on separation efficiency on a theoretical basis is discussed. Second, experimental results are presented on the separation efficiency as function of fluid flow and particle concentrations. Finally, an analysis of the fluid flow distribution of the new sparse deterministic designs is presented.

5.4.1.   Theoretical analysis of particle flow near an obstacle line

Different from conventional, full deterministic ratchets, in which particles are displaced by different obstacles and are gradually concentrated along the length of the ratchet, in *sparse* ratchets all particles are displaced by the same obstacles and thus quickly accumulate on one side of the line. As described by Davis and Leighton [57] and Leighton and Acrivos [58, 59] a concentrated flowing particle layer results in particle-particle interactions, which leads to a random displacement, or hydrodynamic (shear-induced) diffusion, of the particles. At the beginning this leads to a diffusion of the particles over a thicker concentration polarization layer, but it also displaces those particles that are nearest to the obstacles, from the polarization layer, across the critical lane, into the gaps between the obstacles. Since this occurs because of particle-particle interactions in which at least two or even three particles are involved, this phenomenon increases strongly at higher particle concentrations. As the polarization increases with increasing length of the obstacle line, this transmission of particles is low at the beginning (no or low polarization) and then increases with increasing polarization. At some point, the transmission of particles through the obstacle lines is just as large as the inflow of particles through the polarization layer, and a steady state is reached.

In this paragraph we analyze the particle flux along an obstacle line in a sparse deterministic ratchet and the effect of the particle polarization on the retention by the obstacle line. We follow the analysis that was developed by Romero and Davis [60] for the development of concentration polarization on microfiltration membranes, modified to describe the transmission of particles through the obstacle lines. Particles larger than a minimum size are displaced by the line of obstacles, and thus accumulate on one side of this line. They flow along the obstacle line, and increase in concentration. The excess particle flux Q, of those particles along the obstacle line is given by:

$$Q = \int_0^\delta v_y(\phi - \phi_s)dy \tag{5.1}$$

with y the distance from and perpendicular to the line of obstacles, v_y the component of the fluid velocity parallel to the line at distance y (zero at the surface of the line, and increasing in size with increasing y), ϕ is the local particle volume fraction, and ϕ_s is the volume fraction in the bulk of the fluid, far away from the obstacles. Since the velocity of the fluid is not completely parallel to the obstacle line, but somewhat inclined, there is an additional (smaller) component, called u, which is the velocity perpendicular to and through the line so:

$$\vec{v} = \vec{v}_y + \vec{u} \tag{5.2}$$

We assume that u does not depend on the coordinate along the line of obstacles, x. If we assume that v_y is only dependent of y (i.e. it is a two-dimensional ratchet), we may assume that:

$$\dot{\gamma} = \frac{dv_y}{dy} = \frac{\tau}{\eta} \tag{5.3}$$

with $\dot{\gamma}$ the shear rate, τ the shear stress and η the fluid viscosity. Combining equation 5.1 and 5.3 gives:

$$Q = \int_0^\delta \left(\int \frac{\tau}{\eta} dy \right) (\phi - \phi_s) dy \tag{5.4}$$

We may change the coordinate y into the volume fraction by using the continuity equation:

$$-D \frac{\partial \phi}{\partial y} + u\phi = uK\phi_w^2 \tag{5.5}$$

in which D is the hydrodynamic (shear-induced) diffusion coefficient, resulting from the hydrodynamic interaction between adjacent particles. The term on the right hand side of the equality sign is the amount of particles that is transmitted through the obstacle line; ϕ_w is the volume fraction at the obstacle line and K is a proportionality constant, which determines how many of the particles at the obstacle line will be displaced by inter-particle interactions through the obstacle line. Since inter-particle interactions require at least two particles, we assume that this passage is proportional to the square of the concentration near the obstacle line ϕ_w. Thus, the passage of the particles through the line is equal to $uK\phi_w^2$.

Combining equation 5.4 and 5.5 and changing y into ϕ gives:

$$Q = \int\limits_{\phi'=\phi_s}^{\phi'=\phi_w} \left(\int\limits_{\psi=\phi_s}^{\psi=\phi'} \frac{\tau}{\eta} \frac{D}{(u\psi - uK\phi_w^2)} d\psi \right) \frac{D(\phi' - \phi_s)}{(u\phi' - uK\phi_w^2)} d\phi' \tag{5.6}$$

In which we assume that (following Leighton and Acrivos [58, 59]):

$$\eta = \eta_0 \left(\frac{\phi_m - 0.13\phi}{\phi_m - \phi} \right)^2 \tag{5.7}$$

$$D = a^2 \dot{\gamma} 0.33\phi^2 \left(1 + 0.5e^{8.8\phi} \right) \tag{5.8}$$

with the maximum volume fraction ϕ_m = 0.58 and, a the particle radius. With this, the description of the polarization layer is fully determined. Appendix A gives more detailed derivation of equation 5.6, and the calculation of the volume fractions that are transmitted through the obstacle line.

Fig. 5.3 gives the volume fraction and the retention of particles near the obstacle line as a function of the distance along the line. At the beginning, there is a strong increase in accumulation of particles near the line, since most of them are retained, and thus accumulate. As soon as more and more particles accumulate, the chance of particle-particle interactions adjacent to the obstacle line becomes much larger, and particles are 'pushed' through the obstacle line. This results in less additional accumulation; after a certain line length, the amount of particles supplied to the line is just as large as the amount of particles transmitted through the line (asymptotes in fig. 5.3). At this point no separation takes place anymore.

This process is strongly dependent on the initial particle concentration and K. To increase the particle recovery, an additional line of obstacles may be placed after the first line; this will then translate the particles over an additional distance. Of course, those particles that are retained at the second line will also accumulate at a certain increased line length and may at some point affect the retention here as well. Even more lines may be required then to fully displace all particles to one side of the device.
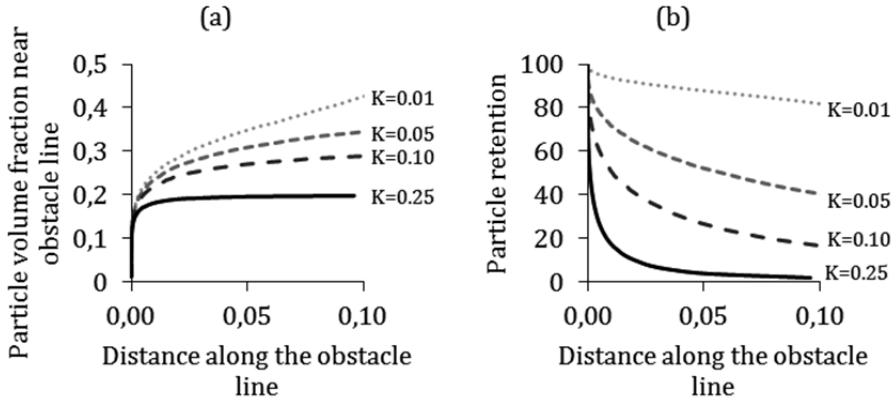
Fig.5.3. (a) Particle volume fraction near the obstacle line and (b) particle retention as function of the distance along the obstacle line. K = 0.01 (dotted line), K = 0.05 (short dashed line), K = 0.1 (long dashed line), K = 0.25 (solid line). The volume fraction in the bulk, ϕ_s = 0.01.

5.4.2. Experiments

In fig. 5.4 the outlet concentrations as a function of the flow rate and particle size are shown for both designs. The outlet concentrations were dependent on the entrance flow rate. This dependency, which we described before [40, 45, 55], is caused by inertial flow effects in the form of vortices behind obstacles. These vortices grow larger with increasing flow rate and form an additional barrier for particles, which enhances the separation. This effect was also found in other studies [46, 47, 61]. The highest particle concentrations were expected for outlet 5, on the basis of deterministic displacement behavior and the previous results using regular ratchet designs, but outlet 4 was found to have the highest outlet concentration in all four experiments. As mentioned in our theoretical analysis this may be explained by particle-particle interactions, pushing particles through the first obstacle line between outlet 4 and 5. Another explanation may be the strong fluid flow between outlet 4 and 5, which is a result of the pressure over the outlet tubing. This flow could drag particles from outlet 4 to 5 as will be discussed in paragraph 5.4.3. When the inlet concentration is 2.8 v/v%, particles are quickly concentrated at the obstacle lines. From high speed video camera images it can be estimated that the local

concentrations approximate 14 v/v% (fig. 5.7). At those concentrations the particles collide with each other, changing the particle displacement track.

Larger particles (fig. 5.4b and fig. 5.4d) showed increased displacement behavior, although with smaller particles (fig. 5.4a and fig. 5.4c) still a significant separation can be obtained. Especially with the larger particles there is a complete removal of particles from outlet 1 and 2 (at high flow rates). There is only a small effect of the obstacle shape: the quadrilateral obstacles perform slightly better, which is explained by the formation of larger vortices behind obstacles [45].
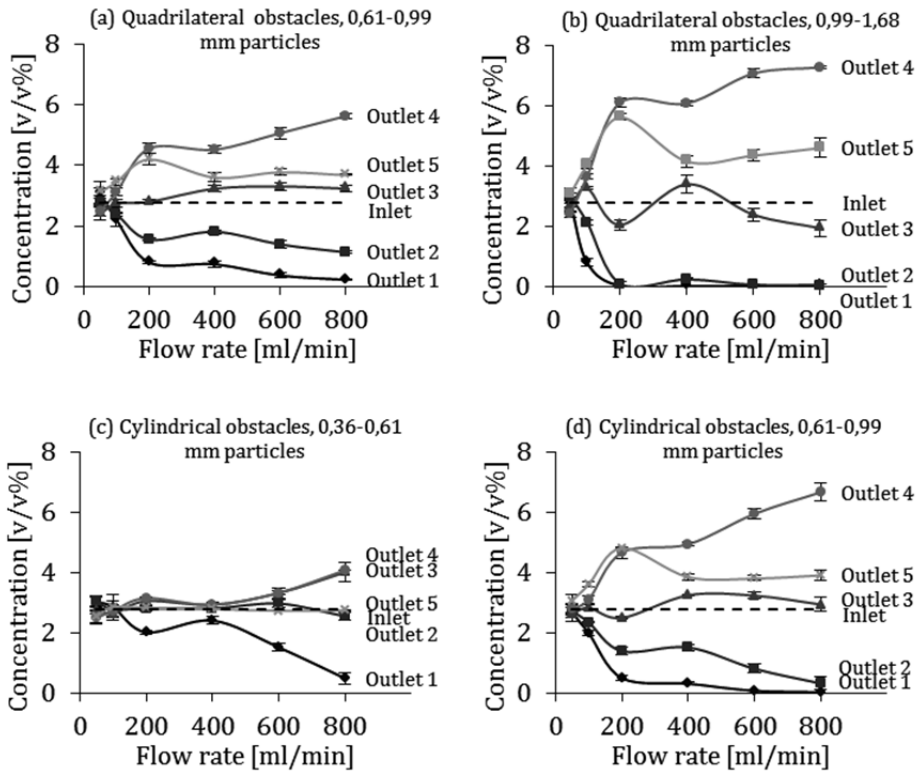
Fig. 5.4. Outlet concentrations as function of the flow rate. (a) Quadrilateral obstacles, particles 0.61-0.99 mm; (b) Quadrilateral obstacles, particles 0.99-1.68 mm; (c) Cylindrical obstacles, particles 0.36-0.61 mm; (d) Cylindrical obstacles, particles 0.61-0.99 mm. The inlet concentration (dashed line) is for all experiments 2.8 v/v%. Experiments are done in triplicate. The error bars show the 95% confidence interval of the measurements. Symbols: diamonds = outlet 1, squares = outlet 2, triangles = outlet 3, circles = outlet 4, crosses = outlet 5. Lines are drawn to guide the eye.

The effect of particle-particle interactions is further investigated with suspensions having different particle volume fractions. Fig. 5.5 shows the recoveries at different flow rates for inlet concentrations from 0.1-7.0 v/v%. The highest recovery for an inlet concentration of 0.1 v/v% is observed in outlet 5. The other recoveries were found equal to the theoretically expected values.

This is visualized in fig. 5.6 where experimental outlet concentrations and outlet concentrations on the basis of complete (ideal) displacement behavior are shown. Note that because two obstacle lines start from the top of the device (fig. 5.2), not all the particles will be displaced to outlet 5. At larger inlet concentration, the particle concentrations in the other outlets were found to increase as well, starting with outlet 4, due to the previously discussed effect of particle-particle interactions. At a critical concentration, the particles are forced from their streamlines by collisions with other particles and flow through the line to the adjacent outlet. At higher concentrations, the frequency of inter-particle interactions increases strongly, and many more particles are displaced to the next obstacle line. There the concentration will increase as well and particle-particle interactions start to occur again.

Thus the higher the inlet concentration the more particles are expected to deviate from their streamlines. This decreases the separation efficiency of sparse deterministic ratchets. In addition to particle-particle interactions, the fluid flow may have an effect as well. As discussed with the CFD simulations (fig. 5.8), there is a strong flow between lines, close to the outlets. Particles may be dragged along by this flow and move to adjacent outlets.
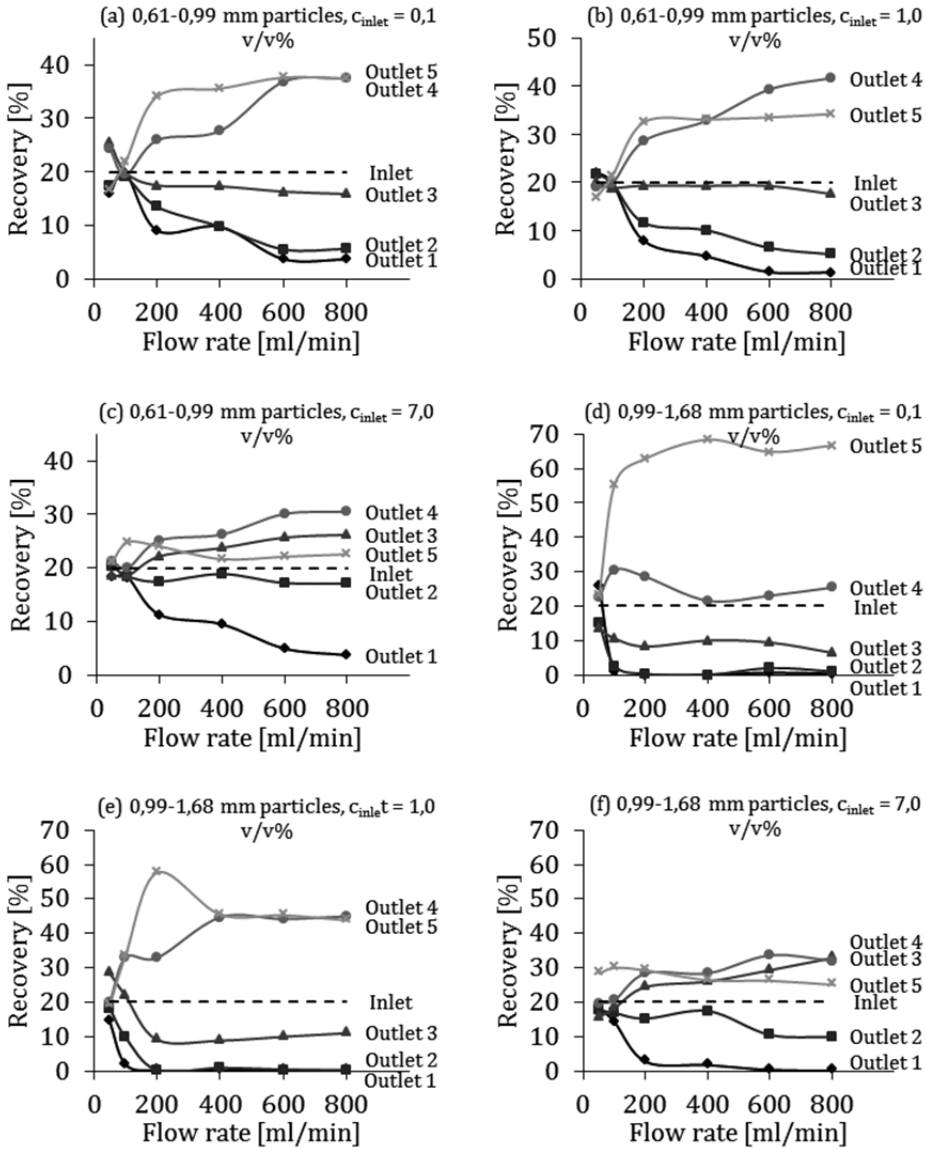
Fig. 5.5. The figures show the recovery as function of the flow rate for different inlet concentrations. The data presented are obtained with the quadrilateral obstacle design. (a,b,c) particle size 0.61-0.99 mm, inlet concentration (a) 0.1, (b) 1.0, (c) 7.0 v/v%; (d, e, f) particle size 0.99-1.68 mm, inlet concentration (d) 0.1, (e) 1.0, (f) 7.0 v/v%. Symbols: diamonds = outlet 1, squares = outlet 2, triangles = outlet 3, circles = outlet 4, crosses = outlet 5. Lines are drawn to guide the eye.
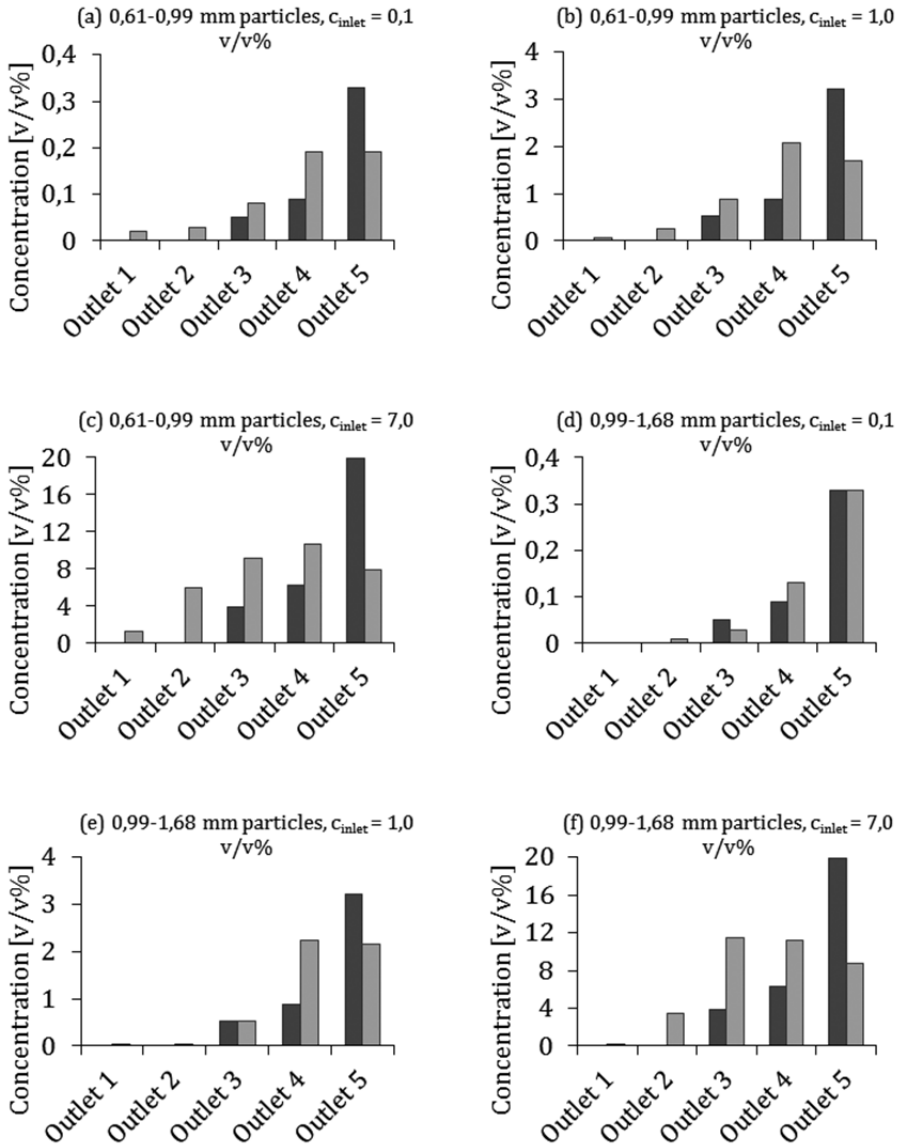
Fig.5.6. Outlet concentrations for complete (ideal) particle displacement (dark grey bars) versus experimental data (light grey bars). Data are obtained with the quadrilateral obstacle design. (a,b,c) particle size 0.61-0.99 mm, inlet concentration (a) 0.1, (b) 1.0, (c) 7.0 v/v%; (d, e, f) particle size 0.99-1.68 mm, inlet concentration (d) 0.1, (e) 1.0, (f) 7.0 v/v%.

The behavior of the particles near the obstacle line was observed and recorded with a high speed camera (fig. 5.7). At the bottom of the device many particles flow close to the line. To estimate the local particle concentration in such a polarization layer we estimated (from the pictures) the number of particles within two average particle diameters (1.6 mm) from the line. At 100 ml/min the concentrations are (from the left to the right line) 6.7, 7.0 and 8.7 v/v%, at 400 ml/min 0.7, 10.7 and 14.1 v/v% and at 800 ml/min 0.2, 4.7 and 13.7 v/v%. These values might be an underestimation, because only the particles which were in focus are counted. A video of the flow at the bottom and 800 ml/min is provided as supplementary material. From this video, but also from the picture, one can observe the building up of a particle layer and particles moving through the gaps. From the pictures the concentration differences between the outlets can be observed, which are in line with the quantitative results provided in fig. 5.4d.

Chapter
5
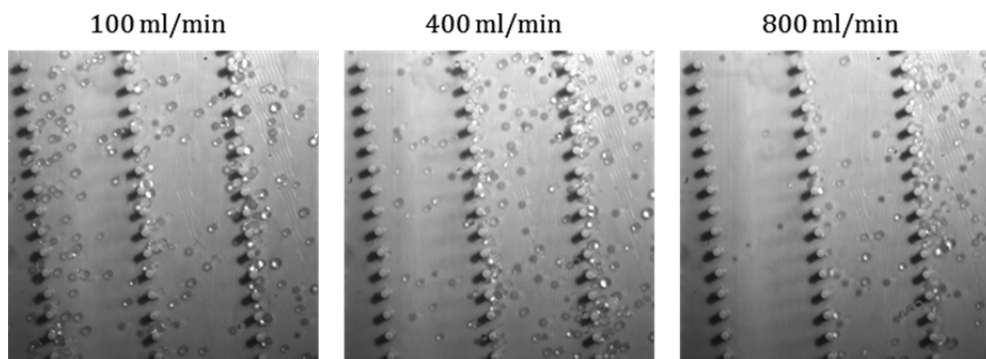
Fig.5.7. High speed camera images taken at the bottom of the device at 100, 400 and 800 ml/min. The pictures show the lines between outlet 1-2, 2-3 and 3-4.

5.4.3. CFD modeling of the fluid flow distribution

Two different boundary conditions for the outlets were applied. The first assumes free outflow, where the outlet flows result from the pressure differences across the ratchet geometry. The second boundary condition for the outlet assumes equal fluid flow for all five outlets. This was achieved by defining equal (negative, thus out-flowing) fluid flows per outlet to create a flow from top to bottom. This condition is more realistic

for our experimental system, in which the pressure difference across the outlet tubing is somewhat larger than the pressure drop across the ratchet, and thus results in similar flows from each outlet. The pressure drop across the length of the ratchet is calculated at 6 mbar for 100 ml/min and 40 mbar for 800 ml/min, while the pressure drop across the tubes is estimated 10 mbar for 100 ml/min and 78 mbar for 800 ml/min.

From the simulations we obtained outlet velocities for the sparse deterministic ratchet with cylindrical obstacles for both boundary conditions and inlet velocities. For the first boundary condition the maximum velocity in outlet 5 was 0.03 m/s at 100 ml/min and 0.30 m/s at 800 ml/min, while the velocity in the other outlets was 30 to 50% smaller. This unequal distribution may be less desired since this may limit the final concentration of the separation process. For the second boundary condition the outlet velocities were equal; 0.015 m/s at 100 ml/min and 0.12 m/s at 800 ml/min. Here, the fluid is forced (especially at the end of the device) through the obstacle arrays (fig. 5.8). Particles might be dragged along by this flow and as a consequence this may have a negative effect on the separation efficiency.
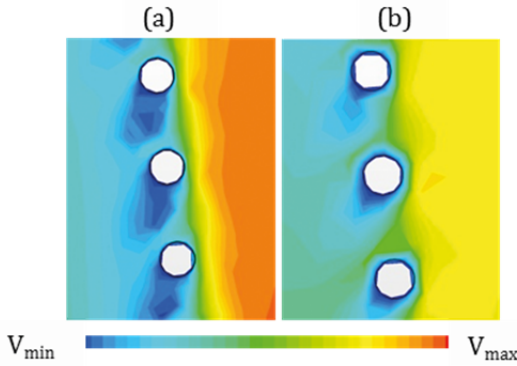
Fig.5.8. STAR-CCM+ scalar velocity plots of the obstacles near outlet 4 and 5. The velocity ranges from 0.00 (Vmin) to 0.30 m/s (Vmax). The input flow rate is 800 ml/min. (a) Outlet flow is assumed not restricted by separate outlets and (b) outlet flux is assumed influenced by high flow resistance in outlet tubing.

Combining all results we see that sparse deterministic ratchets are able to displace particles. Where the size of the gap between the obstacles, combined with the angle of

the obstacle lines determine the critical particle size for separation, the number of obstacle lines is found to determine the maximum particle volume fraction that can be separated.

Thus, sparse deterministic ratchets can be designed for their purpose: for dilute suspensions one or just a few obstacle lines may be sufficient, while for more concentrated suspensions, one may simply add more obstacle lines. The theory given above predicts that this will proceed more or less linearly; a twice as high particle concentration will require twice as many lines.

The finding that the hydrodynamic resistance in a sparse deterministic ratchet is low, in contrast to a full deterministic ratchet, is important here, since it shows that indeed there is freedom to add more lines. While the specific shape of the obstacles, the gap size and angle, and the flow rate all influence the absolute amount of lines required for a given volume fraction, we expect that relatively simple design rules can be based on the findings in this paper. This is important for the translation of the concept of sparse deterministic ratchets to industrial scale application.

5.5. Conclusions

Suspensions can be separated using deterministic ratchets with much simpler design than that of conventional systems. These sparse deterministic ratchets have only one or a few obstacle lines. Particles larger than a critical size follow a deterministic path along the line(s) and form a concentrated stream that can be collected at the outlet.

Particles accumulate rapidly along the obstacle line and are pushed through the gaps between the obstacles by interaction with other particles that have accumulated in a polarization layer. Thus, a single obstacle line can only displace a small amount of particles. Addition of additional obstacle lines can then be used to achieve full displacement with more particles, which will be distributed among the lines.

These theoretical considerations were confirmed by experiments with suspension flow through sparse deterministic ratchets. Diluted suspensions with a volume fraction below 0.1 v/v% particles give full retention with only one line, which is in full agreement with the displacement. At larger volume fractions, the particle retention

was lower, which is in agreement with the occurrence of the inter-particle interactions.

High speed imaging confirmed the accumulation of particles near the obstacle lines to concentrations of roughly 14 v/v%, which is in good agreement with the shear induced diffusion theory. The images also showed particles being pushed through the gaps, due to the particle-particle interactions.

CFD simulations showed that the hydrodynamic resistance of a sparse deterministic ratchet is very small. This indicates that the use of a limited number of lines, to accommodate for sufficient capacity, poses no problem.

This work thus gives the basis for relatively simple design rules for sparse deterministic ratchets. While the combination of the gap size between the object, and the angle of the obstacle lines determine the critical particle size that can be separated, the capacity of the system is determined by the number of lines. One can therefore easily adjust the design to any specific application.

5.6.Acknowledgements

Appendix A. Theoretical analysis of particle flow near an obstacle line

In paragraph 5.4.1 we derived an equation for the excess particle flux Q, near the obstacle line in a sparse deterministic ratchet:

$$Q = \int_{\phi'=\phi_s}^{\phi'=\phi_w} \left(\int_{\psi=\phi_s}^{\psi=\phi'} \frac{\tau}{\eta} \frac{D}{\eta(u\psi - uK\phi_w^2)} d\psi \right) \frac{D(\phi' - \phi_s)}{(u\phi' - uK\phi_w^2)} d\phi' \tag{A.1}$$

With:

$$\eta = \eta_0 \left(\frac{\phi_m - 0.13\phi}{\phi_m - \phi} \right)^2 = \eta_0 \eta_\phi \tag{A.2}$$

$$D = a^2 \dot{\gamma} 0.33\phi^2 (1 + 0.5e^{8.8\phi}) = a^2 \dot{\gamma} D_\phi \tag{A.3}$$

we obtain (once more taking $\dot{\gamma} = \frac{\tau}{\eta}$):

$$Q = \frac{a^4 \tau^3}{u^2 \eta_0^3} \int_{\phi'=\phi_s}^{\phi'=\phi_w} \left(\int_{\psi=\phi_s}^{\psi=\phi'} \frac{D_\phi}{\eta_\phi^2(\psi - K\phi_w^2)} d\psi \right) \frac{D_\phi(\phi' - \phi_s)}{\eta_\phi(\phi' - K\phi_w^2)} d\phi' \tag{A.4}$$

This is the excess flux of particles that accumulates before the line, and is equal to:

$$Q = \int_0^x (u\phi_s - uK\phi_w^2) d\xi \tag{A.5}$$

Equation A.5 is the overall balance of particles, over the length of the line; $u\phi_s$ being the supply from the bulk, and $uK\phi_w^2$ the loss of particles through the ratchet. Thus, we end up with the balance:

$$\int_0^x (u\phi_s - uK\phi_w^2) d\xi$$

$$= \frac{a^4 \tau^3}{u^2 \eta_0^3} \int_{\phi'=\phi_s}^{\phi'=\phi_w} \left(\int_{\psi=\phi_s}^{\psi=\phi_w,\psi} \frac{D_\phi}{\eta_\phi^2(\psi - K\phi_w^2)} d\psi \right) \frac{D_\phi(\phi' - \phi_s)}{\eta_\phi(\phi' - K\phi_w^2)} d\phi' \tag{A.6}$$

which we can use to find the volume fraction at the obstacle line. By using the difference equation:

$$\Delta \hat{x}(\phi_w) = \frac{\Delta \hat{Q}(\phi_w)}{\phi_s - K\phi_w^2} \tag{A.7}$$

with

$$\hat{x} = \frac{xu^3\eta_0^3}{a^4\tau^3}$$

(A.8)

(A.9)

$$\hat{Q}(\phi_w) = \int\limits_{\phi'=\phi_s}^{\phi'=\phi_w} \left(\int\limits_{\psi=\phi_s}^{\psi=\phi_{w,\psi}} \frac{D_\phi}{\eta_\phi^2(\psi - K\phi_w^2)} d\psi \right) \frac{D_\phi(\phi' - \phi_s)}{\eta_\phi(\phi' - K\phi_w^2)} d\phi'$$

we can find the volume fraction along the obstacle line.

The concentration passing through the line of obstacles is equal to $K\phi_w^2$, so the retention R of the line is equal to:

$$R = \frac{(\phi_s - K\phi_w^2)}{\phi_s}$$

(A.10)

The concentration of particles that can be obtained at the right strongly depends on the value of K. A larger K means less retention, and therefore a lower concentration in the concentrated part in the ratchet.

There is a steady state over the line when:

$$-D\frac{\partial \phi}{\partial y} = 0 = -u\phi_s + uK\phi_w^2$$

(A.11)

or $\phi_s = K\phi_w^2$. As soon as the transmitted concentration $(u\phi_p = uK\phi_w^2)$ is equal to the incoming concentration $(u\phi_s)$, there is no capacity for accumulation in the concentrated polarization layer anymore, and the retention has become zero.

General Discussion
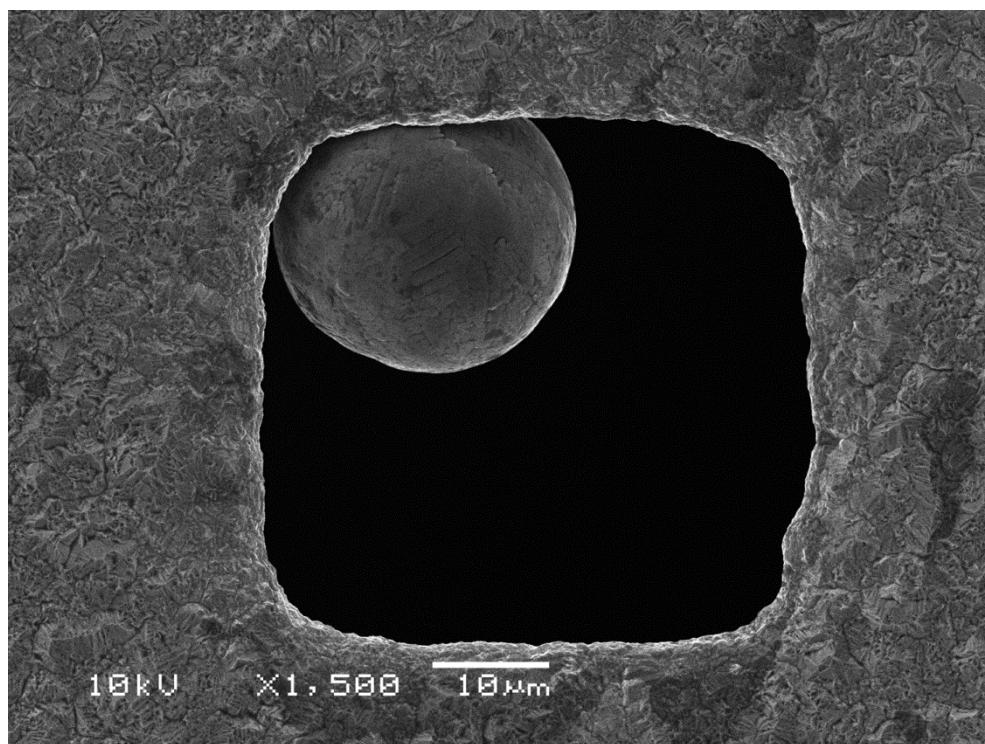
SEM picture of a 50x50 μm pore of a metallic microsieve. In the left corner a polyethylene particle is visible.

6. General Discussion

The development of technologies that can separate insoluble solids from a liquid is important for a wide range of activities in society. A new technology creates opportunities for innovative products, improves current processes and provides options for recycling of process streams to make better use of materials and to reduce waste. A promising technology named deterministic ratchet technology is a size based separation process by means of physical displacement of particles by an obstacle array. This process allows continuous separation and fractionation of concentrated suspensions with a low particle accumulation chance and has potential for large scale applications. The work reported in this thesis contributes to the development of deterministic ratchet technology for larger scale application.

In this chapter the main findings and conclusions are discussed followed by a comparison of out- and up-scaling strategies to larger processing volumes. Subsequently, microfluidic devices made by soft lithography are evaluated for potential large-scale separation and a new design using microsieves as deterministic ratchets is discussed as an option for out or up-scaling. Finally, the obtained results are translated in a conceptual design and compared with traditional membrane technology.

Chapter
6

6.1. Discussion of main findings

While microfluidic deterministic ratchets already were successfully demonstrated for treatment of small and dilute samples, we could show that it is possible to use the technology to a surprisingly high volume fraction of the dispersed phase. However, the application of microfluidic devices to separate industrially relevant product streams is not trivial. To speed up the research process an up-scaled device was constructed to study separation of model suspensions with a substantial volume fraction of particles (**Chapter 2**). A suspension with a particle concentration of 5.4 v/v% was successfully concentrated to 12 v/v%. This, and even higher initial

concentrations did not lead to particle accumulation inside the ratchet. The separation efficiency increased with increasing flow rate. These results pointed out the potential for larger scale application of deterministic ratchets and opened up ways for further research.

The strong dependency of the separation efficiency on the flow rate was not reported before. We evaluated the hypothesis that the hydrodynamic conditions (Re > 1) induced fluid instabilities and inertial effects, by visualizing the flow inside the up-scaled device with a high-speed camera and 2D flow field simulations (**Chapter 3**). A higher flow rate was indeed found to enhance particle displacement by the formation of a vortex pair behind obstacles, and an asymmetric flow profile as a result. In addition inertial forces exerted on particles are expected to influence particle displacement behavior. These factors lead to a decrease of the critical particle size. We can therefore make use of the hydrodynamic conditions to develop new deterministic ratchets facilitating high throughput separation.

To make deterministic ratchets suitable for large-scale application, the design should be effective and simple. The deployment of a mirrored (axisymmetric) obstacle array resulted in more effective displacement of particles (**Chapter 4**). By mirroring, particles can be concentrated in the center or at both sides of the obstacle array. This reduces the distance that particles need to be displaced by a factor two. The new designs allowed 100% displacement of particles to the sides and 88% displacement of particles to the center. A four times smaller up-scaled device was developed to investigate the effect of the length scale on the separation process. Less high volumetric inlet concentrations could be reached, which scaled inversely with the total particle surface area. The movement of small particles did not hamper the displacement of large particles, while a small effect was noticeable for the influence of large particles on small particles. These results show that mirrored designs are promising for cleaning or concentration applications, but that further research is required to make them suitable for larger-scale separation or for fractionation of concentrated suspensions.

A new, simple design is obtained by replacing the obstacle arrays by single lines of obstacles **(Chapter 5)**. This new device, which we named sparse deterministic ratchet,

Chapter
6

has several advantages for up-scaling the technology, like higher throughput and less fouling chance. CFD simulations visualized that the geometry in this sparse design results in unequal fluid distribution over the outlet, but that this can be corrected by using a slightly larger pressure over the outlet tubing. A theoretical analysis of particle fluxes in a sparse deterministic ratchet indicated that high initial particle concentrations result in rapid particle accumulation along the obstacles line and decreased retention caused by particle-particle interactions. It is suggested that the addition of extra obstacle lines could overcome this problem. The number of obstacle lines is thus a function of the volume fraction of dispersed phase. For dilute feeds, only a few lines are sufficient, for more concentrated feeds, one would need to deploy more lines. Camera images of experiments confirmed the formation of a concentrated particle layer at higher inlet concentrations, while almost all particles were retained at diluted concentrations below 0.1 v/v%. It is our conclusion therefore that a sparse deterministic ratchet has potential for larger scale application, and that the degree of sparseness is a design parameter for accommodating differences in concentrations. For each application a specific geometry can be designed based on the particle sizes and concentrations to be separated.

Chapter
6

6.2. Large scale separation

The translation of a lab-scale developed technology to a large-scale process is not trivial. Traditionally, higher throughputs are obtained by resizing of a single device. Alternatively, out-scaling by stacking of numerous small devices can also provide higher throughput.

Out-scaling is generally applied for microfluidic devices [62]. The choice for out-scaling arises from the origin of microfluidic devices. As described by Whitesides [8] the first applications of microfluidic technologies have been in analysis, because of the small sample volume, short analysis time, high resolution and sensitivity, low cost and small footprint. Stacking of multiple single devices implies that the costs of construction depend linearly on the production capacity, and requires complex integration of the devices [62]. Another important consequence of using microfluidics

is the relatively small size of the flow channels, which is usually in the same order as the particles flowing through. The channels are prone to clogging, causing reduced performance and extra cleaning steps might be necessary. The manufacturing of micron-sized pillars has some challenges, like the height-diameter ratio and accuracy. A frequently applied fabrication method for microfluidic devices is soft-lithography with poly(dimethylsiloxane) (PDMS). The fabrication of PDMS devices is shortly described in paragraph 6.3.

Considering these drawbacks for out-scaling, up-scaling might be a more attractive strategy for large-scale ratchet separation, since the costs of construction scale less than linearly with the total production capacity. As already discussed in the research chapters of this thesis, up-scaling requires knowledge about the flow conditions and particle-particle interactions on the process. Therefore, it is recommended to keep the design as simple as possible, such as for example in sparse deterministic ratchets. One of the ways to implement a sparse deterministic ratchet is by using microsieves as 2D obstacle sheets. Microsieves are widely available in a large variety of materials, pore sizes, shapes, porosities and thicknesses, and can be made such, that it is basically a sheet of pillars connected by crossbeams (see fig. 6.1). Because of these possibilities a sparse deterministic structure can be mimicked by microsieves. This idea is translated in a first experimental device (paragraph 6.4).

6.3. PDMS

Soft lithography is a technique to fabricate micron-sized structures. It represents a group of technologies using a patterned elastomer as the stamp, mold or mask (rather than a rigid photo mask) to make microstructures with a minimum feature size of 500 nm [63, 64]. A frequently used elastomer is poly(dimethylsiloxane) (PDMS), because of its mechanical properties, its low cost and ease of solidification by crosslinking [65]. Despite the manufacturing advantages the robustness of PDMS devices is low. Deformation of features with high aspect ratios, which is the height of the feature divided by the width or diameter, occurs easily [66]. Deterministic ratchets consist of obstacles with preferably high aspect ratios. The design of PDMS ratchets is thus

limited by the deformation of the structure. Nevertheless, PDMS has proven to be a suitable material for successful deterministic ratchet devices for biomedical separations, even at high flow rates up to 2 à 3 ml/min for a single device (0.3 m/s, Re = 20) [23, 67]. To investigate PDMS for large-scale application a few devices were produced. The production included two stages; the fabrication of the master mold and the fabrication of the PDMS device. The master mold fabrication was outsourced to Stanford Microfluidics Foundry, part of the Bioengineering Department at Stanford University (Stanford, USA). The fabrication of the PDMS devices was done in house.

6.3.1. Design and manufacturing

Fabrication of the master mold

A master mold contains the negative of the features of the desired microfluidic circuit. It is made by conventional photolithography. First, a mask is made by printing a computer-aided design (CAD) onto a transparency film using a very high resolution printer. Second, a photosensitive polymer (photoresist) is spun onto a silicon wafer. Then, the mask is placed on top of the coated wafer and exposed to UV-light. Finally, the wafers are developed to reveal the transferred design. The method of development depends on the type of photoresist used, positive or negative. A positive resist, AZ or SPR, is used to create rounded channels after hard baking. The portion of photoresist that is exposed to the UV-light becomes soluble to the photoresist developer. A negative resist, SU 8 series, is used to create rectangular type channels after hard baking. The portion of photoresist that is *not* exposed to the UV-light becomes soluble to the photoresist developer.

Fabrication of the PDMS devices

An 11:1 mixture of PDMS prepolymer and curing agent is stirred and degassed under vacuum. New master molds are pre-treated with Trichloro(1H,1H,2H,2H-perfluorooctyl)silane to make them hydrophobic. A thin layer of this PDMS mixture is poured onto the master mold. The mold with PDMS is baked in an oven of 60 °C overnight. The PDMS layer is carefully removed from the mold and oxidized in oxygen

Chapter
6

plasma for 2 minutes. The oxidized surface is irreversibly sealed to a glass slide. The bonded PDMS is heated at 60 °C for 1 hour. Holes are punched to connect the input and output channels with tubing. The flow through the device is controlled by a syringe pump.

Design

The basic geometry of the designed deterministic ratchets is the same as the designs described in Chapter 2 of this thesis. The dimensions are a factor 20 smaller, resulting in quadrilateral obstacles with a width of 40 μm and cylindrical obstacles with a diameter of 34 μm. The height of the obstacles is 50 μm. Cross flow operation is used to feed the suspensions to the ratchet.

6.3.2. Results

A suspension was prepared with 10 ml filtered water, 20 μl (5 w/v%) suspension of 10 μm particles in water and 20 μl (5 w/v%) suspension of 20 μm particles in water. The particles are spherical and made of polystyrene (microParticles GmbH, Germany). This equals a total particle concentration of 0.02 v/v%. Sodium dodecyl sulfate (SDS) was added as a surfactant (1 w/v%). After filling the device with the aqueous SDS solution and removing the air, the suspension was pumped through the ratchet at a flow rate of 0.2 ml/min (0.03 m/s, Re = 1.1). The motion of particles was observed with a microscope (Axiovert, Zeiss).

In all three designs most of the 20 μm particles moved in a displacement trajectory, while the 10 μm particles moved in a zigzag trajectory. This result was promising, because 0.2 ml/min is a relatively high flow rate for microfluidic deterministic ratchets. The initial particle concentration of 0.02 v/v%, or $2 \cdot 10^5$ particles/ml is low compared to those in applications such as the separation of yeast from beer (0.04 v/v%, $6 \cdot 10^6$ cells/ml, average size 5 μm) [68] or the removal of fat globules from milk (4 w/v%, $1.9 \cdot 10^8$ droplets/ml, average size 3.4 μm) [51]. These high initial concentrations were not yet investigated, because despite the clean working conditions and use of filtered water, the ratchet quickly fouled by the rare appearance of a single larger particle, larger than the gap size (e.g. dust), that got stuck and caused

accumulation of following small particles. This risk might be reduced by including a pre-filter just before the inlet. Another aspect that should be considered for increased throughputs is that the aspect ratio of the obstacles that can be made with soft lithography is limited. This fabrication method requires out-scaling rather than up-scaling.

6.4. Microsieves as a sparse deterministic ratchet

A microsieve can be designed in such a way that it looks similar to a single line of obstacles in a sparse deterministic ratchet (fig. 6.1). An obstacle line consists of individual obstacles separated by gaps, while a microsieve is a collection of pores (gaps) held together by the sieve frame (obstacles). The microsieve looks similar to a single obstacle line, if the distance between pores perpendicular to the flow is small compared to the width of the pore and the distance between pores in the flow direction is approximately equal to the pore length (front view fig. 6.1). In that case the sieve porosity is high and the pressure drop low. A low pressure drop is of course beneficial for the energy use. A side view of a microsieve and obstacle line clearly shows a similar geometry. This is the reason to assume that a microsieve can separate suspensions in a similar way as a sparse deterministic ratchet. This means that the pore sizes can be a few times larger than the particles to be separated, while for conventional sieving, microsieves are applied with pores smaller than the particles, leading to quick accumulation of particles on the surface.

6.4.1. Design and manufacturing

The microsieves were developed and kindly supplied by Veco B.V. (Eerbeek, the Netherlands) and are made by electroforming. Electroforming is a specialized process that grows metal, in this case nickel, on a metal substrate. First a photo-sensitive coating is applied on the metal substrate. On top of this coating a photo mask is placed, which is the negative design of the required pattern. The photo mask is exposed to UV light and the uncovered parts of the coating are solved by the UV light. Nickel ions are electro-deposited on areas not masked with photo-resist. In the last step the

microsieve is separated from the metal substrate. A scanning electron microscope (SEM) picture of a microsieve is given in fig. 6.2.
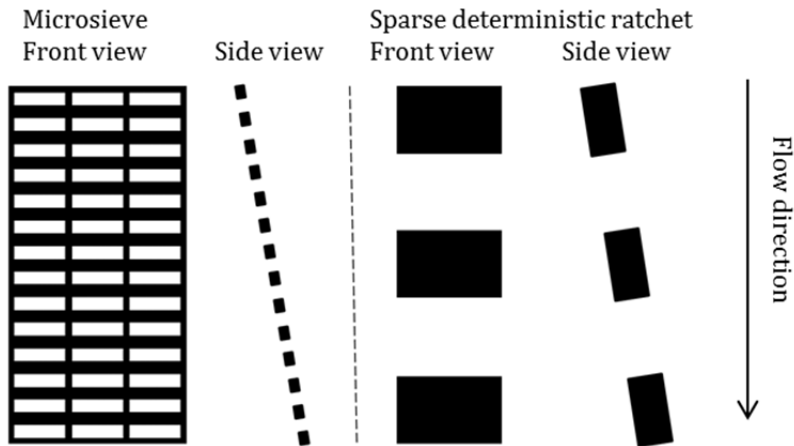
Fig. 6.1. Comparison between the geometry of a microsieve and a sparse deterministic ratchet.
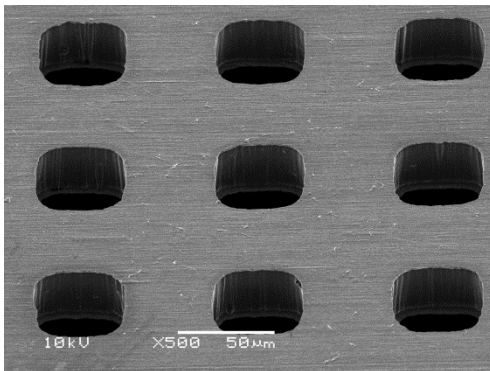
Fig. 6.2. SEM-picture of a microsieve with pore size 50x50 μm and distance between pores 50 μm. Thickness is 35 μm.

The design of the microsieve can be targeted on the particles that need to be separated. Important is the pore size, which should be larger than the particle. The distance between pores perpendicular to the flow is small compared to the width of the pore and the distance between pores in the flow direction is approximately equal

to the pore length. Examples of different geometries are given in fig. 6.3. Other properties that might be of influence to the separation process are the sieve material properties, ratio pore depth and particle size, the pore shape and permeability. Future research should focus on finding the right combination of microsieve design and suspension properties.
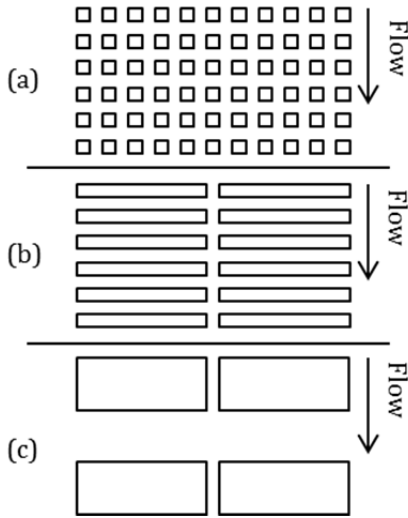
Fig. 6.3. Microsieve designs with pore size (a) 50x50 µm, (b) 50x500 µm and (c) 200x500 µm. The distance between the pores perpendicular to the flow direction is 50 µm, the distance between the pores in the flow direction is (a) 50 µm, (b) 50 µm and (c) 200 µm.

6.4.2.   Design of microsieve obstacle sheets

The up-scaled module as described in chapter 2 and the sparse deterministic ratchet design as described in chapter 5 can be used as starting point for a microsieve obstacle sheet. The microsieve can be cut into narrow strips that match the length of the obstacle lines in a sparse deterministic ratchet. A grooved PVC plate can serve as a holder for the microsieve strips. The grooves determine the displacement angle.

Depending on the composition of the suspension in terms of particle size, concentration and application (concentration or fractionation), different device designs are possible. For the concentration of very diluted suspensions one microsieve might be enough (fig. 6.4a). Keeping in mind the presence of particle-

particle interactions at high initial particle concentrations, a number of microsieves closes to each other can be applied to separate more concentrated suspensions (fig. 6.4b). For fractionation purposes several microsieves with different pore sizes may be combined (fig. 6.4c). Considering the results described in chapter 4 from the use of mirrored designs, similar design can be used for the arrangement of microsieves (fig. 6.4d).
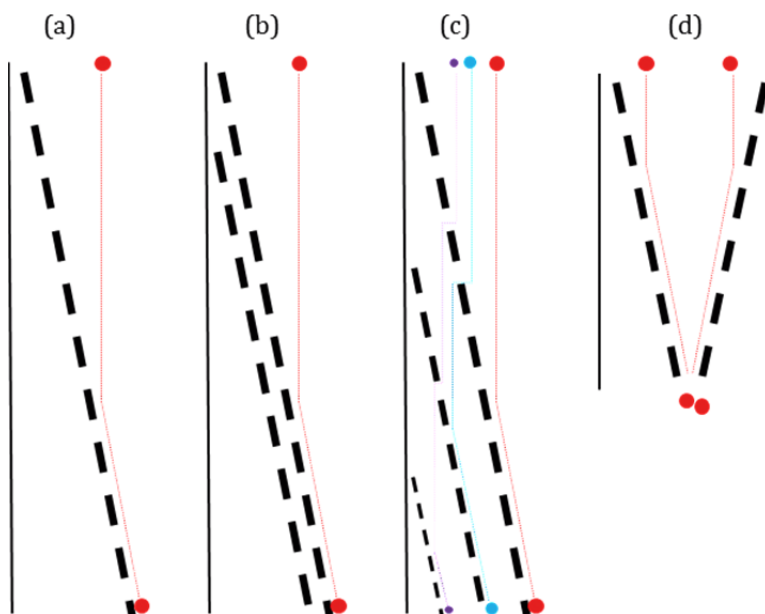
Fig. 6.4. Possible device designs for microsieves.

6.5. Conceptual design for larger-scale separation

The results in this thesis show that deterministic ratchets have potential for larger scale applications. High flow rates enhance the separation efficiency and smart designs allow quick and easy separation. In paragraph 6.2 it was concluded that up-scaling, increasing the volume of a single device, might be the preferred way for larger-scale separation. For the microsieve design the height can be increased easily to get a higher throughput. A hundredfold increase of the height results in a hundredfold increase of the throughput if the same channel flow velocity is applied. There are

however more factors to take into account, such as the Reynolds number, pressure drop and energy consumption. In the following sections rough calculations are presented indicating the effect of up-scaling pressure drop and the energy consumption of microsieve based ratchet separation for varying pore sizes. Finally, these data are compared to the performance of membrane separation. On the basis of previous experimental work on (sparse) deterministic ratchets it can be expected that particle sizes to be separated are approximately a factor 2 to 3 smaller than the actual pore size of the microsieve.

6.5.1.   Reynolds number

The hydrodynamics influence the separation process as explained in chapter 2 and 3. Inertial flow conditions are beneficial for the separation efficiency due to the formation of vortices and inertial lift forces on particles. To develop vortices inside the gaps of a deterministic ratchet or inside the pore of a microsieve, the Reynolds number in the gap (Re_p) should be larger than 1.

$$Re_p = \frac{U_p w_p}{\nu} \tag{6.1}$$

Here, U_p [m/s] is the average flow velocity in the gap, ν [m²/s] is the kinematic viscosity of the fluid and w_p[m] is the gap size in the direction of the flow. U_p is the average channel flow velocity (U_c) divided by the microsieve porosity (ε).

$$U_c = \frac{Q}{wh} \tag{6.2}$$

with Q [m³/s] the volumetric flow rate, w [m] the width and h [m] the height of the microsieve.

The pore size is critical in the separation process and determined by the particle size that needs to be separated. Depending on the available device geometry the throughput can be calculated. In fig. 6.5 the throughput is shown as function of the pore size for two devices at similar Reynolds number. Microsieves with pore sizes of a few micrometers require high throughputs to achieve $Re_p > 1$. In the calculations is chosen for $Re_p = 50$, a value at which larger vortices are expected. A higher Reynolds number might result in even larger vortices en thus enhanced separation, but it also

requires a higher throughput. This will affect the pressure drop across the system and the energy consumption, which will be discussed in the next section.
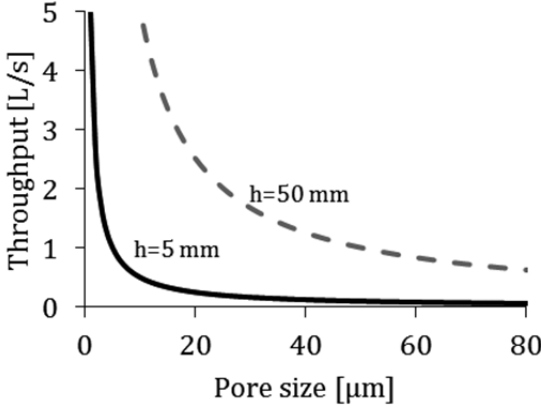
Fig. 6.5. Throughput as function of the pore size for a sieve with a height of 5 mm (black line) and one with a height of 50 mm (grey dashed line). Other parameters for the two devices were kept similar, i.e. w = 44.8 mm, ε = 0.45, v = 1.0·10⁻⁶ m²/s and **Re_p** = 50.

6.5.2. Pressure drop and energy consumption

The pressure drop (Δp) across the device is very relevant for the energy consumption. The pressure drop over a microsieve can be described by [69]:

$$\Delta p = \frac{Q R_p}{N_p} \tag{6.3}$$

in which R_p is the resistance of a pore in the microsieve and N_p is the number of pores per m². For slit-shaped pores having a length l_p, a width w_p ($<< l_p$) and a depth h_p, the following relation holds [69]:

$$R_p = \left(\frac{12 h_p \eta}{l_p w_p{}^3} + \frac{32\eta}{\pi l_p w_p{}^2}\right)\left(\frac{-\pi^2 \epsilon^2}{8\ln\left(\cos\left(\frac{1}{2}\pi\epsilon\right)\right)}\right) \tag{6.4}$$

In which η is the dynamic viscosity of the liquid and ϵ is the porosity of the microsieve. The right hand term in this equation corrects for the synergistic effects of having long slits lying parallel to each other.

In fig. 6.6 the pressure drop is shown as function of the pore size w_p. Here w_p is the distance in the flow direction. Used data: η = 0.001 Pas, ε = 0.45, l_p = 500 μm and h_p = 35 μm. For very narrow pores the pressure drop increases considerably. In fig. 6.4 several microsieve device designs are shown. Some of them contain multiple microsieves to enable fractionation or to increase the separation efficiency. The pressure drop is assumed to increase proportionally with the number of microsieves.

Fig. 6.6. Pressure drop as function of the pore size. Lines represent the number of microsieves; 1 (black line), 2 (dark grey line), 5 (grey line) and 10 (light grey line). The microsieve height is 50 mm.

The energy consumption of the separation process is calculated as follows:

$$E = Q\Delta p\eta_{\text{eff}} \tag{6.5}$$

The pump efficiency, η_{eff}, is assumed to be 0.6. Fig. 6.7 gives the energy consumption as function of the pore size for different number of microsieves.
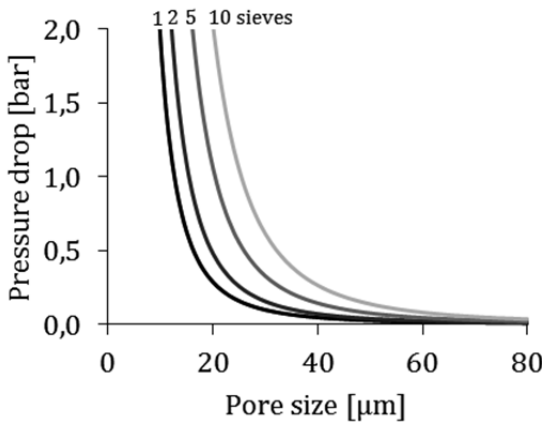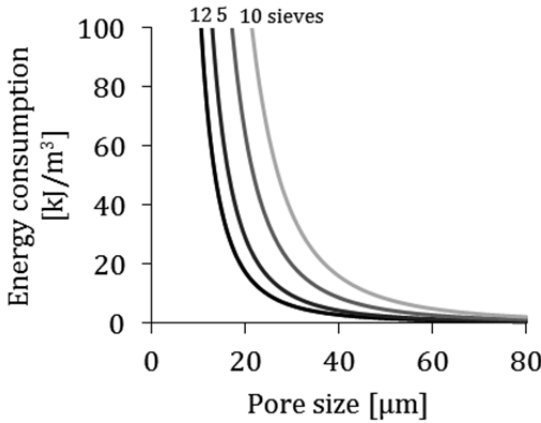
Fig. 6.7. Energy consumption per m³ throughput as function of the pore size. Lines represent the number of microsieves; 1 (black line), 2 (dark grey line), 5 (grey line) and 10 (light grey line). The microsieve height is 50 mm.

6.5.3. Comparison with membrane technology

Membrane technology is a very common size-based separation method and often applied on large scale, because of the relatively simple design and operation. Because the pore size is smaller than the particles that need to be retained, very high separation efficiencies can be obtained. Similar to deterministic ratchets, the separation usually does not require the use of additional water, chemicals or much energy. However, usually a concentration polarization layer develops near the membrane surface, hereby increasing the resistance and the pressure drop.

If we assume that h_p is small relative to w_p, we can observe from equation 6.4 that the hydrodynamic resistance R_s depends on w_p^{-2}. With a deterministic ratchet, the typical gap size D_x is around 3 times larger than the particles to be separated. However, for conventional cross-flow membrane separation, the pore size has to be at least factor 2 smaller than the particle size d_p. Kuiper [69] derived a relation between the required cross-flow velocity and particle/pore ratio to avoid pore blocking by particles:

$$v_c \propto \left(\frac{d_p}{w_p}\right)^3 \tag{6.6}$$

Thus, we may assume reasonable performance (avoidance of pore blocking) with a membrane with a pore size $w_p = \frac{1}{2}d_p$. The ratio of the hydrodynamic resistance exerted by one obstacle having gap size $D_x = 3d_p$ and a microsieve having pore size $w_p = \frac{1}{2}d_p$ is then:

$$\frac{R_{s,\text{ratchet}}}{R_{s,\text{sieve}}} = \frac{\dfrac{12h_p\eta}{l_p D_x^{\,3}} + \dfrac{32\eta}{\pi l_p D_x^{\,2}}}{\dfrac{12h_p\eta}{l_p w_p^3} + \dfrac{32\eta}{\pi l_p w_p^2}} \approx \left(\frac{w_p}{D_x}\right)^2 = \frac{1}{36}$$

Thus, even when the microsieve would have exactly the same thickness, the same porosity and the same elongated shape of the pores, one could employ 36 obstacle sheets in the ratchet, before the ratchet system would have more hydrodynamic resistance, and hence requires a larger pressure drop and energy consumption.

This is without taking into account polarization and particle accumulation on a conventional membrane or microsieve. Under usual operating conditions in the constant flux regime, it is not the membrane (microsieve), but the fouling (cake) layer on top of the membrane that dominates the hydrodynamic resistance through a membrane. The hydrodynamic resistance of this layer is at least one and possibly more than one orders of magnitude higher than that of the sieve itself. The formation of such a layer is not possible in either sparse or conventional ratchets, which implies that the difference in resistance even during normal operation is many times larger than the factor 36 which was based on just the hydrodynamic resistance of the membrane and obstacle sheets.

6.6. Conclusions

Deterministic ratchets have been investigated from a fundamental point of view, i.e. studying the fluid dynamics and the calculation of the critical particle size and their influence on the deterministic ratchet geometry. An up-scaled ratchet system showed

Chapter
6

that fluid instabilities in the form of vortices and inertial forces positively influence the separation process by forcing particles in a displacement movement.

For the design of larger scale systems it is suggested in this chapter to determine the right set of process conditions that induce the desired inertial effects. This means that the flow rate should be sufficiently large to reach Reynolds numbers in the order of one hundred. Small gap sizes in the order of few micrometers would then require very high flow rates. However, such small gap sizes are usually not necessary to separate industrially relevant particle suspensions as the gap size is a factor 2 to 3 larger than the particle diameter.

Simplification of the design lowers the cost of production, makes up-scaling easier and might lower the risk of particle accumulation even further. A good example of such a design is the sparse deterministic ratchet, which contains much less obstacles than a conventional deterministic ratchet. Current developments make it possible to design a microsieve that closely matches the geometry of a sparse deterministic ratchet with very precise gap sizes. Compared to classical microchannel-based deterministic ratchets, a microsieve is easier to make on large scale. Especially in case of fractionation purposes, which require different gap sizes, a stack of microsieves with each a different pore size may be an attractive option.

References

7. References

1.   Ruthven, D.M., *Encyclopedia of separation technology*. Vol. 2. 1997: Wiley New York.

2.   Svarovsky, L., *Solid-liquid separation*. Fourth ed. 2000: Butterworth-Heinemann.

3.   Richardson, J.F., J.H. Harker, and J.R. Backhurst, *Chemical Engineering, Particle Technology and Separation Processes*. 5 ed. Vol. 2. 2002: Butterworth-Heinemann.

4.   Rushton, A., A.S. Ward, and R.G. Holdich, *Solid-liquid filtration and separation technology*. 2008: Wiley. com.

5.   Kemsheadl, J.T. and J. Ugelstad, *Magnetic separation techniques: their application to medicine.* Molecular and Cellular Biochemistry, 1985. **67**(1): p. 11-18.

6.   Cappon, H.J., L.A. Stefanova, and K.J. Keesman, *Concentration based flow control in acoustic separation of suspensions.* Separation and Purification Technology, 2013. **103**(0): p. 321-327.

7.   Neuman, K.C. and S.M. Block, *Optical trapping.* Review of Scientific Instruments, 2004. **75**(9): p. 2787-2809.

8.   Whitesides, G.M., *The origins and the future of microfluidics.* Nature, 2006. **442**(7101): p. 368-373.

9.   van Dinther, A.M.C., C.G.P.H. Schroën, and R.M. Boom, *High-flux membrane separation using fluid skimming dominated convective fluid flow.* Journal of Membrane Science, 2011. **371**(1–2): p. 20-27.

10.   Di Carlo, D., et al., *Continuous inertial focusing, ordering, and separation of particles in microchannels.* Proceedings of the National Academy of Sciences, 2007. **104**(48): p. 18892-18897.

11.   Eijkel, J.C.T. and A. van den Berg, *Nanotechnology for membranes, filters and sieves.* Lab on a Chip, 2006. **6**: p. 19-23.

Chapter
7

12.   Kulrattanarak, T., et al., *Classification and evaluation of microfluidic devices for continuous suspension fractionation.* Advances in Colloid and Interface Science, 2008. **142**(1-2): p. 53-66.

13.   Huang, L.R., et al., *Continuous Particle Separation Through Deterministic Lateral Displacement.* Science, 2004. **304**(5673): p. 987-990.

14.   Feymann, R., R. Leighton, and M. Sands, *The Feynman Lectures on Physics* Addison Wesley, Reading MA, 1966. **Vol. 1, Chapter 46**.

15.   Huang, L.R., et al., *Tilted Brownian Ratchet for DNA Analysis.* Analytical Chemistry, 2003. **75**(24): p. 6963-6967.

16.   Huang, L.R., et al., *Role of Molecular Size in Ratchet Fractionation.* Physical Review Letters, 2002. **89**(17): p. 178301.

17.   Inglis, D.W., et al., *Critical particle size for fractionation by deterministic lateral displacement.* Lab on a Chip, 2006. **6**(5): p. 655-658.

18.   Kulrattanarak, T., et al., *Analysis of mixed motion in deterministic ratchets via experiment and particle simulation.* Microfluidics and Nanofluidics, 2011. **10**(4): p. 843-853.

19.   Kulrattanarak, T., et al., *Mixed motion in deterministic ratchets due to anisotropic permeability.* Journal of Colloid and Interface Science, 2011. **354**(1): p. 7-14.

20.   Loutherback, K., et al., *Improved performance of deterministic lateral displacement arrays with triangular posts.* Microfluidics and Nanofluidics, 2010. **9**(6): p. 1143-1149.

21.   Loutherback, K., et al., *Deterministic Microfluidic Ratchet.* Physical Review Letters, 2009. **102**(4): p. 045301.

22.   Davis, J.A., et al., *Deterministic hydrodynamics: Taking blood apart.* Proceedings of the National Academy of Sciences, 2006. **103**(40): p. 14779-14784.

23.   Loutherback, K., et al., *Deterministic separation of cancer cells from blood at 10 mL/min.* AIP Advances, 2012. **2**(4): p. -.

24. Bargiel, J.T., *Commercialization of lateral displacement array for dewatering of microalgae*, in *Department of Physics*. 2009, Case Western Reserve University: Cleveland. p. 53.

25. Green, J.V., M. Radisic, and S.K. Murthy, *Deterministic Lateral Displacement as a Means to Enrich Large Cells for Tissue Engineering.* Analytical Chemistry, 2009. **81**(21): p. 9178-9182.

26. Holm, S.H., et al., *Separation of parasites from human blood using deterministic lateral displacement.* Lab on a Chip, 2011. **11**(7): p. 1326-1332.

27. Huang, L.R., et al., *A DNA prism for high-speed continuous fractionation of large DNA molecules.* Nat Biotech, 2002. **20**(10): p. 1048-1051.

28. Inglis, D.W., et al., *Scaling deterministic lateral displacement arrays for high throughput and dilution-free enrichment of leukocytes.* Journal of Micromechanics and Microengineering, 2011. **21**(5): p. 054024.

29. Inglis, D.W., N. Herman, and G. Vesey, *Highly accurate deterministic lateral displacement device and its application to purification of fungal spores.* Biomicrofluidics, 2010. **4**(2): p. 024109-8.

30. Joensson, H.N., M. Uhlen, and H.A. Svahn, *Droplet size based separation by deterministic lateral displacement-separating droplets by cell-induced shrinking.* Lab on a Chip, 2011. **11**(7): p. 1305-1310.

31. Morton, K.J., et al., *Hydrodynamic metamaterials: Microfabricated arrays to steer, refract, and focus streams of biomaterials.* Proceedings of the National Academy of Sciences, 2008. **105**(21): p. 7434-7438.

32. Balvin, M., et al., *Directional Locking and the Role of Irreversible Interactions in Deterministic Hydrodynamics Separations in Microfluidic Devices.* Physical Review Letters, 2009. **103**(7): p. 078301.

33. Quek, R., D.V. Le, and K.H. Chiam, *Separation of deformable particles in deterministic lateral displacement devices.* Physical Review E, 2011. **83**(5): p. 056301.

34. Park, J.-S., S.-H. Song, and H.-I. Jung, *Continuous focusing of microparticles using inertial lift force and vorticity via multi-orifice microfluidic channels.* Lab on a Chip, 2009. **9**(7): p. 939-948.

Chapter
7

35.   Han, F., et al., *Density, Viscosity, and Excess Properties for Aqueous Poly(ethylene glycol) Solutions from (298.15 to 323.15) K.* Journal of Chemical & Engineering Data, 2008. **53**(11): p. 2598-2601.

36.   Braun, M.J. and V.V. Kudriavtsev, *Fluid Flow Structures in Staggered Banks of Cylinders Located in a Channel.* Journal of Fluids Engineering, 1995. **117**(1): p. 36-44.

37.   Sumer, B.M. and J. Fredsøe, *Hydrodynamics around cylindrical structures. Revised edition. Chapter 1: Flow around a cylinder in steady current.* Advanced Series on Ocean Engineering, 2006. **26**.

38.   Di Carlo, D., *Inertial microfluidics.* Lab on a Chip, 2009. **9**(21): p. 3038-3046.

39.   Shannon, M.A., et al., *Science and technology for water purification in the coming decades.* Nature, 2008. **452**(7185): p. 301-310.

40.   Lubbersen, Y.S., M.A.I. Schutyser, and R.M. Boom, *Suspension separation with deterministic ratchets at moderate Reynolds numbers.* Chemical Engineering Science, 2012. **73**(0): p. 314-320.

41.   Kulrattanarak, T., *Deterministic ratchets for suspension fractionation*, in *Food Process Engineering*. 2010, Wageningen University: Wageningen.

42.   Bowman, T., J. Frechette, and G. Drazer, *Force driven separation of drops by deterministic lateral displacement.* Lab on a Chip, 2012. **12**(16): p. 2903-2908.

43.   Morton, K.J., et al., *Crossing microfluidic streamlines to lyse, label and wash cells.* Lab on a Chip, 2008. **8**(9): p. 1448-1453.

44.   Loutherback, K., *Microfluidic Devices for High Throughput Cell Sorting and Chemical Treatment*, in *Department of Electrical Engineering*. 2011, Princeton University.

45.   Lubbersen, Y.S., et al., *Visualization of inertial flow in deterministic ratchets.* Separation and Purification Technology, 2013. **109**(0): p. 33-39.

46.   Schutyser, M. and G. Belfort, *Dean Vortex Membrane Microfiltration Non-Newtonian Viscosity Effects.* Industrial & Engineering Chemistry Research, 2002. **41**(3): p. 494-504.

Chapter
7

47.   Schutyser, M., et al., *Dean Vortex Membrane Microfiltration and Diafiltration of rBDNF E.coliInclusion Bodies.* Biotechnology Progress, 2002. **18**(2): p. 322-329.

48.   Raju, N. and E. Meiburg, *The accumulation and dispersion of heavy particles in forced two-dimensional mixing layers. Part 2: The effect of gravity.* Physics of Fluids, 1995. **7**(6): p. 1241-1264.

49.   Tropea, C., A.L. Yarin, and J.F. Foss, *Springer Handbook of Experimental Fluid Mechanics*. Vol. 1. 2007.

50.   Bhagat, A., et al., *Microfluidics for cell separation.* Medical and Biological Engineering and Computing, 2010. **48**(10): p. 999-1014.

51.   Brans, G., et al., *Membrane fractionation of milk: state of the art and challenges.* Journal of Membrane Science, 2004. **243**(1–2): p. 263-272.

52.   Mulder, M., *Basic Principles of Membrane Technology Second Edition*. 1996: Kluwer Academic Pub.

53.   Al-Fandi, M., et al., *New design for the separation of microorganisms using microfluidic deterministic lateral displacement.* Robotics and Computer-Integrated Manufacturing, 2011. **27**(2): p. 237-244.

54.   Inglis, D.W., *Efficient microfluidic particle separation arrays.* Appl. Phys. Lett., 2009. **94**(1): p. 013510.

55.   Lubbersen, Y.S., R.M. Boom, and M.A.I. Schutyser, *High throughput particle separation with a mirrored deterministic ratchet design.* Chemical Engineering and Processing: Process Intensification, 2014. **77**(0): p. 42-49.

56.   D'Avino, G., *Non-Newtonian deterministic lateral displacement separator: theory and simulations.* Rheologica Acta, 2013. **52**(3): p. 221-236.

57.   Davis, R.H. and D.T. Leighton, *Shear-induced transport of a particle layer along a porous wall.* Chemical Engineering Science, 1987. **42**(2): p. 275-281.

58.   Leighton, D. and A. Acrivos, *Viscous resuspension.* Chemical Engineering Science, 1986. **41**(6): p. 1377-1384.

59.   Leighton, D. and A. Acrivos, *The shear-induced migration of particles in concentrated suspensions.* Journal of Fluid Mechanics, 1987. **181**: p. 415-439.

Chapter
7

60.   Romero, C.A. and R.H. Davis, *Transient model of crossflow microfiltration.* Chemical Engineering Science, 1990. **45**(1): p. 13-25.

61.   Hur, S.C., A.J. Mach, and D. Di Carlo, *High-throughput size-based rare cell enrichment using microscale vortices.* Biomicrofluidics, 2011. **5**: p. 022206.

62.   Thorsen, T., S.J. Maerkl, and S.R. Quake, *Microfluidic Large-Scale Integration.* Science, 2002. **298**(5593): p. 580-584.

63.   Xia, Y. and G.M. Whitesides, *Soft Lithography.* Annual Review of Materials Science, 1998. **28**: p. 153-184.

64.   Perl, A., D.N. Reinhoudt, and J. Huskens, *Microcontact Printing: Limitations and Achievements.* Advanced Materials, 2009. **21**(22): p. 2257-2268.

65.   Duffy, D.C., et al., *Rapid Prototyping of Microfluidic Systems in Poly(dimethylsiloxane).* Analytical Chemistry, 1998. **70**(23): p. 4974-4984.

66.   Sharp, K.G., et al., *Effect of Stamp Deformation on the Quality of Microcontact Printing: Theory and Experiment.* Langmuir, 2004. **20**(15): p. 6430-6438.

67.   Liu, Z., et al., *Rapid isolation of cancer cells using microfluidic deterministic lateral displacement structure.* Biomicrofluidics, 2013. **7**(1): p. 011801-10.

68.   Blanpain-Avet, P., et al., *The effect of oscillatory flow on crossflow microfiltration of beer in a tubular mineral membrane system – Membrane fouling resistance decrease and energetic considerations.* Journal of Membrane Science, 1999. **152**(2): p. 151-174.

69.   Kuiper, S., *Development and application of microsieves.* 2000, University of Twente, Enschede, The Netherlands.

Summary

Separation processes are essential unit operations in the process industry to concentrate or fractionate raw materials into a product or stream of desired specifications. This thesis focusses on the separation of suspensions of solid particles in a liquid. Processing industries traditionally process large volumes. Dilution with solvent (water) is avoided, since it makes the volumes to be processed even larger, and the added water has to be removed again, often by evaporation or drying, which is very energy intensive. This requires separation technologies that allow high throughputs, while retaining good separation efficiencies, having low energy use and which do not suffer from fouling problems.

In recent years, there has been strong development in the area of microsystems engineering: systems in which small channels are used to process very small volumes; typically for analytic purposes. Amongst these microfluidic separation technologies, deterministic ratchets have been identified as a separation principle to be applied also to larger scale separation of suspensions. Deterministic ratchet technology, also known as deterministic lateral displacement technology, relies on particle interactions with a series of obstacle arrays positioned in a flow field. Particles above a critical size are forced from their streamlines when they interact with an obstacle and have a migration path other than the main flow direction. The objective of this thesis was to understand the mechanisms relevant for suspension separation with deterministic ratchets to be applied at larger scales, and to develop guidelines for the design of these deterministic ratchets.

An up-scaled device with three different deterministic ratchet designs was constructed (chapter 2). This up-scaled device, with five equal sized outlets, and designs have dimensions 70x larger than microfluidic devices to simplify and speed up the research. They were used to study the separation of model suspensions (polystyrene particles with d_{50} = 441 µm) with a substantial volume fraction of particles. A suspension with a particle concentration of 5.4 v/v% was successfully

Sum-
mary

concentrated to 12 v/v%, with a separation efficiency of 20 (ratio highest and lowest outlet concentrations). This, and even higher initial concentrations did not lead to particle accumulation. The separation efficiency increased with increasing flow rate; from a ratio of 1 at the lowest flow rates (Re = 2), to a ratio of 47 at the highest flow rates (Re = 18). Also the fractionation of small and large particles improved with increasing flow rates. Although experiments were carried out with model particles, the large separation efficiencies and tolerance for high suspension concentrations may open up ways for efficient larger-scale separation processes.

The strong dependency of the separation efficiency on flow rate has not been reported before and was further investigated in chapter 3. The flow field inside the up-scaled device was visualized with a high-speed camera and 2D flow field simulations. At increased Re the critical particle size was reduced by 1) the formation of a pair of vortices behind obstacles, 2) an asymmetric flow profile in the gap between two obstacles on the same row and 3) inertial forces exerted on particles. For cylindrical-shaped obstacles the vortices developed at Re = 9, became larger for higher Re and were about 70% of the gap between rows at Re = 30. For quadrilateral-shaped obstacles the vortices developed at Re = 2 and became 75% of the gap at Re = 26. These vortices, in combination with the anisotropy of the obstacle array, caused asymmetry of the fluid velocity profile in the gaps. The size of the critical flow lane width was decreased and this reduced the critical particle size by 14% (from 264 to 226 µm) for the design with cylindrical-shaped obstacles and by 24% (from 380 to 290 µm) for the design with quadrilateral-shaped obstacles. In addition, inertial lift forces exerted on particles moving between two obstacles are expected to push particles to adjacent flow lanes, which enhances the separation even more. These results provide better understanding of the inertial flow behavior in deterministic ratchets. It shows that specific asymmetric ratchet designs and hydrodynamic conditions can be used to develop new deterministic ratchets which facilitate high throughput.

To render deterministic ratchets suitable for larger scale application, the design should be effective and as simple as possible. Mirrored obstacle array designs were evaluated to concentrate particles in the center or at both sides of the obstacle array (Chapter 4). A mirrored design reduces the distance that particles need to be displaced by a factor two and resulted in more effective displacement of particles. The new designs were tested with model suspensions in the up-scaled module and allowed displacement of 100% of the particles to the sides and 88% of the particles to the center. The lower recoveries for the center mode were explained by the increased particle-particle interactions in the center regions, counter-acting the lateral displacement. Lower volumetric inlet concentrations were required with a four times smaller up-scaled device (critical particle size is 98 µm) that was developed to investigate the effect of the size scale. The separation scaled inversely with the total particle surface area. Fractionation experiments showed that the presence of small particles did not hamper the displacement of large particles, while a small effect was noticeable of the large particles on the displacement of the small particles. Further development will translate these results to practical application, which may be either cleaning (removal of unwanted particles) or concentration of suspensions.

The sparse deterministic ratchet design presented in chapter 5 has a much simpler design than conventional designs and has potential advantages for up-scaling, like higher throughput and less fouling chance. The design is obtained by replacing the obstacle arrays by single lines of obstacles. A theoretical analysis of particle fluxes indicated that high initial particle concentrations result in rapid particle accumulation along the obstacles line and decreased retention caused by particle-particle interactions. Additional obstacle lines can accommodate for sufficient capacity. High speed camera imaging confirmed that at higher inlet concentrations a particle polarization layer is formed with a concentration of roughly 14 v/v%. This was in good agreement with the shear induced diffusion theory. At diluted concentrations below 0.1 v/v% almost all particles were retained. CFD simulations showed that the hydrodynamic resistance of a sparse deterministic ratchet is very small. The latter indicates that the use of a limited number of lines poses no problem in terms of high

pressure drop. For each application a specific geometry can be designed based on the particle sizes and concentrations to be separated.

The last chapter discusses the main findings and conclusions, followed by a discussion of larger scale separation of suspensions (Chapter 6). A comparison between out- and up-scaling strategies was made. For deterministic ratchet technology, up-scaling is suggested as the best option to process large volumes. In addition, a preliminary evaluation was made of microfluidic deterministic ratchets made by soft lithography. Although model particles of 20 µm could be separated, in practice fouling issues arose due to the rare appearance of larger particles causing rapid accumulation of particles at the entrance. Thus, a system was proposed in which microsieves with slit-shaped pores are used to construct deterministic ratchets. The design of a system can be made similar to the design of a sparse deterministic ratchet, with the advantage that the height of the sieve is not limited by the aspect ratio of the obstacle, and the third dimension can be used for up-scaling. The pore size is – just like in deterministic ratchets – assumed to be a factor 2 to 3 larger than the particles to minimize the risk of fouling. Compared to a membrane with a pore size a factor 2 smaller than the particles, such a sparse ratchet would have a much lower hydrodynamic resistance, would have a much simpler design because it does not require cross-flow pump, and is much less sensitive to internal fouling.

Samenvatting

Scheiding is een belangrijke bewerkingsstap in de procesindustrie voor het concentreren en fractioneren van grondstoffen in de juiste productstroom. Dit proefschrift richt zich op de scheiding van waterige suspensies met vaste deeltjes. De meeste processen behandelen grote hoeveelheden grondstoffen. Verdunning van die stromen veroorzaakt nog grotere volumes, terwijl het water dat voor de verdunning nodig is, later vaak door verdamping of drogen moet worden verwijderd. Ideale scheidingstechnologie moet daarom grote hoeveelheden kunnen verwerken met een hoge scheidingsefficiëntie, laag energieverbruik en zonder dat vervuiling optreedt.

In de laatste jaren heeft het gebied van microsysteemtechnologie een grote vlucht genomen: technologie van systemen waarin kleine kanalen zeer kleine volumes vloeistof behandelen, over het algemeen voor analytische doeleinden. Onder deze micro-scheidingstechnieken is een deterministische ratchet geïdentificeerd als een principe dat mogelijk ook toegepast kan worden op grotere schaal. Deterministische ratchet technologie is gebaseerd op interacties van deeltjes met obstakels in een stromingsveld. Door interactie met een obstakel en een beweging in een richting anders dan de hoofdstroomrichting wordt een deeltje dat groter is dan een kritische grootte uit zijn stromingspad geplaatst. Het doel van dit proefschrift was het begrijpen van de achterliggende mechanismes relevant voor het mogelijk op grotere schaal kunnen scheiden van suspensies met deterministische ratchets en richtlijnen te ontwikkelen voor het ontwerp van deze deterministische ratchets.

Een opgeschaald systeem met drie verschillende deterministische ratchet-ontwerpen werd ontworpen en gebouwd (hoofdstuk 2). Om het onderzoek makkelijker te maken en te versnellen heeft dit opgeschaald systeem, met vijf uitgangen van gelijke grootte, een afmeting die 70x groter is dan die van de ratchets op microschaal. Het systeem is gebruikt om de scheiding van modelsuspensies (polystyreendeeltjes met d_{50} = 441 μm in water/glycerol) met een substantiële volumefractie aan deeltjes te onderzoeken.

Een suspensie met een concentratie van 5.4 v/v% kon geconcentreerd worden tot 12 v/v% met een scheidingsefficiëntie van 20 (ratio hoogste en laagste uitgangsconcentratie). Deze en nog hogere beginconcentraties leidden niet tot ophoping van deeltjes. De scheidingsefficiëntie nam toe met een hogere stroomsnelheid; van ratio 1 bij de laagste stroomsnelheid (Re = 2) tot een ratio van 47 bij de hoogste stroomsnelheid (Re = 18). Ook de fractionering van kleine en grote deeltjes verbeterde met hogere stroomsnelheden. Hoewel de experimenten uitgevoerd zijn met modeldeeltjes, zijn de hoge scheidingsefficiëntie en toleranties voor hoge suspensieconcentraties hoopvol voor het ontwerp van efficiënte scheidingsprocessen op grotere schaal.

De sterke afhankelijkheid van de scheidingsefficiëntie van de stroomsnelheid was nog niet eerder beschreven en is nader onderzocht in hoofdstuk 3. Het stromingsveld in het opgeschaald systeem is in verder detail bestudeerd met een hogesnelheidscamera en 2D-stromingsveld (CFD) simulaties. Bij hogere Re nam de kritische deeltjesgrootte af door 1) de vorming van een vortex achter de obstakels, 2) een asymmetrisch stromingsprofiel tussen twee obstakels op dezelfde rij en 3) inertiekrachten die de vloeistof uitoefent op de deeltjes. Met cilindervormige obstakels ontwikkelden de vortices zich bij Re = 9 en werden groter bij hogere Re tot een grootte van 70% van de ruimte tussen de obstakelrijen bij Re = 30. Met vierhoekige obstakels ontwikkelden de vortices zich bij Re = 2 tot een grootte van 75% van de ruimte bij Re = 26. Deze vortices in combinatie met de anisotropie van het obstakelveld veroorzaakten een asymmetrisch stroomsnelheidsprofiel tussen obstakels. De kritische breedte van de stromingspaden (bij zeer lage stroomsnelheid alleen bepaald door het ontwerp) nam af, waardoor de kritische deeltjesgrootte afnam met 14% (van 264 tot 226 μm) voor het ontwerp met cilindervormige obstakels en met 24% (van 380 tot 290 μm) voor het ontwerp met vierhoekige obstakels. Daarbij wordt ook nog eens verwacht dat deeltjes tussen obstakels naar naastgelegen stromingspaden verplaatst worden door inertiekrachten. Deze resultaten laten zien dat specifieke asymmetrische ontwerpen en hydrodynamische condities gebruikt kunnen worden bij de ontwikkeling van nieuwe deterministische ratchets met een hoge doorzet.

Om deterministische ratchets geschikt te maken voor toepassing op grotere schaal moet het ontwerp effectief en zo simpel mogelijk zijn. De concentratie van deeltjes in het midden of aan beide zijkanten van het obstakelveld is onderzocht met ontwerpen van gespiegelde obstakelvelden (hoofdstuk 4). Een gespiegeld ontwerp halveert de verplaatsingsafstand van deeltjes en maakt het verplaatsen dus effectiever. De nieuwe ontwerpen zijn getest met modelsuspensies in het opgeschaalde systeem. Met het centrumontwerp werd 88% van de deeltjes verplaatst naar het centrum en met het zijkantontwerp werd 100% van de deeltjes verplaatst naar een van beide zijkanten. De lagere opbrengst met het centrumontwerp kan verklaard worden door de toegenomen deeltjes-deeltjesinteracties in het midden van het systeem, die de verplaatsing tegenwerken. Lagere beginconcentraties waren nodig voor een viermaal zo klein systeem (kritische deeltjesgrootte is 98 µm), dat ontwikkeld was om het effect van de lengteschaal op het scheidingsproces te onderzoeken. De scheiding bleek omgekeerd evenredig met de totale oppervlakte van alle deeltjes. De experimenten lieten zien dat de bewegingen van kleine deeltjes de bewegingen van grote deeltjes niet beïnvloedden. Omgekeerd was er wel een merkbaar, maar klein effect van de invloed van grote deeltjes op kleine deeltjes. Verdere ontwikkeling is nodig om deze resultaten te vertalen naar praktische toepassingen met als doel een vloeistof te regenereren of suspensies te concentreren.

Het vereenvoudigde deterministische ratchet ontwerp, zoals gepresenteerd in hoofdstuk 5, heeft potentiële voordelen voor opschalen, zoals hogere doorzet en kleinere kans op ophoping van deeltjes. In het ontwerp zijn de obstakelvelden vervangen door enkele lijnen met obstakels. Een theoretische analyse liet zien dat het gebruik van hoge deeltjesconcentraties kan resulteren in een snelle ophoping van deeltjes langs een obstakellijn. Hierdoor worden deeltjes niet meer netjes verplaatst, wat te verwachten is door deeltjes-deeltjesinteracties. De toevoeging van meerdere obstakellijnen kan zorgen voor voldoende capaciteit door het aantal deeltjes te verspreiden over meerdere obstakellijnen. Beelden, gemaakt met een hogesnelheidscamera, bevestigen dat bij hoge beginconcentraties een polarisatielaag

wordt gevormd met een concentratie van ruwweg 14 v/v%. Bij lagere concentraties dan 0.1 v/v% worden alle deeltjes tegengehouden door de obstakellijn. CFD simulaties laten zien dat de hydrodynamische weerstand in het uitgedunde obstakelveld erg laag is. Hierdoor lijkt dat het gebruik van meerdere obstakellijnen geen probleem is wat betreft de drukval over het systeem. Voor elke toepassing kan een specifieke geometrie ontworpen worden gebaseerd op de aanwezige deeltjesgrootte en concentratie.

Het laatste hoofdstuk geeft een discussie van de belangrijkste vindingen en conclusies, gevolgd door een discussie over het op grotere schaal scheiden van suspensies (hoofdstuk 6). Eerst is een vergelijking gemaakt tussen twee opschalingsstrategieën. Het conventionele opschalen door middel van het vergroten van de capaciteit van een enkel apparaat is waarschijnlijk een betere optie dan het opschalen door parallellisatie van kleinere apparaatjes. Zachte lithografie is geëvalueerd voor het maken van micro-deterministische ratchets. Hoewel modeldeeltjes van 20 µm in een voorlopig experiment gescheiden konden worden, ontstonden er wel problemen met enkele ongewenste en grotere deeltjes bij de ingang die zorgden voor snelle ophoping van de andere deeltjes. Daarom is een systeem gepresenteerd, waarin microzeven met spleetvormige poriën worden gebruikt voor de constructie van deterministische ratchets. Het ontwerp van zo'n systeem kan nagenoeg gelijk gemaakt worden aan dat van een obstakellijn in een uitgedunde deterministische ratchet met als voordeel dat de hoogte van de zeef niet beperkt is door de aspectratio van de obstakels, en de derde dimensie dus gebruikt kan worden voor opschaling. Aangenomen is dat de poriegrootte, net als de ruimte tussen obstakels bij deterministische ratchets, een factor 2 tot 3 groter is dan de deeltjes die afgescheiden moeten worden om zo het risico van ophoping van deeltjes te minimaliseren. Vergeleken met een membraan met een poriegrootte die een factor 2 kleiner is dan de deeltjes, heeft een dergelijke uitgedunde ratchet of zeefconstructie een veel lagere hydrodynamische weerstand, heeft een veel simpeler systeemontwerp, omdat geen pomp voor crossflow nodig is, en is veel minder gevoelig voor interne vervuiling.

Dankwoord

Mijn proefschrift is klaar en ik ben er trots op. Dit was echter nooit gelukt zonder de hulp van vele mensen. Bedankt allemaal!

Remko, tijdens mijn MSc thesis overviel je me met de vraag of ik AIO wilde worden. Daar heb ik even over na moeten denken, maar het interessante project en het vertrouwen dat jij en Maarten me gaven hebben me overtuigd. De weinige keren dat we elkaar spraken was je altijd enthousiast en positief en gaf je me genoeg stof om over na te denken.

Maarten, wat heb je me veel geleerd. Zonder al je opmerkingen had ik dit proefschrift nooit kunnen schrijven. De afstand Leeuwarden-Wageningen heeft ons wekelijks contact nooit in de weg gestaan. Alle telefoontjes en talloze e-mails zijn niet voor niets geweest. Heel veel dank voor de plezierige samenwerking.

Mijn project heb ik opgestart in Wageningen. Na dit eerste jaar ben ik regelmatig een dagje teruggekeerd voor uiteenlopende redenen. Binnen de vakgroep van FPE zijn er dan ook veel collega's die ik wil bedanken. Karin en Ruud voor hun inhoudelijke advies, Jos voor de praktische hulp, Joyce, Marjan, en Martin voor de secretariële en administratieve zaken, Maurice voor de vele PDMS-uurtjes en de DIPP-experimenten, Pieter voor alle CFD-simulaties, Martijntje, Lena en Sina voor het gezelschap in onze kamer, Anja, Anna, Carsten, Frascisco, Marta, Nicolas, Nirmal, Petra en Thomas voor de gezellige lunches bij de vijver, Jimmy, Jue, Kashif, Kevin en Pascalle voor de groepsbijeenkomsten en pizza etentjes bij Maarten en natuurlijk alle andere collega's voor de bijdrage of steun op welke manier dan ook. Ondanks dat ik het grootste deel van het project fulltime in Leeuwarden werkte heb ik mij altijd thuis gevoeld bij FPE.

Na mijn verhuizing van Wageningen naar Leeuwarden wachtte mij een warm welkom bij Wetsus. Het waren drie fantastische jaren (en een paar maandjes extra) dankzij een inspirerende omgeving en vele behulpzame mensen. Mijn dank gaat uit naar Cees,

Gert-Jan, Bert en Maarten die mij de PhD-positie bij Wetsus toevertrouwden, Helena, Linda, Roely, Nynke, Trienke en Geke voor het secretariaat en HR, Wim, Jan, Harry en Harm voor de praktische ondersteuning, Ernst en Rienk voor het oplossen van mijn computervragen, Foppe en Poppe-Tjalf voor het afhandelen van al mijn bestellingen, Janneke, Jelmer, Marianne, Mieke, Pieter en Ton voor de analytische hulp in het lab, Luewton en Adam voor de hulp met de hogesnelheidscamera, Jan voor zijn investeringen in de Lego-ratchet, Andrii, Olivier, Odne, Juanma, Bram en Pieter voor de gezellige tijd in Vx1.01, Doede voor de stoelmassages, alle leden van het Wetsus thema Advanced Waste Water Treatment en in het bijzonder Paul en Flip voor alle nuttige discussies en informatie, mijn mede-AIO's in het thema Hans, Johannes, Jouke, Justina, Nadine, Ran, Slawomir en Vytautas en alle anderen die mijn tijd bij Wetsus zo leuk hebben gemaakt.

Tijdens mijn project heb ik twee studenten mogen begeleiden bij hun afstudeeropdracht. Jaap, jouw resultaten vormen de basis van hoofdstuk 3 in dit proefschrift en hebben geleid tot een mooie publicatie. Nu mag jij het stokje van me overnemen en de ratchet technologie verder ontwikkelen. Heel veel succes. Farnoosh, your hard work resulted in a lot of data and is a substantial part of chapter 5 in this thesis. I am glad that you find a PhD position yourself and wish you all the best. Jaap and Farnoosh, I thank you for the enjoyable cooperation.

Op deze plaats wil ik ook mijn paranimfen bedanken. Natasha, it was a pleasure to share many hours as neighbors in the lab. You supported me with positive words and always convinced me that I will succeed. Sanne, we hebben elkaar een jaar of tien geleden in Wageningen leren kennen. Jouw komst naar Wetsus betekende een gezellig weerzien en regelmatig een korfbalpraatje tijdens de pauzes.

Het succesvol volbrengen van een PhD-project is alleen mogelijk met de nodige ontspanning. Daarom bedank ik al mijn korfbalvrienden uit Harderwijk, Wageningen en Leeuwarden voor de sportieve en gezellige tijd na het werk.

Als laatste bedank ik mijn vrienden en familie. Hoewel jullie regelmatig dachten 'het zal allemaal wel', waren jullie altijd positief en enthousiast. Marijke, het was fijn om als collega-AIO de successen en frustraties met je te kunnen delen, maar het is nog fijner om jou als beste vriendin te hebben. Ik hoop dat we nog heel veel leuke uitstapjes gaan maken. Rene, papa, mama, niets is waardevoller dan jullie om me heen te hebben.

Yvette

About the author

Yvette Sylvia Lubbersen was born on November 28, 1985 in Harderwijk, the Netherlands. She finished her secondary education (VWO) in 2004 at the Regionale Scholengemeenschap het Slingerbos in Harderwijk. In the same year she started the study Food Technology at Wageningen University.

During her BSc thesis Yvette investigated the breakup of fibrils by a small molecule (DAPH). This work was carried out at the Food Physics department of Wageningen University. She finished her BSc degree in 2007 and continued with an MSc specialization on process and product design. Her MSc thesis was about the separation of suspensions with deterministic ratchets. This work was carried out at the Food Process Engineering department of Wageningen University. Her internship was performed at Duyvis Wiener in Koog aan de Zaan, where she investigated the cocoa milling process. In August 2009 Yvette obtained her MSc degree.

In October 2009 Yvette started to work as a PhD student at the Food Process Engineering Group of Wageningen University. From October 2010 she continued her research at Wetsus, centre of excellence for sustainable water technology in Leeuwarden. Her research focused on larger-scale separation of suspensions with deterministic ratchets. The results of the work are described in this thesis.

About
the
author

Publications

Thioflavin T fluorescence assay for β-lactoglobulin fibrils hindered by DAPH.
A. Kroes-Nijboer, Y.S. Lubbersen, P. Venema, E. van der Linden
Journal of Structural Biology, 165 (2009) 140-145.

Mixed motion in deterministic ratchets due to anisotropic permeability.
T. Kulrattanarak, R.G.M. van der Sman, Y.S. Lubbersen, C.G.P.H. Schroën, H.T.M. Pham,
P.M. Sarro, R.M. Boom
Journal of Colloid and Interface Science, 354 (2011) 7-14.

Suspension separation with deterministic ratchets at moderate Reynolds numbers.
Y.S. Lubbersen, M.A.I. Schutyser, R.M. Boom
Chemical Engineering Science, 73 (2012) 314-320.

Visualization of inertial flow in deterministic ratchets.
Y.S. Lubbersen, J.P. Dijkshoorn, M.A.I. Schutyser, R.M. Boom
Separation and Purification Technology, 109 (2013) 33-39.

High throughput particle separation with mirrored deterministic ratchet designs.
Y.S. Lubbersen, R.M. Boom, M.A.I. Schutyser
Chemical Engineering & Processing: Process Intensification, 77 (2014) 42-49.

Suspension separation with sparse deterministic ratchets.
Y.S. Lubbersen, F. Fasaei, P. Kroon, R.M. Boom, M.A.I. Schutyser
Submitted for publication.

Publi-
cations

Overview of completed training activities

Discipline-specific training activities - Courses

Numerical Methods in Chemical Engineering, OSPT, Enschede	2010
Sustainability Analysis in Food Production, VLAG, Wageningen	2011
Process Economics and Cost Engineering, OSPT, Enschede	2012
Sustainable Process, Product and System Design, OSPT, Amersfoort	2012

Discipline-specific training activities - Conferences

Wetsus Congress, Leeuwarden	2009-2012
MicroNano Conference, Delft	2009
Netherlands Process Technology Symposium, Arnhem (poster and pitch)	2011
11th World Filtration Congress, Graz, Austria (oral)	2012
Food Balt, Kaunas, Lithuania (oral)	2012
Symposium Nederlandse Werkgroep Drogen, Utrecht (oral)	2012
9th European Congress on Chemical Engineering, Den Haag (oral)	2013

General training activities

PhD Competence Assessment, WGS, Wageningen	2010
Project and Time Management, WGS, Wageningen	2010
PhD week, VLAG, Baarlo	2010
Philosophy & Ethics of Food Science and Technology, VLAG, Wageningen	2011
Techniques for Writing & Presenting a Scientific Paper, WGS, Wageningen	2011
Communication with the Media and General Public, WGS, Wageningen	2012
Career Perspectives, WGS, Wageningen	2013
Presentation training, VanZelf, Leeuwarden	2013

Training activities

Optional training activities

Writing of Project Proposal	2009
Food Process Engineering Group day	2009-2012
Wetsus Internal Congress	2009-2012
Wetsus theme meetings	2009-2012
Food Process Engineering PhD study tour to the USA	2010
Organizing Wetsus Water Challenge	2012
Food Process Engineering PhD study tour to Finland and the Baltic States	2012

Training
activities